Final report: DOE-UMICH-07465

Robust, Reliable Low Emission Gas Turbine Combustion of High Hydrogen Content Fuels

FINAL REPORT

Federal Agency and Organization Element to Which Report is Submitted	National Energy Technology Laboratory, Department of Energy
Federal Grant Number	DE-FE0007465
Project Title	Robust, Reliable Low Emission Gas Turbine Combustion of High Hydrogen Content Fuels
PI Name	Margaret S. Wooldridge
PI Title	Arthur F. Thurnau Professor Departments of Mechanical and Aerospace Engineering
PI Contact Information	Department of Mechanical Engineering University of Michigan 2350 Hayward Street Ann Arbor, Michigan 48109-2125
Submission Date	December 12, 2016
DUNS Number	073133571
Recipient Organization:	The Regents of the University of Michigan Ann Arbor, Michigan 48109
Project/Grant Period:	10/1/11-9/26/16
Reporting Period End Date:	9/26/16
Report Submission Date:	12/16/16
Report Term:	FINAL REPORT
Signature of Submitting Official	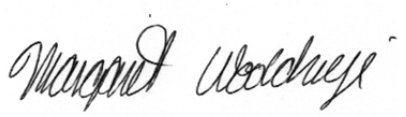

DISCLAIMER

This report was prepared as an account of work sponsored by an agency of the United States Government. Neither the United States Government nor any agency thereof, nor any of their employees, makes any warrantee, express or implied, or assumes any legal liability or responsibility for the accuracy, completeness, or usefulness of any information, apparatus, product, or process disclosed, or represents that its use would not infringe privately owned rights. Reference herein to any specific commercial product, process, or service by trade name, trademark, manufacturer, or otherwise does not necessarily constitute or imply its endorsement, recommendation, or favoring by the United States Government or any agency thereof. The views and opinions of authors expressed herein do not necessarily state or reflect those of the United States Government or any agency thereof.

Robust, Reliable Low Emission Gas Turbine Combustion of High Hydrogen Content Fuels
FINAL REPORT

Abstract

The effects of high hydrogen content fuels were studied using experimental, computational and theoretical approaches to understand the effects of mixture and state conditions on the ignition behavior of the fuels. A rapid compression facility (RCF) was used to measure the ignition delay time of hydrogen and carbon monoxide mixtures. The data were combined with results of previous studies to develop ignition regime criteria. Analytical theory and direct numerical simulation were used to validate and interpret the RCF ignition data. Based on the integrated information the ignition regime criteria were extended to non-dimensional metrics which enable application of the results to practical gas turbine combustion systems.

Keywords: Syngas, hydrogen, carbon monoxide, ignition, impurities

Table of Contents

Abstract…… i

Table of Contents…… 1

Executive Summary…… 3

Project Objectives…… 4

Technical Approach…… 5

Technical Approach - UM RCF Autoignition Studies…… 5

Technical Approach –DNS Autoignition Studies…… 8

Results……10

Results - UM RCF Autoignition Studies…… 10

Results - UM RCF Autoignition Studies of Impurities.…… 11

Results - UM RCF Autoignition Studies of OH Time Histories..……12

Results – Combustion Theory…… 14

Results –DNS Autoignition Studies……15

Conclusions……18

Acknowledgements…… 20

References……21

Appendices……22

Mansfield, A. B., Wooldridge, M. S., (2014) "High-pressure low-temperature ignition behavior of syngas mixtures," Combustion and Flame, 161, pp. 2242-2251……22

Mansfield, A. B., Wooldridge, M. S., Di, H., He, X., (2015) "Low-Temperature Ignition Behavior of Iso-Octane Mixtures," Fuel, 139, pp. 79-86……32

Mansfield, A. B., Wooldridge, M. S., (2015) "The Effect of Impurities on Syngas Combustion," Combustion and Flame, 162, pp. 2286-2295……41

Im, H. G., Pal, P., Wooldridge, M. S., Mansfield, A. B. (2015) "A Regime Diagram for

Autoignition of Homogeneous Reactant Mixtures with Turbulent Velocity and Temperature Fluctuations," Combustion Science and Technology, 187, pp. 1263-1275……51

Pal, P., Mansfield, A. B., Wooldridge, M. S., Im, H. G., (2015) "A Computational Study of Syngas Auto-Ignition Characteristics at High-Pressure and Low-Temperature Conditions with Thermal Inhomogeneities," Combustion Theory and Modeling, 19, pp. 587-601…….. 66

Pal, P., Valorani, M., Arias, P. G., Im, H. G., Wooldridge, M. S., Ciottoli, P. P., Galassi, R. M., (2016) "Computational characterization of ignition regimes in a syngas/air mixture with temperature fluctuations," Proceedings of the Combustion Institute, 36, pp. 1-12……82

Executive Summary

The objective of the project was to develop a thorough and quantitative understanding of the combustion properties of high hydrogen content fuels at conditions relevant to gas turbine operation. Auto-ignition properties and flame/autoignition interactions were determined using state-of-the-art experimental and computational facilities. The University of Michigan (UM) rapid compression facility (RCF) was used to measure ignition properties of hydrogen and carbon monoxide mixtures over a range of state conditions and for a range of fuel/air compositions including the effects of impurities. The effects of trimethylsilanol and hexamethyldisiloxane impurities (common landfill gases) were to significantly promote ignition, causing drastic reductions in auto-ignition delay time of almost an order of magnitude. Additional metrics studied included the ignition regime, the ignition delay time, rate of reaction front propagation (for ignition experiments in the mixed ignition regime) the time of the first stage of heat release (for conditions where multiple stages were observed), and OH time histories during ignition. The results for the ignition delay times were in excellent agreement with model predictions when autoignition occurred in the strong ignition regime. When conditions were in the weak or mixed ignition regime, the experimentally measured autoignition delay times were systematically faster than zero-dimensional model predictions based on elementary reaction chemistry. Ignition regime criteria were developed based on the chemical sensitivity of the reactant mixture to temperature gradients in the experimental system. The thermal sensitivity criteria captured the trends observed in the current work as well as in previous experimental studies of hydrogen ignition regimes. Combustion theory was used to extend the ignition criteria to a more general format using non-dimensional thermodynamic parameters such as the Reynold's and Damköhler numbers. The theory was validated using the RCF ignition regime data and via one-dimensional computational simulations. The direct numerical simulations provided further confidence in the ignition regime theory. Further two-dimensional direct numerical simulations were used to include the effects of turbulence on the ignition regime criteria. A major conclusion of the study is the definitive explanation of previously observed discrepancies in measured and predicted ignition delay times for syngas (and other fuels) at low temperatures. The cumulative results of this project show with high confidence the discrepancies are due to a break-down in the model assumptions of zero-dimensional behavior, i.e. the experiments exhibit spatial effects which are not captured by the models. The spatial effects in turn are attributed to the sensitivity of the syngas combustion system to temperature gradients and competing effects of flame propagation and auto-ignition. Details of these results are provided in several journal articles, and highlights of the work are reported here.

Project Objectives

The primary goal of this project was to develop a thorough and quantitative understanding of important HHC fuel combustion properties at conditions relevant to gas turbine operation. Flammability limits and flame/auto-ignition interactions were determined computationally and experimentally. The experimental data provided rigorous targets for development of accurate, well-validated models for detailed and simplified chemical kinetic reaction mechanisms for HHC combustion. The efforts included distillation of the fundamental data into forms that will aid the rapid transfer of information into syngas turbine design and provide new quantitative assessment of HHC combustion at conditions directly applicable to gas turbines.

The specific project objectives were:

- To develop an accurate and rigorous experimental and computational database of HHC fuel combustion covering reaction kinetics, flame speeds, and flammability limits of HHC fuels, including mixtures with high levels of exhaust gases.
- To develop detailed and simplified models of HHC chemical reactions that accurately reproduce the new experimental data as well as data in the literature.
- To develop a quantitative understanding of the stability of HHC combustion in relation to fluctuations in the flow field, including the opportunities and challenges of exhaust gas recirculation (EGR)/dilution on extinction, ignition, and flame stability.
- To develop domain maps that identify the range of conditions (e.g., percent EGR) where HHC combustion can be effective in both positive and negative manners such as expanded or restricted flammability limits.

Technical Approach

The technical approach used to meet the overall project goal and the specific project objectives was a combination of experimental, computational and combustion theory efforts. All experiments were conducted using the University of Michigan (UM) rapid compression facility (RCF). The numerical efforts used one-dimensional (1-D) and two-dimensional (2-D) direct numerical simulations (DNS). The following sections describe the details of experimental and computational efforts. The combustion theory is developed and presented in the **Results** section.

Technical Approach - UM RCF Ignition Studies

Ignition experiments were conducted for realistic but simple syngas mixtures for two values of equivalence ratio (φ = 0.1 and 0.5), designed to represent lean syngas mixtures used in the power industry. Both mixtures contained only H_2 and CO as fuel, with a molar ratio of H_2:CO = 0.70, and were approximately air-dilute with N_2, i.e. molar O_2 to inert gas ratio of 1:3.76. In some cases small amounts of the N_2 diluent gas were replaced by Ar and/or CO_2 to modify the test temperature. Ignition experiments were conducted at approximately 3, 5, 10, and 15 atm for the broadest range of temperatures allowable in the UM-RCF for these mixtures (~950-1150 K, based on experimental test times). The composition of the gas mixture and the thermodynamic state corresponding to each auto-ignition delay time measurement are given in Mansfield and Wooldridge [1].

Regarding the experimental apparatus, the UM-RCF is uniquely designed to create uniform thermodynamic conditions through an isentropic compression process [2]. A schematic of the UM RCF is presented in **Figure 1**. A detailed description of the UM-RCF and results of studies characterizing its performance can be found in Donovan et al. [2] and He et al. [3]. Briefly, the apparatus consists of a long cylinder, the Driven Section, in which a gas mixture is rapidly compressed by the motion of a free piston (Sabot). Prior to compression, the test volume is evacuated with a pump and then filled with a specific test gas mixture. Upon firing, the Sabot travels the length of the Driven Section compressing the test gas mixture into the Test Section – a small cylindrical volume located at the end of the Driven Section (~ 50 mm length and 50 mm diameter). As the Sabot reaches its final position near the Test Section, the Sabot achieves an annular interference fit, thereby sealing the test gas mixture in the Test Section. At this point, the Test Section is filled with a uniform and isentropically compressed test gas mixture at the desired initial thermodynamic condition. This is achieved in large part because cool boundary layer gases from the Driven section are trapped in an external volume formed by the geometry of the Sabot.

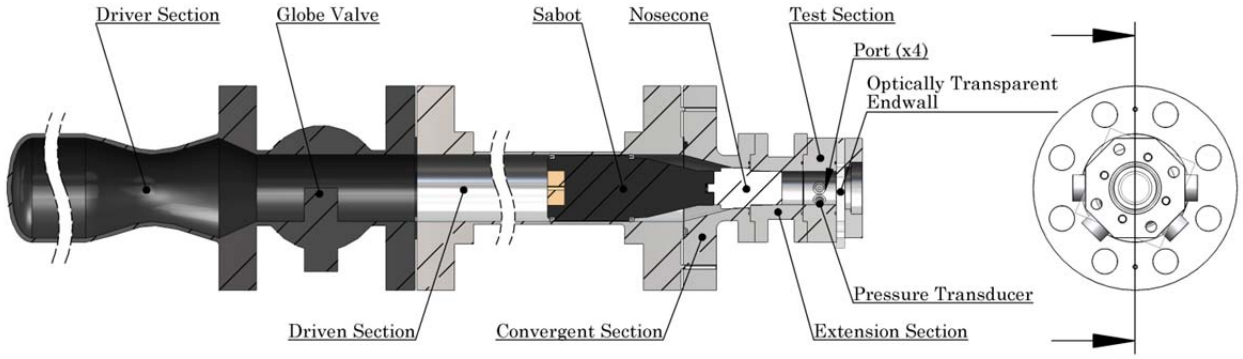

Figure 1. Schematic of the UM RCF as configured for high speed imaging.

For this study, the Test Section was instrumented with a piezoelectric transducer (6125B Kistler, Amherst, NY) and charge amplifier (5010, Kistler, Amherst, NY) for pressure measurements, and a transparent polycarbonate end-wall to permit high-speed imaging of the ignition process. During each experiment the pressure time history was recorded using the pressure transducer at 100 kHz sampling frequency. The uncertainty in the pressure measurements is estimated as ≤ 1% (~ 0.1 atm) considering both the signal-to-noise ratio in the post-ignition pressure time-history data and the non-linearity limits defined by Kistler during the calibration process. High-speed color imaging was recorded using a digital video camera (V711-8G-MAG-C, Vision Research, Phantom) with a Navitar 50mm lens (F0.95), a Hoya 62 mm lens (+2 zoom), and a Hoya 62 mm UV(0) filter. Video sequences were recorded at 25,000 frames/second with a CMOS array resolution of 512 x 512 pixels, resulting in an exposure time of 39.3 μs.

All test gas mixtures were made using a dedicated stainless steel tank and the mixture composition was determined by measurement of the relative partial pressures of the components. After filling, the tank was left to rest for at least one hour before the test gas was used for an experiment, during which time the mixture homogenized by diffusion. Error in the mixture composition is assumed to be negligible and have negligible effect on the ignition results, considering ~80-95% of the mixture is comprised of N_2 and O_2.

Some experiments were conducted of iso-octane ignition in order to confirm the hypotheses of the combustion theory developed as part of this work. For the sake of brevity, those results are not reported here. The details of the iso-octane study are presented in Mansfield et al. [4].

For the RCF studies of impurities, the same experimental apparatus and approach was used as for the ignition regime studies. For the studies of OH formed during ignition, a narrow-line ultraviolet laser absorption system was used as shown in **Figure 2**. The laser apparatus consisted of an intra-cavity frequency-doubled ring dye laser (Coherent 899-05) using Rhodamine 6G dye and a potassium deuterated phosphorus (KDP) doubling crystal. The ring

dye laser was pumped with a Coherent Verdi G7 solid state laser (~7 W @ 532nm). This system was used to generate a beam with specific wavelength corresponding to the $R_1(5)$ line of the $A^2\Sigma^+ \leftarrow X^2\Pi_i$ (0,0) band of the OH spectrum (ν_0 = 32606.556 cm^{-1} or ~ 306.687nm). As illustrated in **Figure 2**, once generated this beam was split into a reference and probe beam, using various optics and fiber optic components. The test beam was passed through the UM-RCF Test Section then both reference and probe beams were targeted on a pair of well-matched large area photodetectors (contained in one assembly) for continuous time monitoring of the power. The window ports though which the probe beam passes are heated for ~ 20 min prior to each experiment using installed resistance heaters, in order to avoid water condensation on the windows during the experiment. System components are labeled in the schematic presented in **Figure 2**.

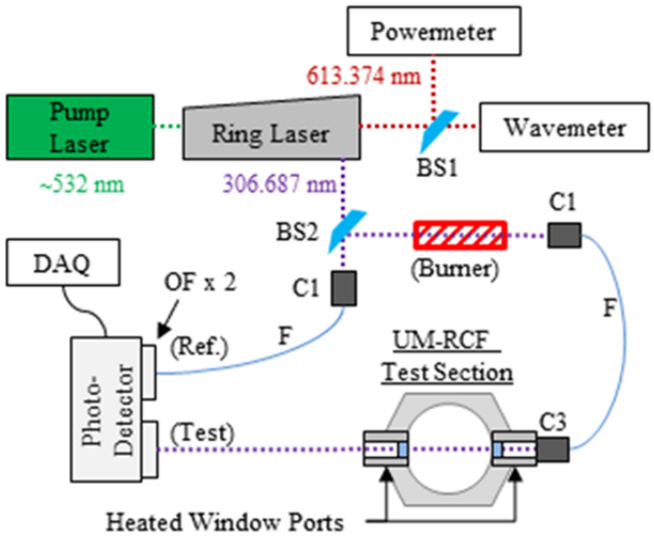

Figure 2. Schematic of the OH laser absorptionspectroscopy system. BS = beam splitter, C = collimator , F = fiber optic cable, OF = optical filter, DAQ = data acquisition system.

Using this system, it was possible to measure the fractional absorption of the test beam in the Test Section during auto-ignition and then calculate the corresponding concentration of OH molecules. Assuming a basic Beer-Lambert relation for a non-saturating linearly absorbing medium with homogeneous conditions along the path length, the fractional absorption of the test beam power can be related to a wavelength dependent absorption coefficient, k_ν, via:

$$-\ln\left(\frac{I}{I_0}\right) = k_\nu L \qquad (6\text{-}1)$$

where, I_0 is the probe beam intensity before passing through the Test Section, I is the probe beam intensity after passing through the Test Section, and L is the path length of the beam through the absorbing medium. The analysis of the laser signals to determine the OH time history is described in detail in Mansfield [5].

Technical Approach - DNS Autoignition Studies

The 1-D DNS used the code S3D [6] which solves the compressible, Navier-Stokes, species continuity and total energy equations. A fourth-order explicit Runge-Kutta method and an eighth-order central differencing scheme were used for time integration and spatial discretization. A detailed H_2/CO mechanism with 12 species and 33 chemical reactions [7] was employed. The mechanism was used with standard source code for evaluating the reaction rates and thermodynamic and mixture-averaged transport properties. Periodic boundary conditions were imposed such that heat release in the computational domain led to pressure rise and compression heating of the reactants.

A number of parametric conditions were considered for initial pressures (P_0) of 10 atm and 20 atm, and the initial mean temperature (T_0) ranging 850-1100 K, as typically encountered in gas turbines. A uniform syngas/air mixture with H_2:CO molar ratio of 0.7:1 and fuel-air equivalence ratio of 0.5 was chosen. For the 1-D study temperature non-uniformities were represented by two types of initial conditions. First, to represent moderate global temperature variations, a sinusoidal temperature profile was superimposed on the initial mean temperature, with a prescribed root-mean-square (RMS) fluctuation, T', and wavelength spanning the domain length, L. Alternatively, to represent a localized ignition source, a hot spot was represented by superimposing a Gaussian temperature profile, T_{hs}, onto the mean temperature:

$$T_{hs}(x) = \frac{A}{\pi}\exp\left[\frac{-2n^2(x-L/2)^2}{L^2}\right] - \frac{A}{2.5n}$$

where the factor n governs the size of the hot spot and A determines the amplitude. The amplitude (ΔT) of the hot spot is varied in the range 25-100 K, while the size of the hot spot was kept constant at 6 mm.

For the 2-D DNS simulations, the same DNS and chemistry codes and the same syngas reaction mechanism were used. A uniform syngas/air reactant mixture of equivalence ratio of 0.5, H_2:CO molar ratio of 0.7:1, an initial pressure of 20 atm, was chosen. In addition, the mixture was diluted with excess nitrogen equal to twice the amount of nitrogen present in the air, resulting in the overall molar ratio of N_2:O_2=11.28 in the reactant mixture, to ensure the pressure rise was sufficiently high to serve as an indicator of auto-ignition, but also to avoid shock wave formation, which cannot be captured by the employed computational schemes at present.

Turbulent velocity fluctuations were superimposed on a stationary mean velocity field based on an isotropic kinetic energy spectrum function. A similar random temperature spectrum, uncorrelated with the turbulent kinetic energy spectrum, was superimposed on a constant mean temperature field. In addition, a thermal hot spot was superimposed on the temperature field and the peak temperature of the hot spot was approximately 100 K, which is the upper limit of the local temperature fluctuations commonly observed in ignition experiments.

A total of eight DNS cases A-H were considered by varying the initial mean temperature, T_o, and the level of turbulence (l_d) and u'. For the four different T_o values of 1100, 1020, 990 and 970 K considered, the computed laminar flame speed values were 67.7, 27.8, 20.5, and 16.5 cm/s, respectively. L = 1.075 cm and 1.5 cm for cases A-E and F-H, respectively. The

magnitude of the temperature fluctuation was fixed at 15 K for all cases. Details of the physical parameters for the different cases and the expected ignition regimes are provided in Pal et al. [8]. All the parametric cases are plotted on the regime diagram in the *Results* section below (**Figure 9**).

Results

Results - UM RCF Autoignition Regime Studies

As noted above, several types of ignition experiments were conducted, including experiments to identify ignition regime, to quantify ignition delay time, to quantify the effects of impurities on ignition delay time and to measure the formation of hydroxyl radicals during ignition. A summary of the results of the ignition regime data is provided in **Figure 3**. The data show the ignition behavior is strongly related to initial thermodynamic state and is repeatable, with generally clear boundaries between different regions. Also shown in Figure 3 are the thermal sensitivity iso-contours based on the Sankaran Criterion [9] and the critical thermal iso-contour is highlighted in bold. There is excellent agreement between the critical iso-contour and the observed strong ignition limit at all pressures. The results quantitatively show the ignition regime behavior is a competition between the laminar flame and the auto-ignition characteristics of the syngas mixture and the local and global state conditions.

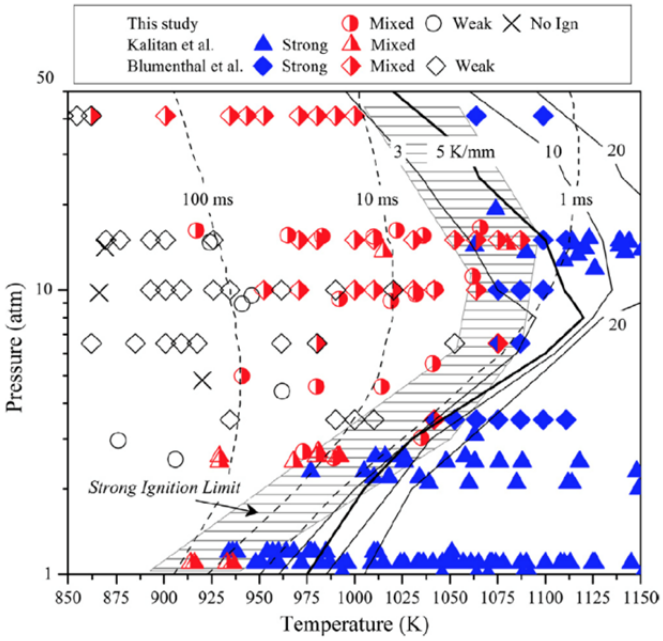

Figure 3. Ignition behavior as a function of thermodynamic state for syngas mixtures with ϕ = 0.5. The strong ignition limit is shown as a hashed area. Results are from the present work, Kalitan et al. [10], and Blumenthal et al. [11]. Predicted locations of the strong ignition limit are shown as solid lines and calculated iso-contours of auto-ignition delay time are shown as dotted lines. The most accurate predicted strong ignition limit, for a 5 K/mm gradient, is the bold solid line.

Considering the success of this criterion it was apparent that localized thermal gradients are the dominant driver of inhomogeneous ignition behavior in this work and the studies by

Blumenthal et al. [11] and Kalitan et al. [10]. Non-uniformities will be present in any experimental or practical combustion system and could come from a number of sources such as heat transfer, mixing, or the presence of minute reactive or non-reactive particles like those considered in Chaos and Dryer [12]. Previously, Chaos and Dryer [12] and Blumenthal et al. [11] predicted that hot spots of 150-200 K would be necessary to cause inhomogeneous auto-ignition. The present work highlights the importance of considering not only the absolute temperature of hot spots, but also the corresponding thermal gradients, as those on the order of merely 3-5 K/mm were found to drive inhomogeneous ignition behaviors in the current work.

This work was the first experimental validation of the Sankaran criterion and showed the theory can be used for a priori prediction of the strong ignition limit. Validating this criterion was fundamentally important, as the criterion quantitatively describing the roles of chemical kinetics, thermo-physical properties, and device dependent thermal characteristics in determining auto-ignition behavior. Overall both the demonstration of the application of the Sankaran Criterion and the ignition behavior maps created in the present work provide important, new, and unique tools that can be used in the design of combustion devices using high hydrogen content fuels like syngas.

Results - UM RCF Autoignition Studies of Impurities

The effects of a range of impurities on syngas ignition were explored. A summary of the results can be found in Mansfield and Wooldridge [13]. Briefly, methane (CH_4), trimethylsilanol (TMS) and hexamethyldisiloxane (HMDSO) were added in small part per million levels to reference syngas mixtures and conditions, and the changes in the autoignition delay time was measured. **Figures 4 and 5** show the results for the effects of TMS and HMDSO, respectively. As demonstrated in **Figure 4**, the effect of TMS addition on the auto-ignition delay time is dramatic and highly pressure dependent, with significantly larger magnitude impact at 15 atm. While 10 ppm TMS addition had minimal impact on the pressure dependence of the reference syngas mixture, the addition of 100 ppm of TMS completely suppressed the syngas pressure dependence of the auto-ignition delay time. As the pressure dependence of syngas is attributed to HO_2 and H_2O_2 chemistry, the results suggests the promoting effect of TMS is related to interaction with these species.

Figure 5 shows the pressure time histories of syngas ignition with and without the addition of HMDSO. HMDSO also had a significant accelerating effect on syngas ignition. The similarities in the chemical structure of TMS and HMDSO allowed further insight into the chemical reaction pathways affected by these organosilicon compounds. These impurities are particularly relevant as siloxanes are increasingly present in land-fill gases. This work was not only the first study of silicon organic compounds; the work also provided the first direct observations of sometimes drastic effects, and highlighted trends in behavior that extended beyond the initial TMS compound studied. Project such as these are vital to the safe and effective application of real syngas and other high-hydrogen content fuels, especially when used in modern high-pressure low-temperature combustion strategies like dry low-NO_x combustors.

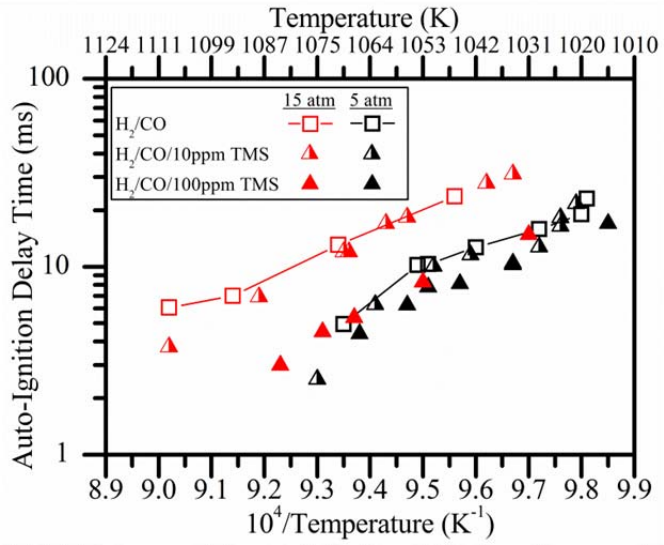

Figure 4. Measured auto-ignition delay time of the second step of ignition as a function of inverse temperature for P = 5 and 15 atm for pure syngas and syngas with TMS mixtures. The solid lines are provided for visual reference to the pure syngas data.

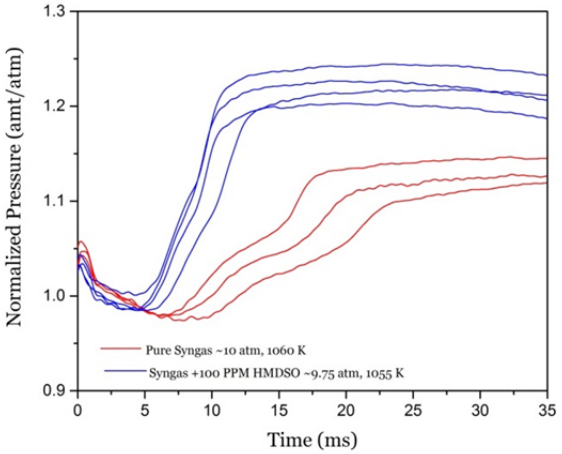

Figure 5. Pressure time histories of pure syngas (blue lines) and syngas with 100 ppm of HMDSO (red lines).

Results - UM RCF Autoignition Studies of OH Time Histories

For the OH studies, for each experiment the fractional absorption (I/I_0) time history was calculated by dividing the output laser signal by the input then smoothing the result using a 50-point smoothing algorithm to reduce noise. A typical result can be seen in **Figure 6** for the measured OH time history. A clear peak in fractional absorption is apparent and an alternate auto-ignition delay time ($\tau_{ign,\ OH}$) was defined as the time from the end of compression the maximum OH mole fraction (χ_{OH}).

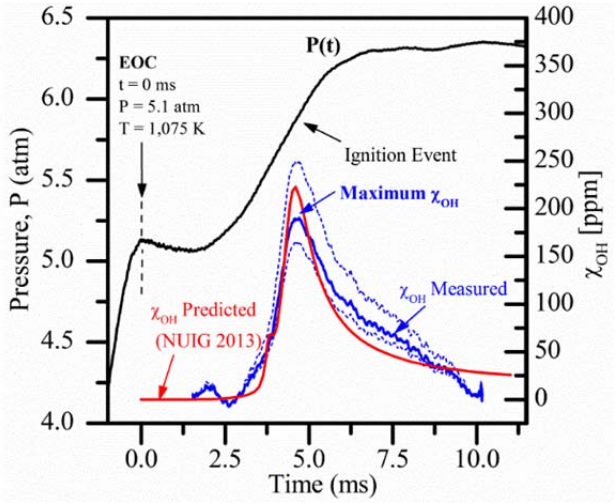

Figure 6. Typical pressure time history, P(t), and OH mole fraction based on the measured fractional absorption (I/I_0) for experimental conditions P = 5.1 atm, T = 1075 K. $\tau_{ign,OH}$ is the auto-ignition delay time corresponding to peak fractional absorption and therefore peak χ_{OH}.

Figure 7 shows the measured and predicted values for peak χ_{OH} as a function of inverse temperature. As evidenced, the measurement results range between ~~100 and 225 ppm. There is excellent agreement between measurements and predictions for T < ~ 1050 K using both the Li et al. [7] and NUIG Kéromnès et al. [14] mechanisms, with nearly identical nominal values and largely overlapping uncertainty bounds; whereas, for T > ~ 1050 K the measurements agree within the uncertainty bounds for predictions using the Kéromnès et al. [14] mechanism only. Predictions for the Li et al. [7] mechanism are above the upper uncertainty bounds of the measurements at these higher temperatures. Overall these results are an excellent indication that the laser spectroscopy system yielded valuable results and the Kéromnès et al. [14] mechanism applied to a homogeneous reactor physical model can accurately predict peak values of χ_{OH} during the auto-ignition process at the conditions studied.

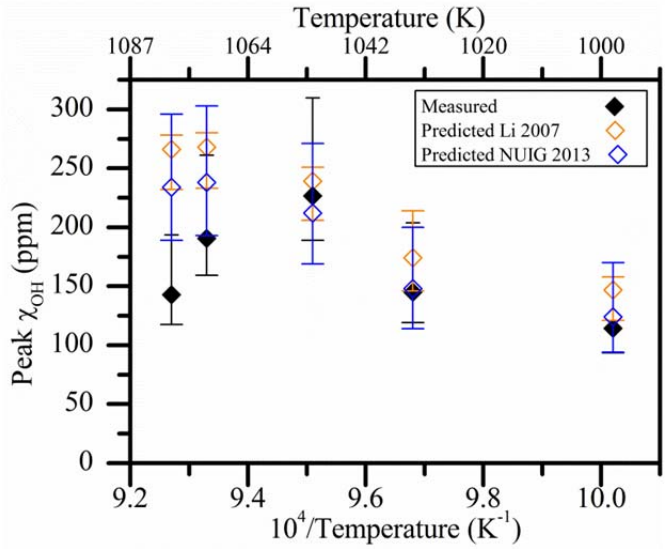

Figure 7. Measured and predicted maximum values of χ_{OH} as a function of inverse temperature; where uncertainty in the measurements and predictions are presented as the error bars.

This aspect of the project represented a unique and important investigation of the OH concentration throughout the auto-ignition process of syngas fuel at practical combustor conditions, providing the first data of its kind for this fuel at any conditions. Studies such as this are vital to the effective development and application of syngas and other high-hydrogen content fuels, considering that the accuracy of chemical kinetic mechanisms directly corresponds to the accuracy of any reacting system models to which it is applied. Furthermore, the results of this work are an important validation of the new laser absorption apparatus applied to the UM-RCF.

Results – Combustion Theory

The experimental results of the ignition regime studies motivated the development of a more universal method of characterizing the limits of the ignition regimes in terms of the scalar properties of the combustion systems. Moreover, we wanted to include the effects of turbulence on the ignition regime criterion. The theoretical scaling analysis to extend the regime criterion in terms of non-dimensional parameters that are commonly used in characterizing turbulent combustion systems is presented in Im et al. [15]. The relevant physical quantities are defined in addition to the simplifying assumptions in that work, as well as the derivations of relevant scaling relations that lead to the ignition regime criterion with turbulent combustion parameters. The outcome is the predicted regime diagram presented in **Figure 8**.

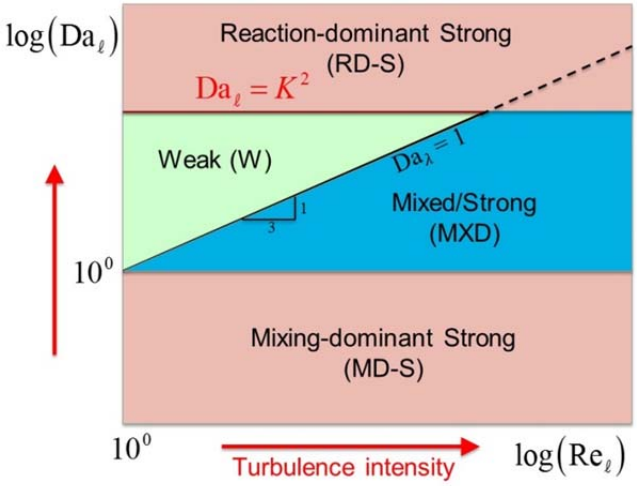

Figure 8. Regime diagram for strong and weak ignition for nearly homogeneous reactant mixture with temperature fluctuations.

As seen in **Figure 8**, the primary factor to determine the ignition regime is Damköhler number, while the Reynolds number modifies the conditions further. For a given Re_ℓ, the Zeldovich-Sankaran criterion indicates the weak/mixed ignition regime is possible for $1 < \mathrm{Da}_\ell < K^2$, where K is a the normalized thermal ignition sensitivity. If $\mathrm{Da}_\ell > K^2$, then the reactant mixture is either too reactive (small τ_{ig}) or the mixture ignition characteristics are not sensitive to the temperature fluctuations (small $d\tau_{ig}/dT$), such that the entire mixture ignites

almost at the same time despite some level of temperature fluctuations. This is referred to as the *reaction-dominant* strong ignition regime. On the other hand, if $\mathrm{Da}_\ell < 1$, then the turbulent mixing is rapid (small τ_ℓ) such that the temperature fluctuations are dissipated before the local ignition takes place. In contrast to the $\mathrm{Da}_\ell > K^2$ case, this is referred to as the *mixing-dominant* strong ignition regime. Note that the K parameter includes the ignition delay sensitivity, which is more than just a time scale characterization, and depends strongly on the ignition chemistry of the specific fuel. Between the limits $1 < \mathrm{Da}_\ell < K^2$, weak ignition is possible; however, the mixing Damköhler number, Da_λ, provides an additional criterion for this region of the regime diagram.

The regime diagram was validated with the UM RCF syngas ignition data and with 1-D and 2-D DNS simulations. The results of the work provided a more unified and comprehensive understanding of the physical and chemical mechanisms controlling ignition characteristics compared to the existing experimental maps in previous studies (e.g. [1]), which were solely based on the ignition delay sensitivity

Results –DNS Autoignition Studies

The 1-D DNS studies are summarized in Pal et al. [16]. The 2-D DNS are highlighted here and additional detail on the 2-D DNS results are presented in Pal et al. [8]. Details of the physical parameters for the different cases and the expected ignition regimes are listed in **Table 1/Figure 9**. Snapshots of the predicted temperature fields for Case A at three times during the simulation are provided in **Figure 10**.

P_0 = 20 atm, φ = 0.5, H_2: CO = 0.7:1 (molar)

Case	T_0(K)	τ_{ig} (ms)	K^2	ℓ_e (mm)	u' (m/s)	τ_t (ms)	Da_ℓ	Re_ℓ	Da_λ	Ignition Regime
A	990	25.8	4.05	4.3	0.05	86.0	3.34	35.3	1.02	W
B	1100	2.07	2.51	4.3	0.05	86.0	41.6	29.4	13.5	RD-S
C	990	25.8	4.05	4.3	1.5	2.87	0.11	1057	0.01	MD-S
D	1100	2.07	2.51	1.4	0.325	4.31	2.08	62.2	0.6	MXD
E	1020	12.7	3.28	4.0	0.3	13.33	1.05	185	0.2	MXD
F	1100	2.07	2.51	6.0	0.2	30.0	14.5	164	2.65	RD-S
G	990	25.8						97	0.2	MXD
H	970	41.8						0.0	0.8	MXD

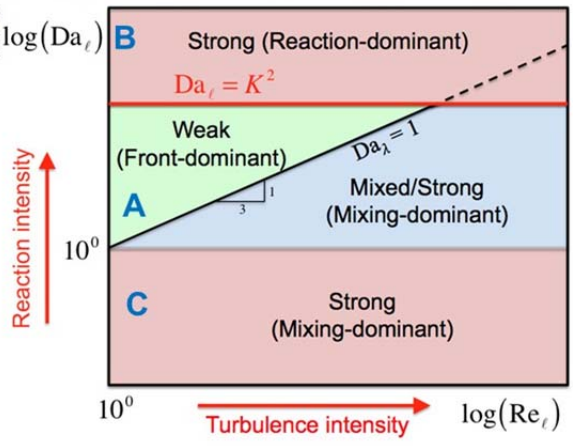

Figure 9/ Table 1. Physical and regime diagram parameters for the 2-D DNS syngas cases studied.

As seen in **Figure 10**, a reaction front emanates from the hot spot at the centre of the domain and consumes the majority of the reactant mixture. The characteristics of this simulation are of a flame consuming the majority of the fuel/air mixture, which is consistent with a system in the weak ignition regime. In comparison, **Figure 11** shows the simulation results for Case C, which had the same initial conditions as Case A. The stronger turbulence levels of Case C lead to rapid scalar dissipation of the temperature fluctuations. Due to strong turbulent mixing, T' decreases from the initial value of 15 K to a minimum value of 6 K in Case C, before any ignition fronts develop. Consequently, the reactant mixture auto-ignites almost homogeneously throughout the domain as seen in **Figure 11**, consistent with the expected characteristics for the strong/mixing dominated ignition regime. In both Cases A and C, the autoignition delay time was faster relative to the homogeneous condition at the same initial average temperature.

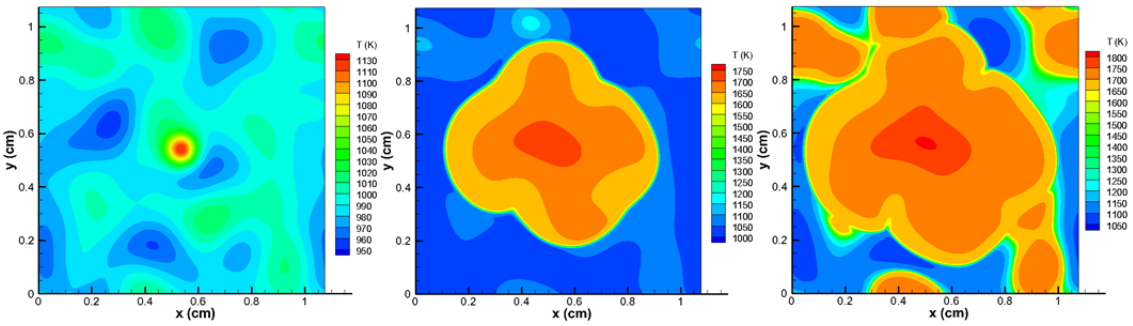

Figure 10. Predicted temperature fields for Case A at (a) $t/\tau_{ig} = 0.0$, the initial condition for the simulation; (b) $t/\tau_{ig} = 0.41$ and (c) $t/\tau_{ig} = 0.48$.

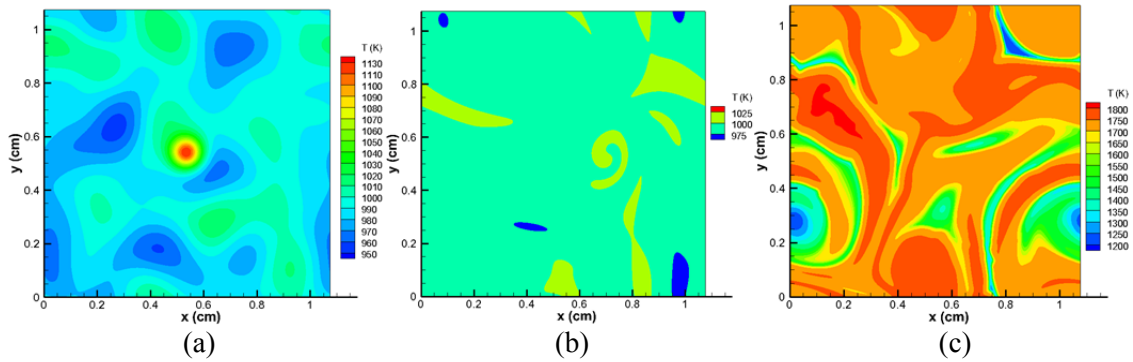

Figure 11. Predicted temperature fields for Case C at (a) $t/\tau_{ig} = 0.0$, the initial condition for the simulation; (b) $t/\tau_{ig} = 0.33$ and (c) $t/\tau_{ig} = 0.94$.

For all the simulation cases, the observed ignition behaviors consistently agreed with the

predictions of the regime diagram. Providing further confidence in the ignition regime theory developed as part of this research program.

Conclusions

The development and implementation of syngas fuel is of great interest, as it can enable a gradual transition from fossil to renewable fuel sources while simultaneously reducing the emissions associated with both. While it is a seemingly simple mixture composed primarily of H_2 and CO, there are still fundamental issues preventing successful application of syngas fuels to commercially viable combustion systems. These issues arise largely within the context of increasing NO_x emission standards, which are driving the development of combustors toward lean pre-mixed, low-temperature, and high-pressure conditions often outside the scope of historical syngas and H_2 combustion research. While understanding of syngas fuels has indeed expanded in recent decades to include these conditions in some respects, research has focused largely on the combustion of pure mixtures of H_2 and CO in highly homogeneous environments. This is far from reality for actual syngas mixtures burned in practical gas turbine or reciprocating engine systems. Indeed recent research and experiences by those in industry have revealed that the effects of both chemical and physical disturbances in syngas fueled combustors can be dramatic and are not well-understood. These effects are manifested quite visibly as uncontrolled auto-ignition in homogeneous environments like those in shock tubes and rapid compression machines. Furthermore, drastic changes in reactivity have been observed for syngas fuels with the addition of sometimes very small quantities of various chemical impurities.

The results of this research project include important quantitative studies of syngas fuel combustion, aimed specifically at comprehensively understanding the effects of specific chemical and physical disturbances. The findings here will help facilitate a more predictable and controllable application of syngas and other fuels to practical devices. The studies were completed using the UM RCF, a unique, well characterized, quiescent, constant volume equipped with state of the art diagnostics and the highest fidelity computational methods. The use of the UM RCF eliminates turbulence and other flow field and fuel/air mixing effects and thus allowed for a focus on the underlying chemical kinetics and ignition regime criteria. The use of DNS allowed the expansion of the learning and outcomes from the RCF studies to turbulent systems and a larger range of state conditions.

The study included many key aspects and outcomes. First, the auto-ignition behavior of syngas fuel at practical combustor conditions was investigated. These behaviors were mapped over a wide range of thermodynamic and mixture conditions for numerous experimental facilities, revealing consistent and well grouped behaviors strongly related to the initial thermodynamic and mixture state. This unique mapping, intrinsically valuable to combustor designers and other investigators, was then used to investigate predictive models and the fundamental source of inhomogeneous behaviors in these experimental systems. It was discovered the Sankaran Criterion, a previously proposed relationship between dominant chemical kinetics, transport properties, and thermal characteristics of the system, could predict the occurrence (albeit not the magnitude) of inhomogeneous auto-ignition behavior with remarkable accuracy. The success of the Sankaran Criterion is a strong indication that minor thermal disturbances distributed throughout the test volume can be the underlying source of

inhomogeneous auto-ignition behavior in syngas mixtures. This predictive capability and newfound fundamental description of inhomogeneous behaviors exhibited by syngas mixtures is an important contribution to both the scientific and industrial communities, which until now have either ignored categorizing the behavior or avoided low-temperature high-pressure conditions entirely. This work represents the first attempt to integrate results from diverse experimental platforms to describe common auto-ignition behaviors in high-hydrogen content fuels, and further to provide a quantitative basis for predicting and interpreting data of other ignition studies, beyond syngas and the conditions studied here. To this end, auto-ignition behaviors were also investigated and mapped for iso-octane fuel (not described in detail here but available in Mansfield et al. [4]), an important primary reference fuel for gasoline. The results indicated the Sankaran Criterion was again successful in predicting the conditions at which inhomogeneous auto-ignition will occur – providing an important tool potentially useful to the successful implementation of modern boosted direct injection combustion strategies in automotive engines.

Regarding the impact of inhomogeneous auto-ignition for both syngas and iso-octane fuels, the effect of these behaviors on the accuracy of basic auto-ignition delay time predictions was also investigated. For both fuels these behaviors indeed impacted the accuracy of predictions at certain mixture conditions, leading to global auto-ignition up to several orders of magnitude faster than predictions. This is an important indication that while inhomogeneous behaviors are localized in nature, they can impact global phenomena significantly and their consideration is therefore critical. This is especially true at low-temperature conditions where inhomogeneous ignition behaviors are far more prominent.

After exploring ignition behaviors, the effects of impurities on the combustion of syngas were then investigated. The studies included effects of CH_4, a common component of syngas, and trimethylsilanol (TMS) and hexamethyldisiloxane (HMDSO), impurities commonly found in landfill-based syngas. Interestingly, through the course of this study multi-stage auto-ignition behaviors were observed; where the pressure rise associated with ignition had two distinct regions of rapid heat release. This behavior has not been reported prior to the present work and was found to depend strongly on pressure and the relative concentration of CO in the mixture. The impact of CH_4 impurity was to inhibit ignition, evidenced by auto-ignition delay time increases by up to a factor of 3. This effect is likely through OH scavenging early in the ignition process. On the other hand the impact of the TMS and HMDSO impurities was to promote ignition, causing drastic reductions in auto-ignition delay time of up to 70%. This is likely related to enhanced consumption and/or reduced production of HO_2, though the precise chemical kinetic effects cannot be resolved with existing kinetic mechanisms.

The drastic effects of TMS and HMDSO have significant safety implications, as pronounced early auto-ignition can lead to catastrophic failures. Furthermore, the upward trend in organic Si content in syngas mixtures and the current movement toward higher pressure combustion systems means consideration of these effects is of increasing importance. The impact of TMS and HMDSO addition observed here is remarkably similar to that for SiH_4 in

pure H_2 made in previous investigations. This suggests a possible trend for Si-based species to promote auto-ignition in syngas and hydrogen mixtures. Overall, this work represents a unique investigation on the effects of common yet understudied impurities on the combustion of syngas fuel at practical combustor conditions, providing not only the first direct observations of these sometimes drastic effects, but also highlighting trends in behavior that may extend beyond the specific compounds evaluated in the present work.

The combustion theory expanded and developed for turbulent ignition regimes was validated using multiple methods including experimental and computational data. The regime diagram provides a tool that can be directly used by turbine designers to verify operating conditions for expected behavior. Specifically, the Zeldovich-Sankaran criterion predicts weak/strong ignition behavior in terms of global combustion parameters. The ignition sensitivity parameter *K* is more than just a characteristic time scale and the use of K to define the ignition regime created the additional fidelity required to describe the ignition/combustion phenomena, where a conventional Da-Re characterization was not sufficient. Furthermore, it was determined that high-*K* mixtures are more susceptible to weak ignition, which happens at low temperatures for hydrogen/syngas mixtures.

Lastly, the overwhelming evidence of the results of the experimental, computational, and combustion theory produced from this research demonstrate the observed ignition advancement for syngas at low temperatures is attributable to weak ignition behavior.

Acknowledgements

The University of Michigan acknowledge the generous financial support of U.S. DOE University Turbine System Research program via NETL award number DE-FE0007465.

References

1. Mansfield, Wooldridge, (2014) "High-pressure low-temperature ignition behavior of syngas mixtures," Combustion and Flame, 161, pp. 2242-2251.
2. Donovan, He, Zigler, Palmer, Wooldridge, and Atreya, (2004) "Demonstration of a free-piston rapid compression facility for the study of high temperature combustion phenomena," Combust. Flame, 137, pp. 351–365.
3. He, Zigler, Walton, Wooldridge, and Atreya, (2006) "A rapid compression facility study of OH time histories during iso-octane ignition," Combust. Flame, 145, pp. 552–570.
4. Mansfield, Wooldridge, Di, He, (2015) "Low-Temperature ignition behavior of iso-octane mixtures," Fuel, 139, pp. 79-86.
5. Mansfield, Ph.D. Dissertation Thesis (2014) *Experimental Study of Synthesis Gas Combustion Chemistry and Ignition Behaviors* University of Michigan.
6. Chen, Choudhary, de Supinski, DeVries, Hawkes, Klasky, Liao, Ma, Mellor-Crummey, Podhorszki, Sankaran, Shende, Yoo, (2009) "Terascale direct numerical simulations of turbulent combustion using S3D", Comput. Sci. Disc., 2, p. 015001.
7. Li, Zhao, Kazakov, Chaos, Dryer, Scire, (2007) "A comprehensive kinetic mechanism for CO, CH_2O and CH_3OH combustion," Int. J. Chem. Kinet., 39, pp. 109–136.
8. Pal, Valorani, Arias, Im, Wooldridge, Ciottoli, Galassi, (2016) "Computational characterization of ignition regimes in a syngas/air mixture with temperature fluctuations," Proc. Combust. Inst., 36, pp. 1-12.
9. Sankaran, Im, Hawkes, and Chen, (2005) "The effects of non-uniform temperature distribution on the ignition of a lean homogeneous hydrogen–air mixture," Proc. Combust. Inst., 30, pp. 875–882.
10. Kalitan, Mertens, Crofton, and Petersen, (2007) "Ignition and oxidation of lean CO/H_2 fuel blends in air," J. Propuls. Power, 23, pp. 1291–1303.
11. Blumenthal, Fieweger, and Komp, (1995) "Self-ignition of H_2-air mixtures at high pressure and low temperature," Proc. Combust. Inst., 20.
12. Chaos and Dryer, (2008) "Syngas combustion kinetics and applications," Combust. Sci. Technol., 180, pp. 1053–1096.
13. Mansfield, Wooldridge, (2015) "The effect of impurities on syngas combustion," Combust. Flame, 162, pp. 2286-2295.
14. Kéromnès, Metcalfe, Heufer, Donohoe, Das, Sung, Herzler, Naumann, Griebel, Mathieu, Krejci, Petersen, Pitz, and Curran, (2013) "An experimental and detailed chemical kinetic modeling study of hydrogen and syngas mixture oxidation at elevated pressures," Combust. Flame, 160, pp. 995–1011.
15. Im, Pal, Wooldridge, Mansfield, (2015) "A regime diagram for autoignition of homogeneous reactant mixtures with turbulent velocity and temperature fluctuations," Combust. Sci. Tech., 187, pp. 1263-1275.
16. Pal, Mansfield, Wooldridge, Im, (2015) "A computational study of syngas auto-ignition characteristics at high-pressure and low-temperature conditions with thermal inhomogeneities," Combust. Theory Model., 19, pp. 587-601.

Appendices

The appendices contain the journal reprints of the following papers there were produced as a result of this project.

Official reprint of Mansfield, A. B., Wooldridge, M. S., (2014) "High-pressure low-temperature ignition behavior of syngas mixtures," Combustion and Flame, 161, pp. 2242-2251, http://dx.doi.org/10.1016/j.combustflame.2014.03.001.

Official reprint of Mansfield, A. B., Wooldridge, M. S., Di, H., He, X., (2015) "Low-Temperature Ignition Behavior of Iso-Octane Mixtures," Fuel, 139, pp. 79-86.

Official reprint of Mansfield, A. B., Wooldridge, M. S., (2015) "The Effect of Impurities on Syngas Combustion," Combustion and Flame, 162, pp. 2286-2295.

Official reprint of Im, H. G., Pal, P., Wooldridge, M. S., Mansfield, A. B. (2015) "A Regime Diagram for Autoignition of Homogeneous Reactant Mixtures with Turbulent Velocity and Temperature Fluctuations," Combustion Science and Technology, 187, pp. 1263-1275.

Official reprint of Pal, P., Mansfield, A. B., Wooldridge, M. S., Im, H. G., (2015) "A Computational Study of Syngas Auto-Ignition Characteristics at High-Pressure and Low-Temperature Conditions with Thermal Inhomogeneities," Combustion Theory and Modeling, 19, pp. 587-601.

Official reprint of Pal, P., Valorani, M., Arias, P. G., Im, H. G., Wooldridge, M. S., Ciottoli, P. P., Galassi, R. M., (2016) "Computational characterization of ignition regimes in a syngas/air mixture with temperature fluctuations," *Proceedings of the Combustion Institute*, **36**, pp. 1-12.

Combustion and Flame 161 (2014) 2242–2251

Contents lists available at ScienceDirect

Combustion and Flame

journal homepage: www.elsevier.com/locate/combustflame

High-pressure low-temperature ignition behavior of syngas mixtures

Andrew B. Mansfield [a,*], Margaret S. Wooldridge [a,b]

[a] Department of Mechanical Engineering, University of Michigan, Ann Arbor, MI 48109, USA
[b] Department of Aerospace Engineering, University of Michigan, Ann Arbor, MI 48109, USA

ARTICLE INFO

Article history:
Received 11 September 2013
Received in revised form 28 December 2013
Accepted 1 March 2014
Available online 26 March 2014

Keywords:
Syngas
Hydrogen
Strong and weak ignition
Rapid compression facility

ABSTRACT

Ignition properties of simulated syngas mixtures were systematically investigated at high-pressure low-temperature conditions relevant to gas turbine combustor operation using the University of Michigan Rapid Compression Facility. Pressure time history measurements and high-speed imaging of the ignition process in this facility were used to determine auto-ignition delay times and observe and characterize ignition behaviors. The simulated syngas mixtures were composed of H_2 and CO with a molar ratio of 0.7, for equivalence ratios (φ) of 0.1 and 0.5, near air dilution (i.e. molar O_2 to inert gas ratio of 1:3.76), with N_2 as the primary diluent gas. The pressures and temperatures after compression ranged from 3–15 atm and 870–1150 K respectively. The comprehensive results of the present work combined with those from previous shocktube studies in the literature clearly illustrate the existence of both homogeneous and inhomogeneous auto-ignition behaviors at these conditions. Analysis of patterns in the ignition behaviors revealed a dependence on temperature, pressure, and equivalence ratio with distinct thermodynamic regions in which the ignition behavior is consistent and repeatable. Predicted locations of the strong ignition limit made using a criterion which compares laminar flame speed to a thermal gradient driven front propagation speed have excellent agreement with the experimental findings for each φ and an assumed gradient of 5 K/mm. Experimental validation of this unique and powerful criterion means that it can be used for *a priori* prediction of the strong ignition limit using basic computational simulations. The validity of this criterion is fundamentally important, quantitatively describing the roles of chemical kinetics, thermo-physical properties, and device dependent thermal characteristics in determining auto-ignition behavior. Additionally, a comparison of the measured auto-ignition delay times to predictions made using zero-dimensional homogeneous reactor modeling revealed that agreement was dependent on φ, with excellent agreement for $\varphi = 0.1$ and large discrepancies for $\varphi = 0.5$. These results indicate that while inhomogeneous ignition phenomena are not entirely avoidable by reducing equivalence ratio, the subsequent effects on the accuracy of typical auto-ignition delay time predictions may be reduced or eliminated.

© 2014 The Combustion Institute. Published by Elsevier Inc. All rights reserved.

1. Introduction

Synthesized gas, or syngas, is a mixture composed primarily of hydrogen and carbon monoxide, which can be produced via gasification of coal and combusted directly in a gas turbine as part of an Integrated Gasification Combined Cycle (IGCC) power plant. Compared to a pulverized coal system, an IGCC plant can achieve reductions in emissions of SO_x, NO_x, particulate matter, and heavy metals without a significant decrease in overall plant efficiency [1]. Currently the gas turbine portion of the IGCC system is in development, with a focus on the abatement of increased NO_x production resulting from the increased flame temperatures of this high-hydrogen-content fuel [2]. A modern method of temperature control is to utilize a lean pre-mixed combustion strategy, otherwise known as "Dry Low-NO_x", with a fuel-to-air equivalence ratio (φ) nearing 0.5 [3]. Given that the behavior of a pre-mixed combustion system is highly dependent on the chemical kinetics of fuel oxidation, it is imperative that both these kinetics and the chemically driven ignition behaviors (auto-ignition) be well understood at gas turbine post-compressor conditions ($P \sim 10$–30 atm, $T < 1000$ K) [4] for air–dilute mixtures over a range of equivalence ratios [5]. Adding to the complexity of such a combustion system is the high variability in syngas fuel composition, where, for example, relative molar fractions of H_2 to CO can range from ~0.4 to 1 for coal-derived syngas [6].

* Corresponding author. Address: 2350 Hayward St., Room 2293 G.G. Brown Building, Ann Arbor, MI 48109, USA.
E-mail addresses: amansfld@umich.edu (A.B. Mansfield), mswool@umich.edu (M.S. Wooldridge).

http://dx.doi.org/10.1016/j.combustflame.2014.03.001
0010-2180/© 2014 The Combustion Institute. Published by Elsevier Inc. All rights reserved.

While the kinetics of syngas and pure hydrogen oxidation have been well studied and modeled, see Chaos and Dryer [4] and the references contained therein, there have been only a few experimental investigations of auto-ignition behavior conducted at a small range of conditions (Voevodsky and Soloukhin [7] – undiluted H_2, Meyer and Oppenheim [8] – air–dilute H_2 $\varphi = 1.0$, Blumenthal et al. [9] – air–dilute H_2 $\varphi = 0.4$, Kalitan et al. [10] – air–dilute syngas $\varphi = 0.4$ and molar H_2:CO = 0.05–4.0, and Walton et al. [11] – air–dilute syngas $\varphi = 0.1$–0.4 and molar H_2:CO = 0.25–4.0). In these studies, optical techniques were employed during ignition measurements in a variety of experimental facilities, which revealed diverse auto-ignition behaviors at thermodynamic conditions relevant to gas turbine operation. The observed behaviors consisted of both homogeneous (spatially uniform emission or detonation wave) and inhomogeneous (localized reaction sites and deflagration) phenomena.

Voevodsky and Soloukhin [7] and Meyer and Oppenheim [8] observed a clear transition between inhomogeneous and homogeneous auto-ignition behavior at varying initial thermodynamic conditions, i.e. the *strong ignition limit*. These studies indicate ignition behaviors are generally repeatable and strongly related to the unburned condition. Voevodsky and Soloukhin [7] further illustrated that the strong ignition limit corresponds to the second explosion limit of hydrogen at low pressures, demonstrating the importance of dominant chemical kinetic pathways in determining ignition behavior. Meyer and Oppenheim [8] expanded on the work by Voevodsky and Soloukhin [7] at low pressures, discovering that a specific value of the temperature derivative of the auto-ignition delay time (which they defined as the *thermal sensitivity* of the system) was well correlated with the strong ignition limit – thus connecting auto-ignition behavior to the dominant chemical kinetic pathway and thermal non-uniformities in the unburned gas. This was an important indication that transitions in auto-ignition behavior can be understood and potentially predicted using thermal sensitivity.

The relationship between thermal non-uniformities and auto-ignition behavior was investigated computationally by Sankaran et al. [12] using high fidelity direct numerical simulations of air–dilute pure H_2 at $\varphi = 0.1$. These simulations revealed that indeed various auto-ignition behaviors could be caused by distributed thermal non-uniformities. A non-dimensional criterion was proposed which compared thermal gradient driven propagation speed and laminar flame speed to indicate the transition between inhomogeneous and homogeneous ignition behaviors. Since a propagation speed determined by a thermal gradient is directly related to thermal sensitivity, this criterion again highlights the importance of the value of the thermal sensitivity. While providing a potentially powerful tool in the prediction of auto-ignition behavior, this criterion had not been experimentally validated prior to the results of the current work.

The understanding and prediction of the occurrence of various auto-ignition behaviors are important, as is the relationship between auto-ignition behaviors and the accuracy of basic homogeneous ignition modeling. As highlighted in Chaos and Dryer [4], it is apparent that auto-ignition delay time measurements for experiments with inhomogeneous ignition behavior are up to several orders of magnitude less than typical model predictions; whereas measurements for experiments with homogeneous ignition behavior are generally in excellent agreement with these predictions. This highlights a potentially catastrophic tendency of syngas fuels to ignite at unexpected locations or times if inhomogeneous ignition behavior occurs. With this in mind, there is currently a lack of understanding as to whether the effects inhomogeneous ignition necessarily lead to inaccuracy in basic auto-ignition delay modeling.

The objectives of the current study were to comprehensively advance the understanding and prediction of the auto-ignition behaviors of air–dilute syngas for a broad range of conditions, and to evaluate the relationship of such behaviors to the predictive accuracy of basic auto-ignition delay time modeling. The objectives were accomplished in part through an experimental investigation of syngas auto-ignition behavior and ignition delay times at lean conditions, using the University of Michigan Rapid Compression Facility (UM-RCF). The results were then combined with those from the shocktube studies of Blumenthal et al. [9] and Kalitan et al. [10] to comprehensively map auto-ignition behavior as a function of initial thermodynamic state and equivalence ratio. On these maps, the strong ignition limit was identified and compared to the second explosion limits of hydrogen and values of thermal sensitivity. The locations of the experimentally determined strong ignition limits were also compared to predictions made using the criterion of Sankaran et al. [12], the first application of this tool to experimental data. Lastly, the auto-ignition delay time measurements were compared to predictions made using typical zero-dimensional homogeneous reactor ignition modeling and the formaldehyde oxidation mechanism of Li et al. [13] (Li 2007 mechanism).

2. Methods

2.1. Experimental

Ignition experiments were conducted for realistic but simple syngas mixtures for two values of equivalence ratio ($\varphi = 0.1$ and 0.5), designed to represent lean syngas mixtures used in the power industry [14]. Both mixtures contained only H_2 and CO as fuel, with a molar ratio of H_2:CO = 0.7, and were approximately air–dilute with N_2, i.e. molar O_2 to inert gas ratio of 1:3.76. In some cases small amounts of the N_2 diluent gas were replaced by Ar and/or CO_2 to modify the test temperature. Ignition experiments were conducted at approximately 3, 5, 10, and 15 atm for the broadest range of temperatures allowable in the UM-RCF for these mixtures (~950–1150 K, based on experimental test times). The composition of the gas mixture and the thermodynamic state corresponding to each auto-ignition delay time measurement are given in the Supplemental material section.

Regarding the experimental apparatus, the UM-RCF is uniquely designed to create uniform thermodynamic conditions through an isentropic compression process [15]. A detailed description of the UM-RCF and results of studies characterizing its performance can be found in Donovan et al. [15] and He et al. [16]. Briefly, the apparatus consists of a long cylinder, the Driven Section, in which a gas mixture is rapidly compressed by the motion of a free piston (Sabot). Prior to compression, the test volume is evacuated with a pump and then filled with a specific test gas mixture. Upon firing, the Sabot travels the length of the Driven Section compressing the test gas mixture into the Test Section – a small cylindrical volume located at the end of the Driven Section (~50 mm length and 50 mm diameter). As the Sabot reaches its final position near the Test Section, the Sabot achieves an annular interference fit, thereby sealing the test gas mixture in the Test Section. At this point, the Test Section is filled with a uniform and isentropically compressed test gas mixture at the desired initial thermodynamic condition. This is achieved in large part because cool boundary layer gases from the Driven Section are trapped in an external volume formed by the geometry of the Sabot [15,17].

For this study, the Test Section was instrumented with a piezoelectric transducer (6125B Kistler, Amherst, NY) and charge amplifier (5010 Kistler, Amherst, NY) for pressure measurements, and a transparent polycarbonate end-wall to permit high-speed imaging

of the ignition process. During each experiment the pressure time history was recorded using the pressure transducer at 100 kHz sampling frequency. The uncertainty in the pressure measurements is estimated as ⩽1% (∼0.1 atm) considering both the signal-to-noise ratio in the post-ignition pressure time history data and the non-linearity limits defined by Kistler during the calibration process. High-speed color imaging was recorded using a digital video camera (V711-8G-MAG-C, Vision Research, Phantom) with a Navitar 50 mm lens (F0.95), a Hoya 62 mm lens (+2 zoom), and a Hoya 62 mm UV(0) filter. Video sequences were recorded at 25,000 frames/s with a CMOS array resolution of 512 × 512 pixels, resulting in an exposure time of 39.3 μs.

All test gas mixtures were made using a dedicated stainless steel tank and the mixture composition was determined by measurement of the relative partial pressures of the components. After filling, the tank was left to rest for at least one hour before the test gas was used for an experiment, during which time the mixture homogenized by diffusion. Error in the mixture composition is assumed to be negligible and have negligible effect on the ignition results, considering ∼80–95% of the mixture is comprised of N_2 and O_2.

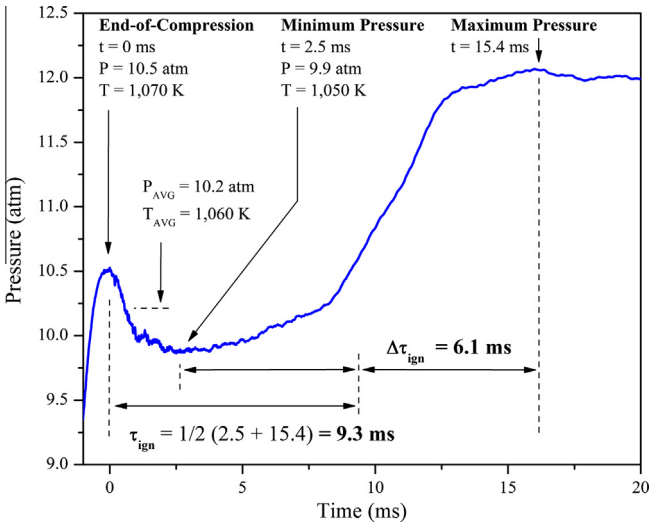

Fig. 1. Typical experimental pressure time history at experimental conditions of $P = 10.2$ atm, $T = 1060$ K, $\varphi = 0.1$; where, τ_{ign} is the auto-ignition delay time and $\Delta\tau_{ign}$ is the symmetric uncertainty of the auto-ignition delay time.

2.2. Computational

Auto-ignition delay time predictions were made using the constant volume adiabatic zero-dimensional homogeneous reactor model in the CHEMKIN software suite [18] with the Li 2007 chemical kinetic mechanism. This mechanism was used only, given its previous success in predicting syngas ignition behavior [4,13] and the minor differences in predictions seen between other H_2 and CO reaction mechanisms in other studies [19]. Using this ignition model, a corresponding auto-ignition delay time prediction was calculated for each ignition experiment conducted in the UM-RCF, using the exact initial thermodynamic condition and mixture composition. For each prediction, quantified uncertainty bounds of the model predictions were calculated using the known uncertainty in the "A-factor" of the Arrhenius reaction rates for the two most sensitive reactions, $H + O_2 = H + OH$ (R1) & $H + O_2 (+M) = HO_2 (+M)$ (R9), selected using OH sensitivity analysis in the CHEMKIN software suite. The rate coefficients used for this reaction are listed in the Supplemental material section. Iso-contours of constant predicted auto-ignition delay time and thermal sensitivity were also calculated using this model for a broad range of initial thermodynamic conditions and nominal reaction rates, though a constant pressure boundary condition was applied when calculating thermal sensitivity.

3. Results and discussion

For each experiment in the UM-RCF, a pressure time history and a high-speed imaging video were recorded, allowing for the determination of an auto-ignition delay time and direct observation and classification of the auto-ignition behavior. A typical pressure time history during an ignition experiment for the present work can be seen in Fig. 1. Trends in the pressure data illustrate a pressure increase during the compression stroke until the Sabot is seated at the end-of-compression event, followed by a slight decrease in pressure due to heat transfer from the test gas volume into the cool Test Section walls, followed by a large and rapid increase in pressure during the ignition event. For each experiment, the time and pressure value was noted at three distinct events: end-of-compression (EOC), minimum pressure (P_{min}), and maximum pressure (P_{max}), denoted in Fig. 1. After filtering the pressure time history with a 75-point smoothing algorithm to reduce signal noise, the pressure and time value for each event was defined mathematically as a local maximum or minimum respectively. The nominal ignition event was defined as occurring at the average time of P_{min} and P_{max} with symmetric uncertainty bounds assigned to span the time from P_{min} to P_{max}. The nominal auto-ignition delay time was defined as the time from EOC to the ignition event, with symmetric uncertainty bounds defined by the uncertainty bounds of the ignition event time. Overall, this definition is quite general and biases the auto-ignition delay times slightly to faster times compared to conventional definitions based on the maximum rate of pressure rise. However, this approach ensures the analysis can be applied to all experiments regardless of ignition behavior, which was critical given the wide range of conditions considered in this work yielding variable pressure time history characteristics. Additionally, the uncertainty limits assigned in this study ensure that the conventional definition of auto-ignition delay time based on the maximum rate of pressure rise is captured within the bounds of the reported measurements.

While the pressure within the Test Section was directly measured throughout each experiment, it was necessary to calculate the bulk temperature using thermodynamic relations. Experimentally verified by Donovan et al. [15], the initial compression stroke in the UM-RCF is well represented as isentropic compression. Furthermore, assuming that the gas volume contained in the Test Section is composed of an "adiabatic core" and a "boundary layer region", as defined in Lee and Hochgreb [20], the pressure decrease after the EOC event can be modeled as isentropic expansion. With these well supported assumptions in place, the initial uncompressed thermodynamic conditions were used in conjunction with isentropic state relations to calculate the temperature at both EOC and P_{min}. Propagation of the pressure measurement uncertainty of ⩽1% through the isentropic state relations yields an uncertainty of ⩽0.4% in the assigned temperature (∼5 K). This is in very good agreement with expected thermal variations in the UM-RCF, experimentally determined by Donovan et al. [15] to be less than ∼10 K by direct thermocouple measurement.

For each experiment a thermodynamic state was assigned, representing the isobaric/isothermal condition at which the experimental was conducted. In most cases, there was no appreciable decrease in temperature between the EOC event and the ignition event (i.e. <10 K change from P_{EOC} to P_{min}), and so the EOC thermodynamic state was assigned to the experimental result. However, for the cases with appreciable decreases in temperature (i.e.

>10 K) in that time period, an average thermodynamic state was assigned. The average pressure was defined mathematically as the arithmetic mean of the pressures at the EOC and P_{min}. The average temperature was calculated thereafter assuming an isentropic expansion from the thermodynamic state at the EOC event to the average pressure. Assignment of an average state captures heat transfer effects on the experiment while retaining critical clarity in both reporting and interpreting the experimental results, thus greatly improving the archival value of the results as compared to using the EOC conditions. Similar methods of assigning an average or "effective state" to experiments exhibiting some non-adiabatic behavior have been successfully applied in numerous past experiments using the UM-RCF [11,15]. Moreover, the use of average conditions allows straightforward interpretation of the data using isobaric and isothermal reporting techniques such as the *P*–*T* diagrams and Arrhenius diagrams presented later in this work.

Other methods to represent the effects of heat transfer on similar rapid compression experiments exist, such as those which integrate a non-reactive pressure time history or a derived "volume trace" into the modeling process as done in Gersen et al. [21], Mittal et al. [22], and Würmel et al. [23]. Different modeling methods were considered in the current work and results are compared in the Supplemental material section. While incorporation of a volume trace is indeed a more time-dependent treatment of heat transfer effects, the merit of implementing such detail is small and may be significantly outweighed by the often overlooked drawbacks. Foremost, if this empirical method is used without appropriate documentation, the archival value of the data is significantly reduced. Without any record of the heat loss profiles, appropriate comparisons cannot be made between experimental facilities or model predictions, and any quantitative understanding of the effects of heat transfer in the experiments is lost. A standard for reporting rapid compression machine heat losses using these empirical corrections has yet to be established or a criterion for when it is appropriate to take such steps to represent heat losses (clearly not all experiments need such attempts, only systems and conditions with high heat transfer rates). As noted above, a criterion of a maximum temperature change of 10 K was applied in this study. Further, comparison of the volume trace and the effective state methods revealed no significant difference between auto-ignition delay time predictions (<15%), which was particularly irrelevant when the uncertainty in the chemical kinetic mechanism was appropriately considered. Thus, the assignment of an effective state allows for both improved archival clarity and equivalent accuracy as compared to the volume trace method.

Typical high-speed imaging results of chemilluminescence during syngas auto-ignition in the UM-RCF are shown in Figs. 2a and 2b, illustrating both homogeneous and inhomogeneous auto-ignition phenomena respectively. As seen in the figure, homogeneous ignition is indicated by spatially uniform chemilluminescence emission; whereas, inhomogeneous ignition is indicated by local emission features forming flame-like structures which propagate and merge. In some experiments, inhomogeneous phenomena were followed by homogeneous ignition of the unburned gas volume. Based on the observed chemilluminescence behavior, each experiment was classified as exhibiting one of three ignition behaviors, strong, weak, or mixed, described in detail in Table 1. In general, the imaging closely resembled previous high-speed imaging results for syngas ignition seen in Walton et al. [11]. In several low-pressure experiments no chemilluminescence was observed, likely due to low energy content and/or low-densities, and the ignition behavior was classified as strong by default.

In order to compare ignition behaviors from the UM-RCF to those observed in Blumenthal et al. [9] and Kalitan et al. [10], it was necessary to re-classify the behavior in these other studies according to the three categories in Table 1. In Blumenthal et al. experiments were originally classified as "Strong", "DDT" (Deflagration to Detonation Transition), or "no DDT" which were defined as strong, mixed, and weak ignition in the present work respectively. In Kalitan et al. experiments were classified as exhibiting "early OH emission" or not, which were defined as mixed and strong ignition in the present work respectively.

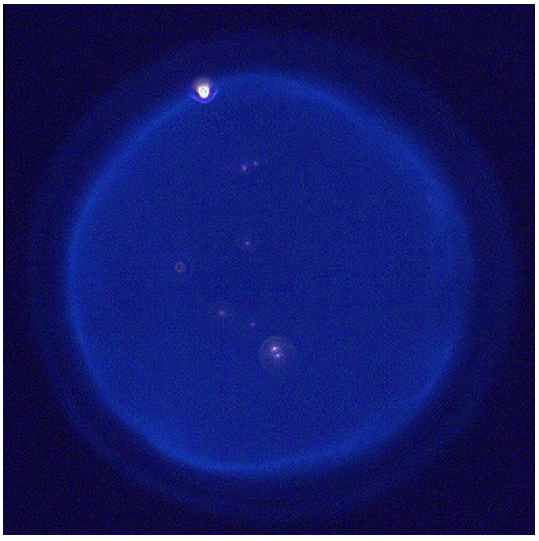

Fig. 2a. Single frame from high-speed imaging of homogeneous ignition behavior, illustrating uniform chemilluminescence for experimental conditions $P = 3.3$ atm, $T = 1043$ K, $\varphi = 0.1$.

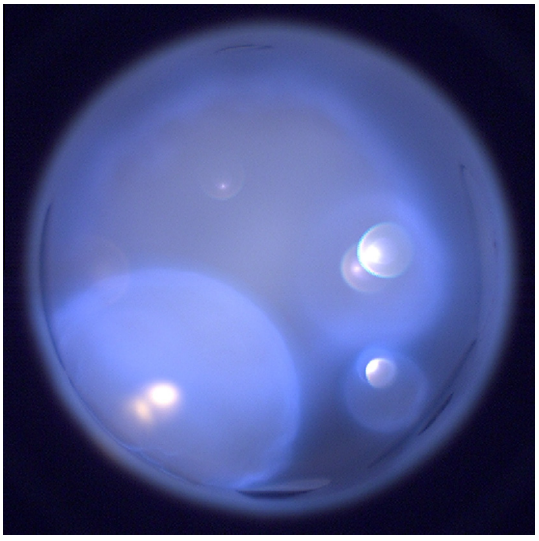

Fig. 2b. Single frame from high-speed imaging of inhomogeneous ignition behavior, illustrating non-uniform chemilluminescence with various localized flame-like structures, for experimental conditions $P = 9.2$ atm, $T = 1019$ K, $\varphi = 0.5$.

3.1. Auto-ignition behavior

Figure 3 presents the observed ignition behavior as a function of thermodynamic state for mixtures with $\varphi = 0.1$. A range of behaviors is evidenced, with strong ignition generally at temperatures above ~1000 K transitioning to mixed and/or no ignition as the temperature decreases. The data show the ignition behavior is strongly related to initial thermodynamic state and is repeatable, with generally clear boundaries between different regions. The boundary between mixed and strong ignition behaviors at lower

Table 1
Classification of ignition behavior based on high-speed imaging results.

Ignition classification	Imaging characteristics	Auto-ignition phenomena
Strong	Spatially uniform only	Homogeneous
Weak	Flame-like structures only	Inhomogeneous
Mixed	Flame-like structures then spatially uniform in unburned gas volume	Inhomogeneous, then homogeneous in unburned gas volume

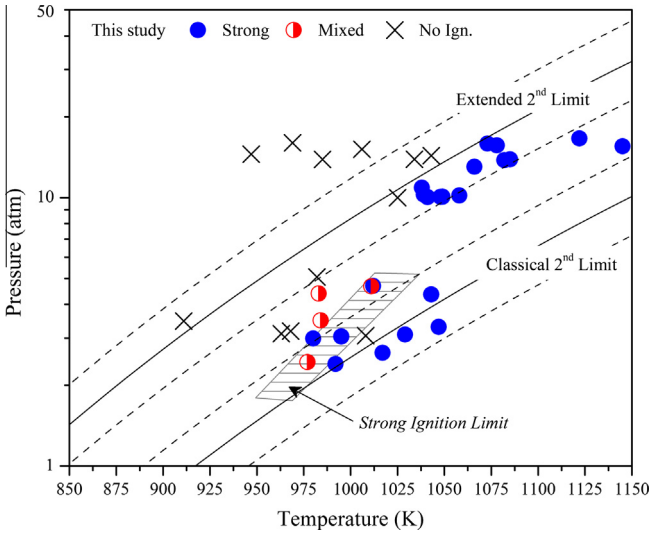

Fig. 3. Ignition behavior as a function of thermodynamic state for mixtures with $\varphi = 0.1$. The strong ignition limit is shown as a hashed area. H_2/O_2 explosion limits are shown as solid lines with upper and lower bounds shown as dashed lines, representing uncertainty in the rate coefficient of reactions R1 and R9.

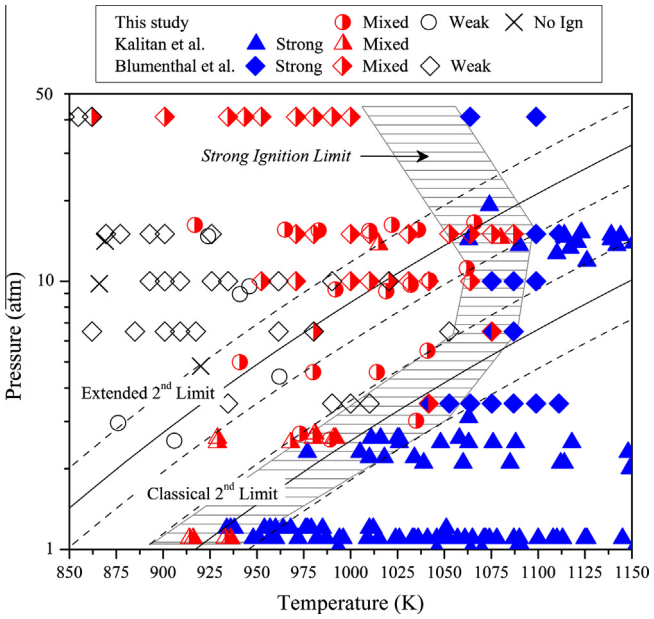

Fig. 4. Ignition behavior as a function of thermodynamic state for mixtures with $\varphi = 0.5$. Results are from the present work, Kalitan et al. [10], and Blumenthal et al. [9]. The strong ignition limit is shown as a hashed area. H_2/O_2 explosion limits are shown as solid lines with upper and lower bounds shown as dashed lines, representing uncertainty in the rate coefficient of reactions R1 and R9.

pressures (2–5 atm) is the strong ignition limit and is marked as a hashed area. A strong ignition limit is not evident at higher pressures (10–15 atm) though, where no mixed ignition is observed at any temperature.

Figure 4 presents the observed ignition behavior as a function of thermodynamic state for mixtures with $\varphi = 0.5$, including results from Blumenthal et al. [9] and Kalitan et al. [10]. Again, a range of behaviors was observed, with strong ignition generally at the highest temperatures transitioning to mixed, then weak, then no ignition as the temperature decreases. There is excellent agreement between the results in the present work and those from Blumenthal et al. [9] and Kalitan et al. [10]. This finding suggests that the ignition behavior of syngas is not highly sensitive to the molar ratio of H_2:CO at these conditions and that the behavior trends are not strongly device dependent. Overall the data show the ignition behavior is strongly related to initial thermodynamic state and is repeatable, with generally clear boundaries between different regions. The boundary between mixed and strong ignition is the strong ignition limit, which exhibits a clear dependence on pressure and is marked as a hashed area. The onset of mixed ignition at higher pressures as the equivalence ratio is increased from 0.1 to 0.5 is an indication that the energy content of the mixture is related to the auto-ignition behavior, in agreement with previous findings that connected inhomogeneous ignition phenomena and "high energy density mixtures" [4]. This relation is not evident at lower pressures, however, where the strong ignition limit seems largely unaffected by changes in the equivalence ratio.

With the strong ignition limit experimentally determined for $\varphi = 0.1$ and 0.5, it was possible to develop a more complete understanding of the transition in auto-ignition behavior. This was accomplished through a comparison of the strong ignition limit in each case to: (1) the second explosion limits of hydrogen, as suggested by Voevodsky and Soloukhin [7], (2) values of thermal sensitivity, as suggested by Meyer and Oppenheim [8], and (3) predicted locations of the strong ignition limit, as proposed by Sankaran et al. [12].

3.1.1. H_2/O_2 second explosion limits

The explosion limits are thermodynamic states which mark a transition between regions of dominant H_2/O_2 chemistry. While Voevodsky and Soloukhin [7] considered only the classical second explosion limit in their analysis, in the present work the extended second explosion limit was also included. A detailed description of these two limits is given in Zheng and Law [24]. Briefly, the classical second limit represents the competition between the dominant chain-branching pathway ($H + O_2 = OH + O$ (R1)), and the dominant chain-terminating pathway (R9). The limit is the thermodynamic state at which the reaction rates of these two reactions are equal and no net radicals (O, OH) are produced. The extended second limit represents a similar balance between radical generation and termination, though it includes HO_2 chemical pathways significant only at pressures greater than ~1 atm, i.e. the second limit represents the competition between the chain-branching reactions ((R1), $HO_2 + H = OH + OH$ (R11)), the chain-propagating reaction ($H + O_2 = HO_2$ (R9)), and the chain-terminating reaction ($HO_2 + H = H_2 + O_2$ (R10)). The extended second limit is the thermodynamic state at which no net radicals (H, O, OH, HO_2) are produced. Note that this formulation for the extended second limit is simplified, as done in Zheng and Law [24], assuming that HO_2 is consumed only by H. The thermodynamic states corresponding to the classical and extended second limits were calculated using formulations from Zheng and Law [24] where,

$$\text{Classical second limit}: \quad [\mathrm{M}] = \frac{2k_1}{k_9} \ [\mathrm{mole/m^3}] \tag{1}$$

$$\text{Extended second limit}: \quad [\mathrm{M}] = \frac{2k_1}{k_9} * \frac{k_{10}}{k_{10} + k_{11}} \tag{2}$$

$$[\mathrm{M}] = \frac{P}{\overline{R}T} \tag{3}$$

$\overline{R}$ = universal gas constant, P = pressure, T = temperature.

The thermodynamic location of the second explosion limits were calculated using the nominal reaction rate values of the Li 2007 mechanism. Uncertainty bounds were assigned using the known uncertainty of the reaction rates of R1 and R9, consistent with the computational work described previously.

The calculated classical and extended second explosion limits are included in the maps of ignition behavior in Fig. 3 and 4. As illustrated in Fig. 3 for $\varphi = 0.1$, the classical explosion limit correlates with the strong ignition limit at low pressures (2–5 atm) and the extended explosion limit correlates well with the transition from strong to no ignition at high pressures (10–15 atm). As illustrated in Fig. 4 for $\varphi = 0.5$, the classical explosion limit correlates well with the strong ignition limit at low pressures (1–5 atm); however, at higher pressures the strong ignition limit is not well described by either the classical or extended explosion limit with progressively worse deviation as pressure increases beyond 5 atm. It is therefore apparent that the classical H_2/O_2 second explosion limit is a good predictor of the location of the strong ignition limit for pressures less than ~5 atm for a range of equivalence ratios; however, the accuracy of such prediction falls off rapidly as pressure increases beyond this value even if the extended second limit is considered. This finding at lower pressures is in excellent agreement with Voevodsky and Soloukhin [7], and suggests that at low pressures the dominant H_2/O_2 chemical pathway is highly correlated to the auto-ignition behavior, whereas at higher pressures other factors must be considered. As discussed in Chaos et al. [25] and the references contained therein, competing chemical kinetic and transport time-scales near the extended second explosion limit at higher pressures are expected and it is likely that consideration of transport phenomena is indeed necessary at higher pressures.

3.1.2. Thermal sensitivity

As previously discussed, Meyer and Oppenheim [8] built on the work by Voevodsky and Soloukhin [7] and devised a method to more deliberately consider the relationship between gas-dynamic effects and the strong ignition limit, based on the assumption that numerous thermal non-uniformities exist within the reacting volume. It was postulated that these non-uniformities will lead to localized reaction centers (inhomogeneous behavior) in regions with higher thermal sensitivity and longer auto-ignition delay times, where chemical kinetic and transport time-scales are similar. It was indeed demonstrated in their study for an air–dilute pure H_2 mixture at $\varphi = 1.0$ that a limiting value of the thermal sensitivity of approximately -2 μs/K exists which corresponds well to the strong ignition limit at pressures below 3 atm; where regions with higher thermal sensitivity exhibit inhomogeneous auto-ignition and regions with lower thermal sensitivity exhibit homogeneous auto-ignition.

In a similar fashion, thermal sensitivity values were calculated in the present work and iso-contours of these values were compared to the experimentally determined strong ignition limit for each equivalence ratio. Figures 5 and 6 present the ignition behavior for $\varphi = 0.1$ and $\varphi = 0.5$, respectively, as a function of initial thermodynamic state with iso-contours of predicted auto-ignition delay time and thermal sensitivity included for comparison. For

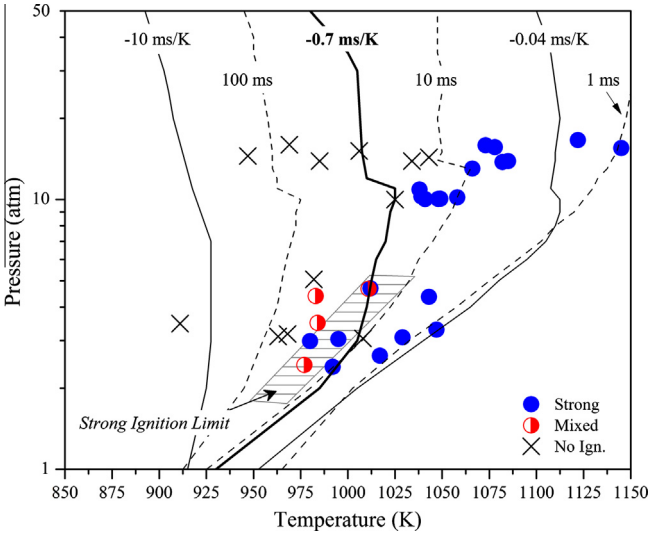

Fig. 5. Ignition behavior as a function of thermodynamic state for mixtures with $\varphi = 0.1$. The strong ignition limit is shown as a hashed area. Calculated iso-contours of thermal sensitivity are shown as solid lines and calculated iso-contours of auto-ignition delay time are shown as dotted lines. The iso-contour of critical thermal sensitivity, −0.7 ms/K, is the bold solid line.

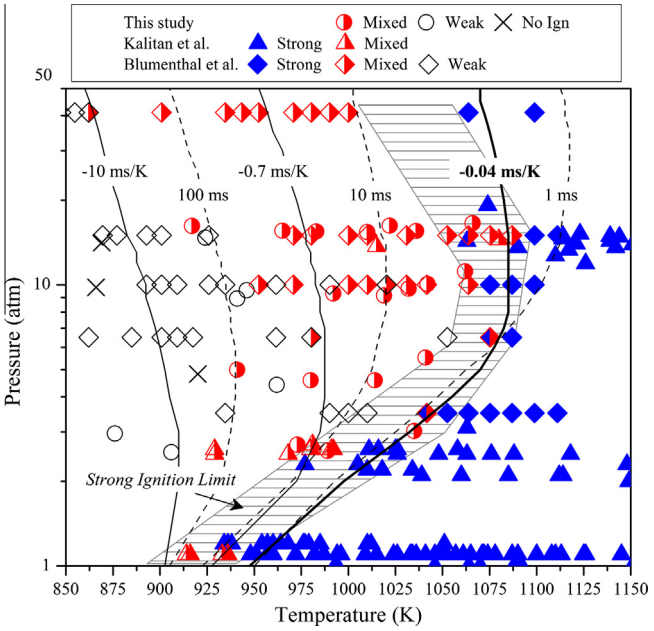

Fig. 6. Ignition behavior as a function of thermodynamic state for mixtures with $\varphi = 0.5$. The strong ignition limit is shown as a hashed area. Results are from the present work, Kalitan et al. [10], and Blumenthal et al. [9]. Calculated iso-contours of thermal sensitivity are shown as solid lines and calculated iso-contours of auto-ignition delay time are shown as dotted lines. The iso-contour of critical thermal sensitivity, −0.04 ms/K, is the bold solid line.

$\varphi = 0.1$ there is a close correlation between the iso-contour of thermal sensitivity ≈−0.7 ms/K and the strong ignition limit. Correspondingly for $\varphi = 0.5$ there is a close correlation between the iso-contour of thermal sensitivity ≈−0.04 ms/K and the strong ignition limit. These two values are therefore considered the critical values of thermal sensitivity for each equivalence ratio and their existence supports the notion of a critical thermal sensitivity previously made by Meyer and Oppenheim [8]. Similar to findings by Meyer and Oppenheim [8], regions with thermal sensitivity in excess of the critical iso-contours exhibited mixed or weak

behavior; whereas, regions with lower sensitivity exhibited only strong behavior. Important to note is the excellent agreement between the critical iso-contour of thermal sensitivity and the strong ignition limit at high pressures for $\varphi = 0.5$, a marked improvement over the predictions using the H_2/O_2 second explosion limits. These findings are strong evidence that the value of thermal sensitivity is indeed an important factor in determining auto-ignition behavior across many mixture and thermodynamic conditions relevant to gas turbine operation. It follows that the assumptions originally made by Meyer and Oppenheim [8] are supported in the present work as well, that thermal non-uniformities and subsequent localized reaction centers are a dominant cause of inhomogeneous ignition behavior.

From the perspective of predicting auto-ignition behavior, using thermal sensitivity is a step forward from using the explosion limits in that high pressure behaviors can be captured. However, in order to determine the critical value of thermal sensitivity of a given mixture it is still necessary to find the strong ignition limit experimentally for at least a few pressure values. These experiments may be avoided for mixtures and conditions sufficiently similar to those studied in the present work. For example, critical values can be estimated for different equivalence ratios by interpolating between the results of the current work ($\varphi = 0.1$ and 0.5) and in Meyer and Oppenheim ($\varphi = 1.0$). Furthermore, it is not clear how these thermal sensitivity limits extend to less ideal combustion devices, which can contain higher magnitudes of thermal non-uniformities and turbulence. Overall, while *a priori* prediction of the strong ignition limit is not possible using thermal sensitivity, establishing the connection between thermal sensitivity and the strong ignition limit at a minimum reduces the number of experiments necessary to define the strong ignition limit for a system.

3.1.3. Sankaran criterion

As previously mentioned, the effect of distributed thermal non-uniformities on auto-ignition behavior in pure H_2 mixtures was investigated in detail by Sankaran et al. [12] using high fidelity direct numerical simulation methods. In that work auto-ignition behavior was investigated for air–dilute H_2 at $\varphi = 0.1$ in a small constant pressure reactor (4.1 mm × 4.1 mm), with a distribution of thermal gradients and a constant turbulence flow field. Two distinct ignition behaviors emanating from thermal hot spots were subsequently observed: *spontaneous propagation* – where a reaction front propagates at a speed (u_p) equal to the inverse of the gradient of the auto-ignition delay time $(d\tau/dx)^{-1}$, and *deflagration* – where a reaction front propagates at the laminar flame speed (s_u^0). Sankaran et al. [12] postulated that a non-dimensional transition parameter, β, exists which indicates the relative dominance of the two ignition behaviors,

$$\beta = \frac{s_u^0}{u_p} = \frac{s_u^0}{\left(\frac{d\tau}{dx}\right)^{-1}} \tag{4}$$

where if $\beta < 1$ a homogeneous explosion (strong ignition) will occur, and if $\beta > 1$ then an inhomogeneous deflagration front (mixed or weak ignition) will occur. If the gradient of the auto-ignition delay time is decomposed into a product of the thermal gradient (dT/dx) and thermal sensitivity ($d\tau/dT$), as was done by Walton et al. [17], then the importance of thermal sensitivity is illustrated in the following criterion (which we define as the Sankaran Criterion),

$$\frac{d\tau}{dT} < \left(\frac{dT}{dx} s_u^0\right)^{-1} \tag{5}$$

where strong ignition will occur if the inequality is true, and mixed or weak ignition will occur if the inequality is false.

In the current work, the Sankaran Criterion was used predict the thermodynamic location of the strong ignition limit by evaluating the inequality across the range of initial temperature and pressure values for each equivalence ratio and a range of initial thermal gradients (3, 5, 10, 20 K/mm). Typical thermal gradients in similar experimental devices are expected to be on the order of 5 K/mm based on findings from Walton et al. [17] and Strozzi et al. [26]. Additional thermal gradient values were included to illustrate the sensitivity of the predicted limits to this parameter and expand the predictions to higher thermal gradients which may be more representative of practical combustion devices. Laminar flame speeds were calculated using the "Premixed Laminar Flame-Speed Calculation" module in the CHEMKIN software suite [18] with the Li 2007 kinetic model [11]. At temperatures above ~1025 K it was necessary to extrapolate laminar flame speeds from lower temperatures, which was done using an exponential fit with correlation coefficients above 0.997. For simplicity, the nominal A-factors and transport parameters provided in the Li 2007 mechanism were used for the calculations. Thermal sensitivity values determined for the iso-contours presented earlier were used for this analysis as well. All calculations were completed with the same syngas mixture used in the experimental work (air–dilute with molar ratio H_2:CO = 0.7).

Figures 7 and 8 present the ignition behavior for $\varphi = 0.1$ and $\varphi = 0.5$, respectively, as a function of initial thermodynamic state with iso-contours of predicted auto-ignition delay time and predicted strong ignition limits for various thermal gradient magnitudes. For $\varphi = 0.1$ there is excellent correlation between the experimental and the predicted strong ignition limit for 5 K/mm. Quite remarkably, the predicted limit moves to drastically lower temperatures as pressure is increased beyond 3 atm, correctly predicting the absence of a strong ignition limit at higher pressures mentioned earlier. This shift to lower temperatures corresponds to a significant decrease in laminar flame speeds as pressure increases beyond 3 atm and is not captured by the critical thermal sensitivity iso-contour. For $\varphi = 0.5$, there is also remarkable correlation between the experimental and the predicted strong ignition limit for 5 K/mm for the entire pressure range considered. The prediction is somewhat less representative of the experimental data closer to 1 atm, predicting a strong ignition limit ~50 K higher than what was measured, but that is most likely within the uncertainty

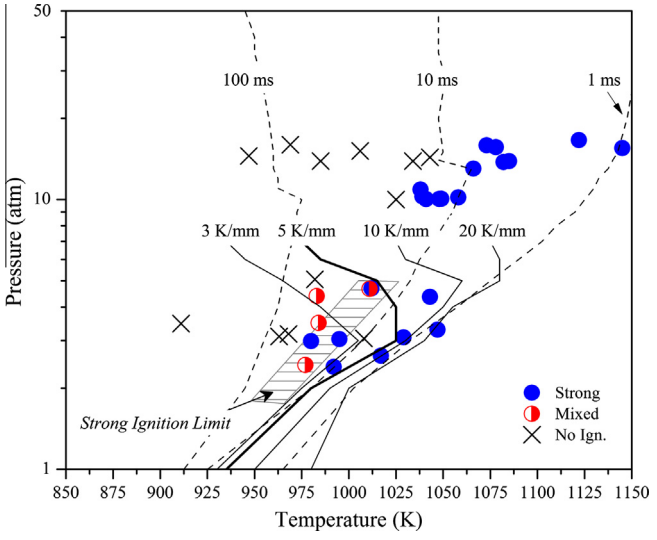

Fig. 7. Ignition behavior as a function of thermodynamic state for mixtures with $\varphi = 0.1$. The strong ignition limit is shown as a hashed area. Predicted locations of the strong ignition limit are shown as solid lines and calculated iso-contours of auto-ignition delay time are shown as dotted lines. The most accurate predicted strong ignition limit, for a 5 K/mm gradient, is the bold solid line.

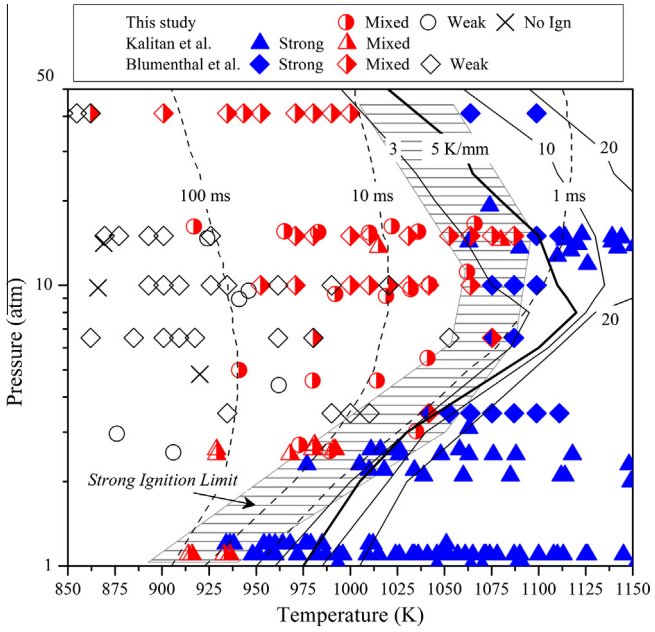

Fig. 8. Ignition behavior as a function of thermodynamic state for mixtures with $\varphi = 0.5$. The strong ignition limit is shown as a hashed area. Predicted locations of the strong ignition limit are shown as solid lines and calculated iso-contours of auto-ignition delay time are shown as dotted lines. The most accurate predicted strong ignition limit, for a 5 K/mm gradient, is the bold solid line.

of the prediction. As opposed to the results for $\varphi = 0.1$, there is general agreement between the predicted strong limit and the critical thermal sensitivity iso-contour for all pressures, which is the result of a gradual decrease in laminar flame speeds as pressure is increased for $\varphi = 0.5$.

Concerning the results for various thermal gradients, there is minimal difference between strong ignition limit predictions at pressures below ~3 atm for $\varphi = 0.1$ and ~7 atm for $\varphi = 0.5$. In both cases, at higher pressures the predicted strong ignition limit shifts to higher temperatures as the thermal gradient is increased. The shift to higher temperatures occurs with decreasing magnitude as the thermal gradient magnitude is increased, suggesting that the strong ignition limit may asymptote as thermal gradients increase to much higher values. It is noteworthy that the thermal gradient of 5 K/mm yielded the most accurate predictions, in excellent agreement with the expected gradient magnitudes in the experimental UM RCF and shock tube equipment.

Overall, these results indicate that the Sankaran Criterion is indeed an excellent tool for *a priori* prediction of the strong ignition limit, with no experimentation necessary for its application. It is accurate and easy to use, requiring only basic computational modeling and the magnitude of characteristic thermal gradients in the system. Beyond the predictive capability, it also provides a straightforward method for extending experimental results to other mixtures, conditions, and devices; a key attribute for combustor designers. The validation of this simple non-dimensional criterion is important, as this criterion quantitatively describes the roles of chemical kinetics, thermo-physical properties, and device dependent thermal characteristics on auto-ignition behavior. In this way, it is not an alternative to the explosion limit and thermal sensitivity methods investigated previously by Voevodsky and Soloukhin [7] and Meyer and Oppenheim [8], but instead is an important integration of these methods with transport phenomena. This criterion not only provides a practical tool for combustor designers and experimentalists, it also sheds light on the fundamental nature of thermally driven auto-ignition behaviors in premixed combustion systems.

Considering the success of this criterion, it is apparent that localized thermal gradients are the dominant driver of inhomogeneous ignition behavior in this work and the studies by Blumenthal et al. [8] and Kalitan et al. [9]. Non-uniformities will be present in any experimental or practical combustion system and could come from a number of sources such as heat transfer, mixing, or the presence of minute reactive or non-reactive particles like those observed in Elsworth et al. [27] and considered in Chaos and Dryer [4]. Previously, Chaos and Dryer [4] and Blumenthal et al. [9] predicted that hot spots of 150–200 K would be necessary to cause inhomogeneous auto-ignition. The present work highlights the importance of considering not only the absolute temperature of hot spots but also the corresponding thermal gradients, as those on the order of merely 3–5 K/mm were found to drive inhomogeneous ignition behaviors in the current work.

Varying levels of turbulence will likely impact the accuracy of the Sankaran Criterion, through an influence on the development of thermal gradients (highlighted in the study by Sankaran et al. [12]), chemical kinetics (highlighted in the study by Ihme [28]), and flame speeds (highlighted in the study by Daniele et al. [29]). While both the UM-RCF and the shocktubes considered in this study are assumed to be nominally quiescent, significantly higher levels of turbulence are expected in practical devices. An investigation of turbulence effects is outside the scope of the present work; however, current computational efforts are underway to expand the work of Sankaran et al. [12] and Bansal and Im [30] to more directly probe the issues of turbulence-chemistry interactions.

3.2. Auto-ignition delay time

As previously discussed, while there are well documented inaccuracies of zero-dimensional homogeneous reactor modeling in predicting auto-ignition delay time in systems with inhomogeneous ignition behavior [4], there is currently a lack of understanding as to whether the occurrence of inhomogeneous ignition necessarily leads to this inaccuracy. Illustrated in Fig. 9 are the measured and predicted auto-ignition delay times as a function of inverse temperature for mixtures with $\varphi = 0.1$ over a range of pressures. Recall that the error bars on the experimental data represent the limits of the definition of the auto-ignition delay time and the error bars on the simulation results represent the effects of the uncertainty limits of R1 and R9. The results indicate excellent agreement between the measured and predicted values, across all thermodynamic conditions investigated and for both ignition behaviors exhibited (strong and mixed). It is therefore apparent that the presence of inhomogeneous ignition phenomena does not significantly affect the predictive accuracy of the zero-dimensional homogeneous reactor model using the Li 2007 mechanism at these conditions. This is likely related to the low energy content of the mixture, limiting the quantity of energy released during local ignition events and/or reducing flame speeds. The results support this notion, given that while high-speed imaging indicates the presence of local ignition events almost immediately after EOC in most cases, inspection of the lower bound of the measured auto-ignition delay time indicates that the first signs of pressure increase occur only just before the auto-ignition event. Important to note is the rather large uncertainty in the predicted auto-ignition delay times for 3 atm, highlighting that consideration of uncertainty in the reaction mechanism is critical when comparing modeling and experimental data.

Illustrated in Fig. 10 are the measured and predicted auto-ignition delay times as a function of inverse temperature for mixtures with $\varphi = 0.5$ over a range of pressures. Unlike the earlier results, these data indicate poor agreement between the measured and predicted auto-ignition delay times, with rapidly increasing error as temperatures decrease below ~1000 K. Note also the limited

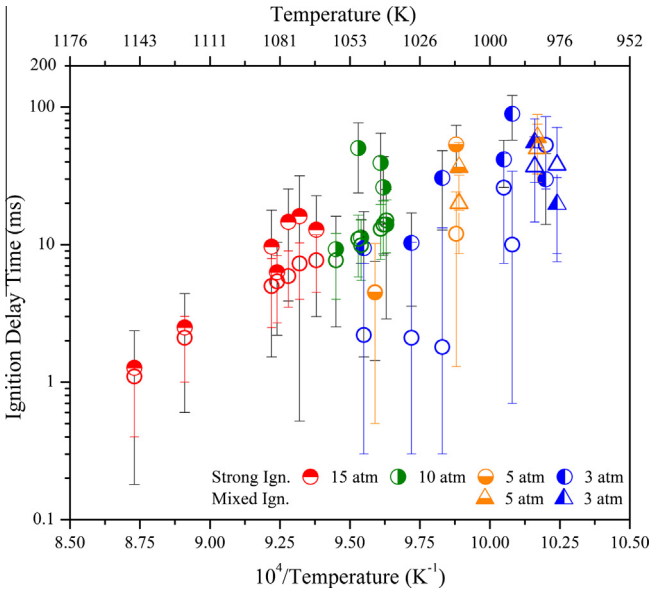

Fig. 9. Measured and predicted auto-ignition delay time as a function of inverse temperature for mixtures with $\varphi = 0.1$. Half-filled symbols are experimental measurements and open symbols are the predictions corresponding to each measurement. Uncertainty bounds of the predictions are the effect of the uncertainty in the rate coefficient of reactions R1 and R9; whereas, uncertainty bounds of the measurements are the limits of the definition of the auto-ignition delay time.

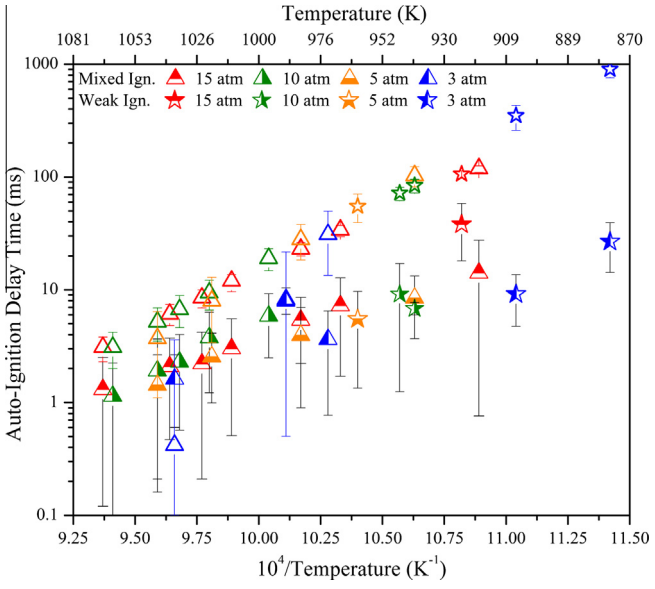

Fig. 10. Measured and predicted auto-ignition delay time as a function of inverse temperature for mixtures with $\varphi = 0.5$. Half-filled symbols are experimental measurements and open symbols are the predictions corresponding to each measurement. Uncertainty bounds of the predictions are the effect of the uncertainty in the rate coefficient of reactions R1 and R9; whereas, uncertainty bounds of the measurements are the limits of the definition of the auto-ignition delay time.

effect of the uncertainty of the reaction mechanism on the predicted values at most of the simulation conditions. The results therefore illustrate that the presence of inhomogeneous ignition phenomena does indeed significantly decrease the predictive accuracy of the zero-dimensional homogeneous reactor model using the Li 2007 mechanism at these conditions. It is assumed here that the discrepancy is not the result of poor performance of this kinetic mechanism at these conditions, given the multitude of previous successful applications [4,13] and the agreement illustrated in the present work for $\varphi = 0.1$. This predictive inaccuracy is instead likely related to the higher energy content of the mixture, leading to larger energy release during local ignition events and/or increased flame speeds. It is clear that nearly all the predicted auto-ignition delay times greatly exceed the measured values, consistent with previous findings highlighted in Chaos and Dryer [4]. These results are expected considering that energy release during inhomogeneous ignition events would cause a temperature increase of the unburned gas mixture, thus accelerating the auto-ignition process. With this in mind, the increasing error trend as temperature decreases can be explained by noting that as auto-ignition delay time increases localized energy release will exist for an increasingly longer time, thus allowing for an increasingly pronounced effect on the unburned gases. Overall the results of the present work illustrate an important finding, that the equivalence ratio or energy content of the mixture is directly related to the predictive accuracy of zero-dimensional homogeneous reactor modeling of auto-ignition delay times in systems with inhomogeneous auto-ignition behaviors.

Unique for $\varphi = 0.5$ is the existence of weak ignition behavior at the lowest temperature conditions, seen as star markers in Fig. 10. Auto-ignition delay time predictions should not be expected to have good agreement with measurements in cases with weak ignition behavior, given that no homogeneous auto-ignition event is observed. These data were still included here to illustrate a potential pitfall in interpreting pressure time history data for low-temperature auto-ignition experiments where inhomogeneous ignition is possible. Had the ignition behavior not been directly observed by imaging and classified appropriately as weak (flame propagation with no observed auto-ignition of the unburned gas), it is quite likely that these data would have been incorrectly categorized as homogeneous auto-ignition events, resulting in potentially unnecessary and inaccurate modification of physical or chemical representations of the combustion system. Diagnostics of ignition behavior are therefore vitally important in any ignition study of syngas or other high-hydrogen content fuels at temperatures below ~1000 K.

4. Conclusions

This work represents the first attempt to integrate results from diverse experimental platforms to describe common auto-ignition behaviors of high-hydrogen content fuels, and further to provide a quantitative basis for predicting and interpreting data of other ignition studies, beyond syngas and the conditions studied here. Studies such as these are vital for enabling low-temperature combustion strategies, such as Dry Low-NO_x. The comprehensive results of the present work clearly illustrate the existence of both homogeneous and inhomogeneous auto-ignition behaviors for lean air–dilute syngas and pure H_2 mixtures at thermodynamic conditions relevant to gas turbine engines and other combustion systems. Analysis of patterns in the ignition behaviors revealed a dependence on temperature, pressure, and equivalence ratio with distinct thermodynamic regions in which the ignition behavior was consistent and repeatable. The strong ignition limit was identified for each equivalence ratio, marking the transition between homogeneous and inhomogeneous ignition behaviors.

The locations of the experimentally determined strong ignition limits were compared to the second explosion limits of hydrogen, iso-contours of thermal sensitivity, and predicted strong ignition

limits using the Sankaran Criterion. These three approaches represent the historical progression of strong ignition limit prediction and analysis methods. The second explosion limits of hydrogen were found to correlate with the strong ignition limits only at pressures below 5 atm, indicating the importance of dominant chemical kinetic pathways in determining auto-ignition behavior at low pressures and the necessity to consider additional factors at higher pressures. Iso-contours of a critical thermal sensitivity described the strong ignition limit well; where any region (i.e. state and mixture conditions) with a sensitivity value in excess of the critical limit exhibited inhomogeneous ignition phenomena and any region with a lower value exhibited homogeneous ignition phenomena. The critical values were equivalence ratio dependent and were found to be approximately -0.7 ms/K for $\varphi = 0.1$ and -0.04 ms/K for $\varphi = 0.5$. It follows that thermal non-uniformities and subsequent localized reaction centers are a dominant cause of inhomogeneous ignition behavior in the present work. Predictions of the strong ignition limit by the Sankaran Criterion, which compares laminar flame speed to a thermal gradient driven front propagation speed, were found to have excellent agreement with the experimentally determined strong ignition limit for both equivalence ratios for an assumed thermal gradient of 5 K/mm. The experimental validation of this criterion, the first of its kind, indicates that it can indeed be used for *a priori* prediction of the strong ignition limit. As this criterion quantitatively describes the roles of chemical kinetics, thermo-physical properties, and device dependent thermal characteristics in determining auto-ignition behavior it also provides unique and critical insight into thermally driven auto-ignition behaviors. Overall both the Sankaran Criterion and the ignition behavior maps created in the present work provide important, new, and unique tools that can be used in the design of combustion devices using high-hydrogen content fuels like syngas.

In order to investigate the relationship between auto-ignition behavior and the accuracy of zero-dimensional homogeneous reactor modeling in predicting auto-ignition delay time, measured and predicted ignition delay times were compared. The results indicate the presence of inhomogeneous ignition phenomena does not significantly affect the predictive accuracy of the zero-dimensional homogeneous reactor model using the Li 2007 mechanism for $\varphi = 0.1$; whereas, the presence of inhomogeneous ignition phenomena does significantly affect the predictive accuracy for $\varphi = 0.5$. This is an important indication that while inhomogeneous ignition phenomena are not avoidable by reducing equivalence ratio, the subsequent effects on the accuracy of typical auto-ignition modeling may be reduced or eliminated. This inaccuracy for $\varphi = 0.5$ is likely related to the higher energy content of the mixture, leading to larger energy release during local ignition events and/or increased flame speeds which can cause a significant violation of the isothermal/isobaric assumptions of the homogeneous reactor model. The importance of properly observing and classifying ignition behaviors was also highlighted, as ignition at the lowest temperatures exhibited no homogeneous auto-ignition, only flame propagation, and the pressure time histories could be confused as consistent with homogeneous auto-ignition behavior if imaging diagnostics had not been applied.

Acknowledgments

The authors acknowledge the generous support of the U.S. Department of Energy via the National Energy Technology Laboratory, Award Number DE-FE0007465 and the Department of Mechanical Engineering at the University of Michigan.

Appendix A. Supplementary material

Supplementary data associated with this article can be found, in the online version, at http://dx.doi.org/10.1016/j.combustflame.2014.03.001.

References

[1] US DOE, Gasifipedia – Power (Integrated Gasification Combined Cycle), 2013. <http://www.netl.doe.gov/research/coal/energy-systems/gasification/gasifipedia/igcc>.
[2] US DOE, Gasifipedia – Hydrogen Turbines, 2013. <http://www.netl.doe.gov/research/coal/energy-systems/turbines/advanced-research>.
[3] G.A. Richards, M.M. McMillian, R.S. Gemmen, W.A. Rogers, S.R. Cully, Prog. Energy Combust. 27 (2001) 141–169.
[4] M. Chaos, F.L. Dryer, Combust. Sci. Technol. 180 (2008) 1053–1096.
[5] T. Lieuwen, V. McDonell, D. Santavicca, T. Sattelmayer, Combust. Sci. Technol. 180 (2008) 1169–1192.
[6] C.L. Miller, D.C. Cicero, M. Ackiewicz, Hydrogen from Coal Program: Research, Development and Demonstration Plan for the Period 2007 through 2016, The United States Department of Energy, National Energy Technology Laboratory, 2007.
[7] V.V. Voevodsky, R.I. Soloukhin, Proc. Combust. Inst. 10 (1965) 279–283.
[8] J.W. Meyer, A.K. Oppenheim, Proc. Combust. Inst. 13 (1971) 1153–1164.
[9] R. Blumenthal, K. Fieweger, K.H. Komp, Proc. Int. Symp. Shock Waves 20 (1995) 935–940.
[10] D.M. Kalitan, J.D. Mertens, M.W. Crofton, E.L. Petersen, J. Propul. Power 23 (2007) 1291–1303.
[11] S.M. Walton, X. He, B.T. Zigler, M.S. Wooldridge, Proc. Combust. Inst. 31 (2007) 3147–3154.
[12] R. Sankaran, H.G. Im, E.R. Hawkes, J.H. Chen, Proc. Combust. Inst. 30 (2005) 875–882.
[13] J. Li, Z. Zhao, A. Kazakov, M. Chaos, F.L. Dryer, J.J. Scire, Int. J. Chem. Kinet. 39 (2007) 109–136.
[14] R.M. Jones, N.Z. Shilling, IGCC Gas Turbines for Refinery Applications, GE Power Systems, Schenectady, NY, 2003.
[15] M.T. Donovan, X. He, B.T. Zigler, T.R. Palmer, M.S. Wooldridge, A. Atreya, Combust. Flame 137 (2004) 351–365.
[16] X. He, B.T. Zigler, S.M. Walton, M.S. Wooldridge, A. Atreya, Combust. Flame 145 (2006) 552–570.
[17] S.M. Walton, X. He, B.T. Zigler, M.S. Wooldridge, A. Atreya, Combust. Flame 150 (2007) 246–262.
[18] CHEMKIN 10101, Reaction Design, San Diego, 2010.
[19] E.L. Petersen, D.M. Kalitan, A.B. Barrett, S.C. Reehal, J.D. Mertens, D.J. Beerer, R.L. Hack, V.G. McDonell, Combust. Flame 149 (2007) 244–247.
[20] D. Lee, S. Hochgreb, Int. J. Chem. Kinet. 30 (1998) 385–406.
[21] S. Gersen, N.B. Anikin, A.V. Mokhov, H.B. Levinsky, Int. J. Hydrogen Energy 33 (2008) 1957–1964.
[22] G. Mittal, C.J. Sung, R.A. Yetter, Int. J. Chem. Kinet. 38 (2006) 516–529.
[23] J. Würmel, E.J. Silke, H.J. Curran, M.S. Ó Conaire, J.M. Simmie, Combust. Flame 151 (2007) 289–302.
[24] X.L. Zheng, C.K. Law, Combust. Flame 136 (2004) 168–179.
[25] M. Chaos, M.P. Burke, Y. Ju, F.L. Dryer, in: T. Lieuwen, V. Yang, R. Yetter (Eds.), Gas Synthesis Combustion: Fundamentals and Applications, CRC Press, Boca Raton, 2010, pp. 29–70.
[26] C. Strozzi, J. Sotton, A. Mura, M. Bellenoue, Meas. Sci. Technol. 20 (2009) 125403.
[27] J.E. Elsworth, W.W. Haskell, I.A. Read, Combust. Flame 13 (1969) 437–438.
[28] M. Ihme, Combust. Flame 159 (2012) 1592–1604.
[29] S. Daniele, P. Jansohn, J. Mantzaras, K. Boulouchos, Proc. Combust. Inst. 33 (2011) 2937–2944.
[30] G. Bansal, H.G. Im, Combust. Flame 158 (2011) 2105–2112.

Fuel 139 (2015) 79–86

Contents lists available at ScienceDirect

Fuel

journal homepage: www.elsevier.com/locate/fuel

Low-temperature ignition behavior of iso-octane

A.B. Mansfield [a,*], M.S. Wooldridge [a,b], H. Di [c], X. He [d]

[a] Department of Mechanical Engineering, University of Michigan, Ann Arbor, MI 48109, USA
[b] Department of Aerospace Engineering, University of Michigan, Ann Arbor, MI 48109, USA
[c] Electrical & Mechanical Engineering College, Qingdao University, Qingdao, Shangdong 266071, China
[d] Center for Combustion Energy and State Key Laboratory of Automotive Safety and Energy, Tsinghua University, Beijing 100084, China

HIGHLIGHTS

- Auto-ignition properties of air-dilute iso-octane investigated at low temperatures.
- Homogeneous and inhomogeneous behaviors observed, strong ignition limits identified.
- Sankaran Criterion accurately predicts location of strong ignition limit *a priori*.
- Measured ignition delay times compared to zero-dimensional model predictions.
- Accuracy of predictions affected by ignition behavior for $\varphi = 1.0$, but not $\varphi = 0.25$.

ARTICLE INFO

Article history:
Received 28 May 2014
Received in revised form 6 August 2014
Accepted 7 August 2014

Keywords:
Iso-octane
Low-temperature
Strong or weak ignition
Rapid Compression Facility

ABSTRACT

Auto-ignition properties of iso-octane mixtures were systematically investigated at conditions relevant to practical combustion devices using the University of Michigan Rapid Compression Facility and the Tsinghua University Rapid Compression Machine. Pressure time history measurements and high-speed imaging of the ignition process were used in both facilities to determine auto-ignition delay times and directly observe physical ignition behaviors. Test mixtures used fuel-to-O_2 equivalence ratios of $\varphi = 0.25$ and 1.0, and were air-dilute, i.e. molar O_2 to diluent gas (N_2, Ar) ratio of 1:3.76. The pressures and temperatures after compression ranged from 3 to 30 atm and 740–1125 K respectively. The comprehensive results of the present work combined with those from previous shocktube studies clearly illustrate the existence of both inhomogeneous and homogeneous auto-ignition behaviors at these conditions. Analysis of patterns in the ignition behaviors revealed a dependence on initial unburned temperature and pressure, as well as equivalence ratio, with distinct regions of thermodynamic state in which the behavior is consistent and repeatable. The strong ignition limits were identified for both φ using the experimental results and compared to predicted locations made using the Sankaran Criterion (the ratio of the laminar flame speed to the thermal gradient driven spontaneous propagation speed). Predictions made using an assumed thermal gradient of 5–10 K/mm were in excellent agreement with measurements at all conditions, clearly indicating that use of this criterion is an effective method for *a priori* prediction of auto-ignition behaviors for iso-octane. This validation of the Sankaran Criterion for iso-octane, an important reference hydrocarbon fuel, importantly broadens the use of this tool and is an indication that ignition processes in hydrocarbon and high hydrogen content fuels are fundamentally similar. Additionally, a comparison of the measured auto-ignition delay times to predictions made using zero-dimensional homogeneous reactor modeling revealed that for experiments with inhomogeneous ignition behaviors, agreement was dependent on φ and the auto-ignition delay time. The presence of inhomogeneous ignition behavior did not significantly affect the accuracy of auto-ignition delay time predictions for mixtures with $\varphi = 0.25$; whereas, for mixtures with $\varphi = 1.0$ the presence of inhomogeneous ignition behavior significantly reduced the accuracy of predictions if the auto-ignition delay time was greater than ~1 ms. These results indicate that while lowering φ may not eliminate inhomogeneous ignition behaviors, the subsequent effect of these behaviors on the predictive accuracy of typical zero-dimensional ignition modeling can be reduced or eliminated.

© 2014 Elsevier Ltd. All rights reserved.

* Corresponding author. Address: 2293 G.G. Brown Building, 2350 Hayward St., Ann Arbor, MI 48109, USA.
E-mail address: amansfld@umich.edu (A.B. Mansfield).

http://dx.doi.org/10.1016/j.fuel.2014.08.019
0016-2361/© 2014 Elsevier Ltd. All rights reserved.

1. Introduction

Low-temperature combustion strategies are used in both transportation and stationary power devices to decrease NO_x emissions and improve efficiency. Reductions in combustion temperature can be achieved using lean, pre-mixed, and/or dilute conditions, which present challenging stability, safety, and control issues. These difficulties stem in part from uncertainties in low-temperature chemistry as well as an increased instance and influence of abnormal ignition behaviors such as knock and misfiring in reciprocating engine systems or flashback and early ignition in gas turbine systems [1]. Therefore, successful application of low-temperature combustion strategies requires improved understanding of both low-temperature oxidation chemistry *and* chemically controlled ignition (auto-ignition) behaviors.

While the oxidation chemistry of iso-octane has been well studied, as indicated in Mehl et al. [2] and the references therein, only Fieweger et al. [3] and Vermeer and Oppenheim [4] have directly investigated the auto-ignition behaviors of iso-octane in a controlled and quiescent experimental apparatus. Vermeer and Oppenheim [4] employed optical techniques during auto-ignition measurements in a shocktube for air-dilute stoichiometric iso-octane, which revealed diverse auto-ignition characteristics at thermodynamic and mixture conditions relevant to practical combustion devices. These behaviors included homogeneous (spatially uniform emission or detonation wave) and inhomogeneous (localized reaction sites and deflagration) phenomena. Vermeer and Oppenheim further observed a clear transition between these auto-ignition behaviors at varying initial thermodynamic conditions, which they defined as the *strong ignition limit*. Fieweger et al. [3] expanded greatly on this work, classifying the auto-ignition behaviors of air-dilute stoichiometric iso-octane in a shocktube over a much broader range of initial temperatures, using pressure and CH emission time history characteristics. Consistent with the previous findings, Fieweger et al. [3] observed both homogeneous and inhomogeneous ignition behaviors and discovered a clearly defined strong ignition limit. The results of these studies are an important illustration that various auto-ignition behaviors are expected at conditions relevant to practical combustion devices using iso-octane, and that these generally repeatable behaviors are strongly related to initial unburned thermodynamic state.

The occurrence of similar auto-ignition behaviors and indeed a strong ignition limit at comparable thermodynamic conditions was reported previously by Meyer and Oppenheim [5] and Mansfield and Wooldridge [6] for air-dilute mixtures of hydrogen and syngas (hydrogen and carbon monoxide), respectively. Importantly, Mansfield and Wooldridge [6] discovered that a criterion first derived by Sankaran et al. [7] (Sankaran Criterion) could accurately predict the location of the strong ignition limit *a priori* using only basic flame and homogeneous reactor modeling. Remarkably, the criterion is a simple comparison of a thermal gradient driven propagation speed to the laminar flame speed. This predictive capability provided a new and unique tool that can be used in the design of combustion devices with high hydrogen content fuels, where auto-ignition behavior prediction and control is critical to performance and safety. Likewise, this ignition behavior criterion would be a valuable tool in the design of low-temperature combustion systems using iso-octane or other higher hydrocarbon fuels. Though its validity has not been evaluated for hydrocarbon fuels previous to the present work, the theoretical foundation of the ignition behavior criterion is not inherently fuel specific and a successful extension to non-hydrogen-based fuels is conceivable. Also highlighted in Mansfield and Wooldridge [6] were equivalence ratio dependent effects of ignition behavior on the accuracy of auto-ignition delay time predictions for syngas fuels made using typical zero-dimensional homogeneous modeling techniques. As auto-ignition delay time measurements were up to several orders of magnitude faster than predictions in cases with inhomogeneous ignition for syngas fuel, identifying and quantifying any effects for iso-octane is vital to its safe and effective use. This is especially important at low-temperature conditions where inhomogeneous behaviors are considerably more prevalent [3,4].

The objectives of the current study were first to evaluate the hypothesis that the Sankaran Criterion could be accurately applied to iso-octane fuel, and second to investigate the effects of auto-ignition behaviors on the predictive accuracy of basic auto-ignition delay time modeling for this fuel. These objectives were accomplished in part through new experimental studies of iso-octane auto-ignition behavior and auto-ignition delay times using the University of Michigan Rapid Compression Facility (UM-RCF) and the Tsinghua University Rapid Compression Machine (TU-RCM). The auto-ignition behavior results were combined with those from the shock tube studies of Fieweger et al. [3] and Vermeer and Oppenheim [4] to map auto-ignition behavior as a function of initial thermodynamic state and equivalence ratio. Using these maps, the strong ignition limit was identified for various equivalence ratios and the location of each limit was compared to predictions made using the Sankaran Criterion. Then the auto-ignition delay time measurements for all experiments were compared to predictions made using typical zero-dimensional homogeneous reactor modeling and the iso-octane oxidation mechanism of Mehl et al. [2] (referred to as the Mehl 2011 mechanism in the remainder of this paper).

2. Methods

2.1. Experimental

Ignition experiments were conducted using mixtures of iso-octane/air with molar fuel-to-O_2 equivalence ratios of $\varphi = 0.25$ and 1.0, at air levels of dilution, i.e. molar O_2-to-diluent gas ratio of 1:3.76. In the UM-RCF N_2 was the primary diluent, with small volumes of Ar and/or CO_2 added to modify the test temperature, and in the TU-RCM Ar was the primary diluent, with small volumes of N_2 added to modify the test temperature. In the UM-RCF, ignition experiments for $\varphi = 0.25$ were conducted between 3 and 20 atm for temperatures ~900–1125 K and experiments for $\varphi = 1.0$ were conducted at ~8 and 18 atm for temperatures ~830–975 K. In the TU-RCM, ignition experiments were conducted between at $\varphi = 0.25$ for 5–30 atm and temperatures ~740–1050 K. The reactant composition and initial state conditions for each auto-ignition experiment are provided in the Supplemental Material.

A detailed description and characterization of the UM-RCF can be found in Donovan et al. [8]. Briefly, the UM-RCF consists of the Driven Section, in which a gas mixture is rapidly compressed by the motion of a free piston (Sabot). Prior to compression, the test volume is evacuated and then filled with the test gas mixture. Upon firing, the Sabot travels the length of the Driven Section compressing the test gas mixture into the Test Section – a small cylindrical volume located at the end of the Driven Section. As the Sabot reaches its final position near the Test Section, the Sabot achieves an annular interference fit, sealing the test gas mixture in the Test Section. At this point, the Test Section is filled with a uniform and isentropically compressed test gas mixture at the desired initial thermodynamic condition. For this study, the Test Section was instrumented with a piezoelectric transducer (6125B Kistler, Amherst, NY) and charge amplifier (5010, Kistler, Amherst, NY) for pressure measurements at 100 kHz sampling frequency, and a transparent polycarbonate end-wall to permit high-speed imaging

of the ignition process. The uncertainty in the pressure measurements is estimated as ⩽1% (~0.1 atm). High-speed color imaging was recorded using a digital video camera (V711-8G-MAG-C, Vision Research, Phantom, CMOS array, 512 × 512 pixels) with a 50 mm lens (Navitar, F0.95), a 62 mm lens (Hoya, +2 zoom), and a 62 mm UV(0) filter (Hoya). Video sequences were recorded at 25,000 frames/s with an exposure time of 39.3 μs. All test gas mixtures were made using a continuously stirred stainless steel tank and the mixture composition was determined by measurement of the relative partial pressures of the components.

A detailed description of the TU-RCM can be found in Di et al. [9]. Briefly, the TU-RCM consists of a Driven Section in which a gas mixture is rapidly compressed by a piston. Prior to compression, the test volume is evacuated with a pump and then filled with a specific test gas mixture. Upon firing, high pressure air drives the piston into the Driven Section compressing the test gas mixture into the Test Section. As the piston reaches its final position hydraulic oil pressure dampens the motion. At this point, the Test Section is filled with a uniform and isentropically compressed test gas mixture at the desired initial thermodynamic condition. For the current study, the TU-RCM test section was instrumented with a piezoelectric pressure transducer (Kistler 6052CU20, Amherst, NY) combined with a charger amplifier (Kistler 5018A1000, Amherst, NY) for pressure measurements. The data were recorded at 100 kHz using a data acquisition system (National Instruments cDAQ-9178 chassis coupled with analog input model cDAQ-9223). The uncertainty in the pressure measurements is estimated as ⩽1%. High-speed color imaging was recorded using a high speed camera (Phantom V7.3, Vision Research, CMOS array, 128 × 128 pixels) with a 105 mm lens (Sigma, F2.3). Video sequences were recorded at 10,000 frames/s with an exposure time of 98 μs. All test gas mixtures were made using a dedicated stainless steel tank and the mixture composition was determined by measurement of the relative partial pressures of the components.

2.2. Computational

Auto-ignition delay time predictions were made using the constant volume adiabatic zero-dimensional reactor model in the CHEMKIN software suite [10] with the Mehl 2011 mechanism [2]. Using this ignition model, a corresponding auto-ignition delay time prediction was calculated for each ignition experiment conducted in the UM-RCF and TU-RCM, using the specific unburned thermodynamic condition and mixture composition of each experiment. Uncertainty bounds were calculated for the model predictions, reflecting the uncertainties in the pre-exponential "A-factor" of the Arrhenius reaction rates for the three most important reactions ($H + O_2 = OH + O$ (R1), H_2O_2 (+M) = OH + OH (+M) (R16), and $I\text{-}C_8H_{18} = Y\text{-}C_7H_{15} + CH_3$ (R3214)), determined via OH sensitivity analysis using the CHEMKIN software suite. The precise values of the rate coefficients used for these reactions are listed in the Supplemental Material. Iso-contours of constant predicted auto-ignition delay times were also calculated for a broad range of initial thermodynamic conditions, using the nominal A-factors for simplicity.

Predicted locations of the strong ignition limit were calculated using the Sankaran Criterion as done previously in Mansfield and Wooldridge [6]. The Sankaran Criterion, given in Eq. (1), is derived through a comparison of the spontaneous propagation speed, equal to the inverse of the gradient of the auto-ignition delay time $(d\tau/dx)^{-1}$, and the laminar flame speed (s_u^0),

$$\left|\frac{d\tau}{dT}\cdot\frac{dT}{dx}\right| < s_u^{0-1} \tag{1}$$

where $d\tau/dT$ is the thermal sensitivity of the ignition delay time, and dT/dx is a characteristic thermal gradient associated with the physical system. It is assumed that when this inequality is true, homogeneous ignition is expected to occur and when it is false inhomogeneous ignition behavior is expected. Therefore, the predicted thermodynamic location (P,T) of the strong ignition limit is where the two sides of this inequality are equal. It is thereby possible to calculate the predicted location of the strong ignition limit by systematically evaluating the thermal sensitivity and laminar flame speed values across a broad range of initial thermodynamic conditions (P,T) and combining these with an assumed value of the thermal gradient; 5, 10, 20 K/mm were used in this work. Thermal sensitivity values were calculated in this study using the same zero-dimensional reactor model and the Mehl 2011 mechanism used for predicting ignition delay times; although a constant pressure boundary condition was applied, consistent with previous studies by Vermeer and Oppenheim [4], Meyer and Oppenheim [5], and Mansfield and Wooldridge [6]. It is assumed that the formation and early existence of localized flame-like structures, the primary concern of predictions in the present work, occur in a nominally constant pressure environment. Laminar flame speed values were calculated using the correlations developed by Middleton et al. [11] for premixed iso-octane. The flame speed correlation was validated in that study by comparison with a wide range of experimental and computational works at initial temperatures between 298 and 1000 K. As a consequence, predictions of the location of the strong ignition limit in the present work were intentionally limited to initial temperatures less than ~1100 K. Valid laminar flame speed data at higher temperatures would allow the predictions in the present work to be extended to higher temperatures.

At the foundation of the Sankaran Criterion is an assumption made first by Meyer and Oppenheim [5] that distributed thermal fluctuations exist within the adiabatic core region of the Test Section of the UM-RCF, TU-RCM, and other similar experimental devices, and that inhomogeneous auto-ignition behavior consists of localized flame-like structures which are generated as a result of, and propagate through, these gradients. In support of this assumption, temperature measurements have been evaluated experimentally in the UM-RCF by Donovan et al. [8] and in an RCM with a very different hardware design by Strozzi et al. [12] with both studies indicating that distributed thermal gradients on the order of 5–10 K/mm are expected in the adiabatic core region of an RCM-like device.

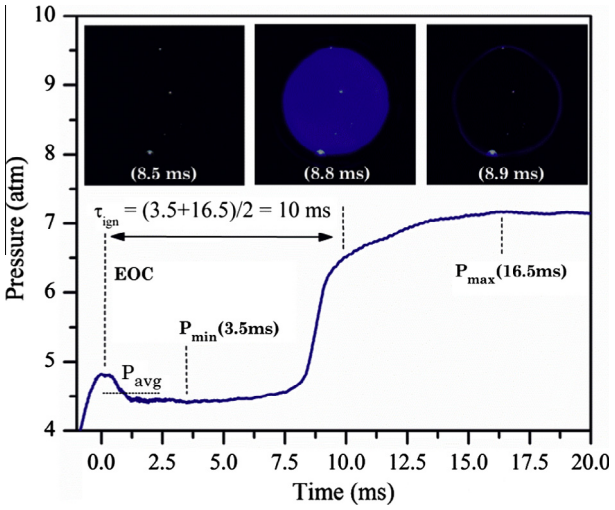

Fig. 1. Typical experimental result for pressure time history in the UM-RCF during homogeneous ignition, for initial conditions P_{avg} = 4.5 atm, T_{avg} = 1035 K, φ = 0.25; where τ_{ign} is the auto-ignition delay time. Three frames from the corresponding high-speed imaging illustrate uniform chemiluminescence during auto-ignition.

3. Results and discussion

For each experiment in the UM-RCF and TU-RCM, a pressure time history and a high-speed imaging video were recorded, allowing for the determination of an auto-ignition delay time and direct observation and classification of the auto-ignition behavior. Fig. 1 presents a typical pressure time history and corresponding still frames from the high-speed video of a UM-RCF experiment exhibiting homogeneous ignition. Trends in the time history data illustrate a pressure increase during the compression stroke until the Sabot is seated at the end-of-compression (EOC), followed by a slight decrease in pressure due to heat transfer from the test gas volume into the cool Test Section walls, followed by a large and rapid increase in pressure during the ignition event. As seen in the frames from the high-speed video, the spatial uniformity of the chemiluminescence is a clear indication the ignition occurs homogeneously in the Test Section. Fig. 2 presents a typical pressure time history with corresponding still frames from the high-speed video of a UM-RCF experiment exhibiting inhomogeneous ignition. The characteristics of the pressure time history are not remarkably different than those for homogeneous ignition in Fig. 1, though it is clear that the heat addition and corresponding pressure increase occurs over nearly twice the time. As seen in the high-speed imaging sequence there are two localized flame-like structures which propagate and consume some of the test-gas mixture prior to homogeneous ignition of the remainder of the test gas volume. This sequence of ignition behaviors occurred in every experiment which exhibited inhomogeneous ignition. Inspection of the imaging results for all experiments exhibiting inhomogeneous ignition revealed that local flame-like structures initiate in widely varying locations within the UM RCF Test Section, indicating that the behavior is likely related to a distribution of disturbances not a single ignition source. Fig. 3 presents a typical pressure time history with corresponding still frames from the high-speed video of a TU-RCM experiment exhibiting homogeneous ignition. The characteristics of the pressure time history and the high-speed imaging are quite similar to homogeneous ignition data of Fig. 1 indicating similar homogeneous behaviors are observed in both experimental facilities. No experiments in the TU-RCM exhibited inhomogeneous ignition behaviors for the conditions and compositions studied.

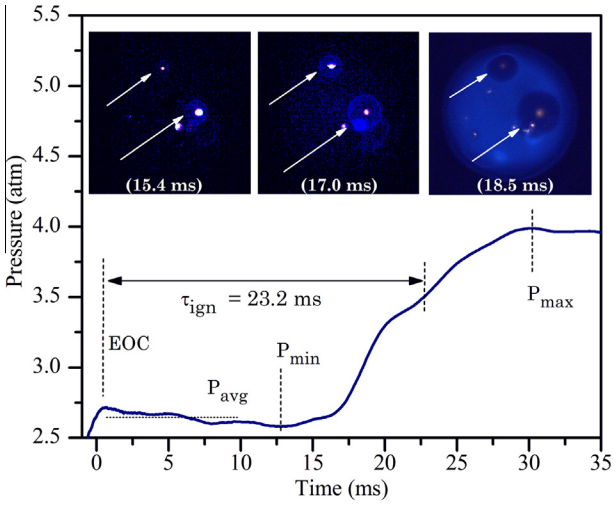

Fig. 2. Typical experimental result for pressure time history in the UM-RCF during inhomogeneous ignition, for initial conditions P_{avg} = 2.7 atm, T_{avg} = 1016 K, φ = 0.25. Three frames from the corresponding high-speed imaging illustrate the formation and propagation of localized flame-like fronts prior to the subsequent auto-ignition of the unburned charge.

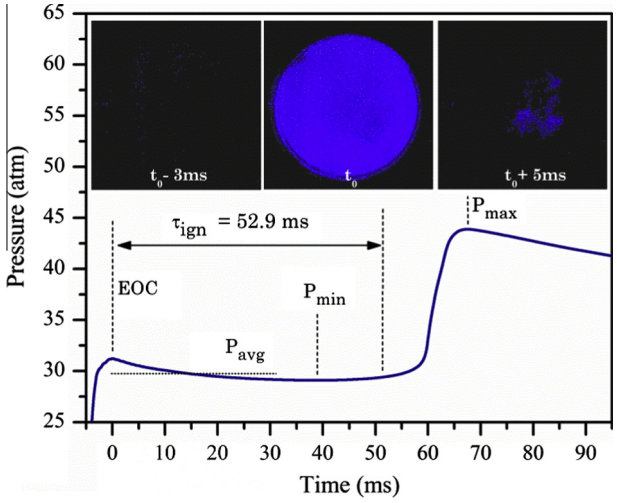

Fig. 3. Typical experimental result for pressure time history in the TU-RCM during homogeneous ignition, for initial conditions P_{avg} = 29.7 atm, T_{avg} = 784 K, φ = 0.25. Three frames from the corresponding high-speed imaging illustrate uniform chemiluminescence during auto-ignition. The time, t_0, corresponds approximately to the auto-ignition delay event (~62 ms).

For each experiment, the time and pressure data were noted at three distinct events: EOC, minimum pressure (P_{min}), and maximum pressure (P_{max}), denoted in Figs. 1–3. After filtering the pressure time history with a 75-point smoothing algorithm, the nominal auto-ignition delay time was defined as the time difference between the EOC and the average of P_{max} and P_{min}, with the uncertainty of the reported ignition delay time defined as one-half the time difference between P_{max} and P_{min}. Overall, this definition biases the auto-ignition delay times to slightly faster values compared to conventional definitions based on the maximum rate of pressure rise; however, this approach ensures the analysis can be applied to all experiments regardless of ignition behavior, which was critical given the wide range of behaviors considered in this work yielding variable pressure time history characteristics. Additionally, the assigned uncertainty limits assigned ensure that any reasonable definition of auto-ignition delay time is well captured within the bounds of the reported measurements.

While the pressure of the Test Section was measured directly, the temperatures for each experiment were calculated using thermodynamic relations. Based on previous findings [8,13] both the compression process and the subsequent expansion of the adiabatic core region due to minor heat transfer can be modeled as isentropic processes. With this well supported assumption in place, the initial thermodynamic conditions were used with isentropic state relations to calculate the temperature at EOC and at P_{min}. Propagation of the pressure measurement uncertainty through the isentropic state relations yields an uncertainty of $\leqslant$0.4% in the assigned temperatures (~5 K).

For each experiment a thermodynamic state was assigned, representing the isobaric/isothermal condition at which the experiment was conducted. In most cases, there was no appreciable decrease in temperature between EOC and the start of the ignition event (i.e., <10 K) and so the EOC thermodynamic state was assigned to that experiment. In the cases where the temperature decrease between EOC and the start of the ignition event was 10 K or more, an average thermodynamic state was assigned. The average pressure was calculated as the arithmetic mean of all pressure measurements between the EOC and P_{min} events, and the average temperature was calculated using an isentropic expansion from the EOC to the average pressure. The assignment of an average state in this manner incorporates heat transfer effects on the

measurements during the time before ignition, and has been successfully applied in numerous previous works [6,8,14]. A detailed review of other methods of assigning a state to an experiment and subsequently simulating each experiment is given in Mansfield and Wooldridge [6]. As discussed in that work, assignment of an average state accurately captures heat transfer effects on the experiment while retaining critical clarity in both reporting and interpreting the experimental results, thus greatly improving the archival value of the results as compared to using the EOC conditions.

In order to compare the auto-ignition behaviors observed in the current work with those from the previous shocktube studies (Fieweger et al. [3] and Vermeer and Oppenheim [4]) it was necessary to systematically categorize the behaviors. Two ignition classifications were defined for the present work: (1) *strong ignition*, where only homogeneous ignition occured, and (2) *mixed ignition*, where local ignition and flame-like propagation occured and is followed by homogeneous ignition of the unburned gas volume. In the present work new experiments exhibiting homogeneous ignition behavior only (shown in Fig. 1) were classified as strong and those exhibiting initial inhomogeneous behavior (shown in Fig. 2) were classified as mixed. Fieweger et al. [3] and Vermeer and Oppenheim [4] categorized experiments as exhibiting strong or mild ignition, where strong ignition was described as the appearance of an essentially instantaneous shock, induced by an explosion, and mild ignition was described as the appearance of numerous localized flames gradually developing into an explosion and shock. Therefore, experiments classified as exhibiting strong ignition in those Shocktube studies were also classified as strong in the present work, and those classified as mild were re-classified as mixed in the present work.

3.1. Auto-ignition behavior

Fig. 4 presents the observed ignition behavior as a function of thermodynamic state for mixtures with $\varphi = 0.25$. A range of behaviors is evident, with strong ignition at all conditions except the lowest pressures (3–5 atm) where there is a transition from strong to mixed to no ignition as temperature decreases from ~1100 K to 950 K. There is excellent agreement between experimental results from the UM-RCF and those from the TU-RCM at the higher pressure conditions, suggesting that behaviors are device independent. Overall the data show the ignition behaviors are well grouped and strongly related to the initial thermodynamic state, with a clearly defined strong ignition limit at lower pressures, marked as a hashed area in Fig. 4. The transition to no ignition at the lowest temperatures for $P = 3$ and 5 atm was not expected, as the predicted auto-ignition delay times in this region are well within the normal limits of the UM-RCF (~75 ms); however, reduced pressure rise rates during mixed ignition, previously highlighted in Fig. 2, likely lead to more significant heat transfer effects at these conditions and could result in unexpected quenching of the test gas mixture. Also presented in Fig. 4 is the location of the predicted strong ignition limit for three thermal gradients, illustrating excellent correlation between the location of the experimentally observed strong ignition limit and the prediction which uses a 10 K/mm thermal gradient magnitude. This is an indication that the Sankaran Criterion can accurately predict the strong ignition limit for iso-octane at these conditions. Interestingly, the most accurate prediction corresponds to an assumed thermal gradient magnitude in close agreement with the experimental findings of Donovan et al. [8] and Strozzi et al. [12].

The experimental results indicate the propensity for strong ignition behavior greatly increases near the negative temperature coefficient (NTC) region (as predicted using the Mehl 2011 mechanism), highlighted in gray in Fig. 4. Remarkably, the Sankaran Criterion correctly forecasts the leftward curvature in the strong ignition limit as the NTC region is approached. Within the NTC region, an inverse relationship between temperature and auto-ignition delay time is predicted by the Mehl 2011 mechanism, i.e. the auto-ignition delay time increases with increasing temperature. Therefore, as temperature is lowered and the NTC region is crossed from the high-temperature side, the magnitude of the thermal sensitivity rapidly decreases and the sign of the thermal sensitivity changes from negative to positive. As indicated by the Sankaran Criterion, Eq. (1), a reduction in thermal sensitivity magnitude indeed corresponds to an increased likeliness for strong ignition behavior.

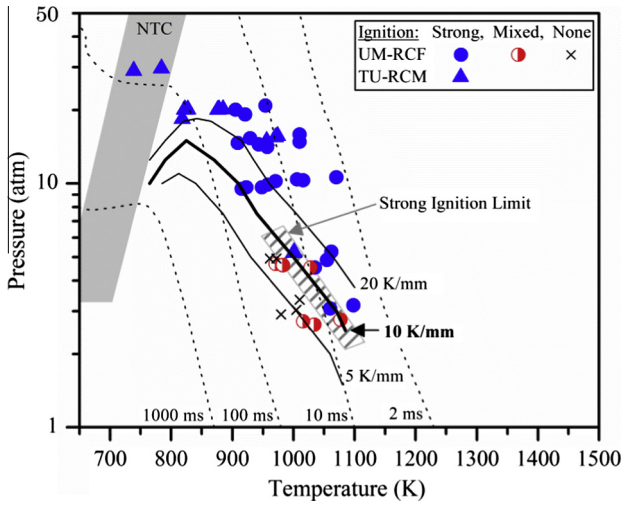

Fig. 4. Ignition behavior as a function of initial thermodynamic state for mixtures with $\varphi = 0.25$. The strong ignition limit identified by the experimental data is shown as the hashed area, and the NTC region identified by model predictions is shown as the gray area. Iso-contours of predicted auto-ignition delay time are shown as dotted lines, and predicted locations of the strong ignition limit are shown as solid lines. The most accurate prediction of the strong ignition limit, for a 10 K/mm gradient, is the bold solid line.

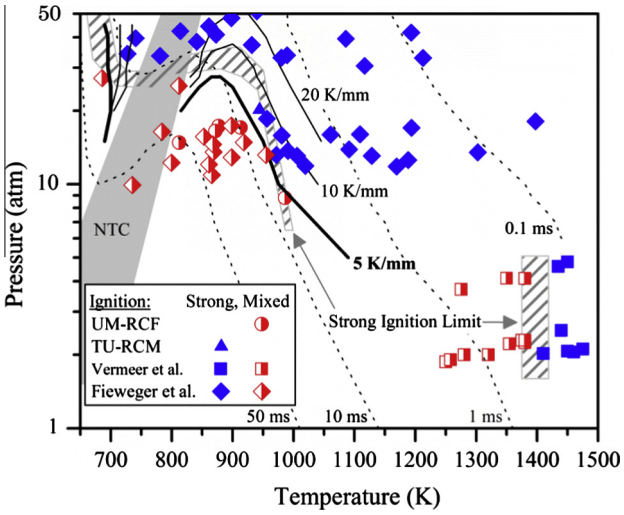

Fig. 5. Ignition behavior as a function of initial thermodynamic state for mixtures with $\varphi = 1.0$. The strong ignition limit identified by the experimental data is shown as the hashed areas and the NTC region identified by model predictions is shown as the gray area. Results are from the present work, Vermeer and Oppenheim [4], and Fieweger et al. [3]. Iso-contours of predicted auto-ignition delay time are shown as dotted lines, and predicted locations of the strong ignition limit are shown as solid lines. The most accurate prediction of the strong ignition limit, for a 5 K/mm gradient, is the bold solid line.

Therefore, increased propensity for strong ignition behaviors near the NTC region is likely due to a corresponding decrease in the magnitude of the thermal sensitivity of the ignition delay time.

Fig. 5 presents the observed ignition behavior as a function of thermodynamic state for mixtures with $\varphi = 1.0$. A range of behaviors is evident, with strong ignition generally occurring at higher temperatures and a highly pressure dependent transition to mixed ignition occurring as temperature is decreased. There is excellent agreement between the experimental results from the UM-RCF, TU-RCM, and those from Fieweger et al. [3], where the latter results span a larger range of pressures and temperatures. As the results from Vermeer and Oppenheim [4] are at much higher temperatures and lower pressures than the other three data sets, it was not possible to directly compare their results to the others; however, the same trend of strong ignition at higher temperatures and mixed ignition at lower temperatures is evident. Overall the data show the ignition behaviors are consistent between devices, well grouped, and strongly related to the initial thermodynamic state, with a clearly defined strong ignition limit spanning 1000–650 K for $P > 10$ atm and $\sim$1400 K for $P < 5$ atm. The measured strong ignition limit is marked as the two hashed areas in Fig. 5. Regarding the effect of equivalence ratio on the location of the strong ignition limit, there is a shift toward higher temperatures as φ is increased from 0.25 to 1.0, in agreement with the trend observed in hydrogen based fuels by Mansfield and Wooldridge [6]. As discussed in that work, this is likely related to the energy content of the mixture and the relative amount of energy released during local ignition events.

Also presented in Fig. 5 is the location of the predicted strong ignition limit for three thermal gradients, illustrating excellent correlation between the measured strong ignition limit and the predicted location for 5 K/mm at $P > 10$ atm. This correlation is a clear indication that the Sankaran Criterion can accurately predict the location of the strong ignition limit for iso-octane at higher equivalence ratio conditions. As the calculation of a predicted strong ignition limit for initial temperatures above 1100 K was not reasonable using the flame speed correlation from Middleton et al. [12], predictions could not be compared to the measured limit around $\sim$1400 K; however, the trajectory of the predictions is consistent with the measured strong ignition limit at high temperatures.

Quite remarkably, for $\varphi = 1.0$ the predicted strong ignition limit for a 5 K/mm thermal gradient accurately predicts the location of the experimentally observed strong ignition limit on both the high and low temperature sides of the NTC region. Consistent with the results for lower φ, the strong ignition limits curve toward lower pressures at temperatures near the NTC region from both low and high temperature directions. This is again due to the rapid reduction in the magnitude of thermal sensitivity near the NTC region. Strong ignition limit predictions were not calculated for points within the NTC region as the inverted sign of the thermal sensitivity values contradicts the physical foundation of the Sankaran Criterion. The basis of this criterion assumes the existence of a spontaneous propagation and/or laminar flame moving from high-temperature to low-temperature down a thermal gradient centered at a thermal hot spot. It is presently unclear if and how flame and/or propagation front motion would be affected if the thermal sensitivity were positive, meaning the lower temperature regions would ignite earlier. However, as evidenced by the results in Fig. 5 the trend of the strong ignition limit is not significantly changed as the NTC region is traversed. This suggests that the underlying mechanism governing ignition behavior is also not significantly changed in this region, though more detailed experimentation in this region would be necessary to more directly validate such an assertion.

Overall, these results illustrate that the Sankaran Criterion is indeed an excellent tool for *a priori* prediction of the strong ignition limit for iso-octane fuels across a broad range of thermodynamic and mixture conditions. As highlighted previously by Mansfield and Wooldridge [6] this is an important and useful tool, which not only provides a practical and simple approach to predicting complex ignition behaviors, but it also describes the roles of chemical kinetics, thermo-physical properties, and device dependent thermal characteristics in governing these behaviors. Importantly, in conjunction with the previous findings for syngas fuels [6], the results of the present work are a strong indication that the Sankaran Criterion can be applied to a broad range of fuels – beyond the important hydrocarbon primary reference fuel iso-octane and fuels with high hydrogen content. Furthermore, the similarity in thermal gradient values which result in the most accurate predictions for both fuels and a range of equivalence ratios suggests that an assumption of a 5–10 K/mm gradient can be reasonably applied for a broad range of fuel types and mixture compositions.

The quantitative nature of the Sankaran Criterion is particularly important to the extension of this criterion to more practical combustion systems like internal combustion engines, which will experience much larger magnitudes of thermal gradients (up to $\sim$50 K/mm, approximated using experimental data from Einecke et al. [15]) as well as mixture inhomogeneities and turbulence. As indicated in Figs. 4 and 5, increasing the value of thermal gradient shifts the predicted location of the strong ignition limit toward higher pressures. Considering the approximate magnitude of thermal gradients in real engine systems, mixed ignition behaviors are likely to occur at pressures up to and exceeding 50 atm for $T \leqslant \sim$1100 K, conditions particularly important to modern boosted low-temperature engine operation. As such, it is possible that "pre-ignition" and "super-knock" behaviors at high-pressure low-temperature conditions, like those described by Kalghatgi and Bradley [16], are related to the inhomogeneous ignition behaviors observed in the present work.

Regarding the influence of mixture inhomogeneity and turbulence in practical combustion systems, these factors are expected to influence the accuracy and utility of the Sankaran Criterion in predicting ignition behaviors. Although quantifying these effects is outside the scope of the current study, these topics are valuable directions for future work. A computational investigation of the influence of turbulence and mixture inhomogeneities on the success of the Sankaran Criterion is currently underway by Pal and Im [17] for syngas fuels, expanding on the previous computational work by Sankaran et al. [7] and Bansal and Im [18]. Additional experimental studies are also important to further bridge the results of the current work to engine development.

3.2. Auto-ignition delay time

Figs. 6a and 6b present the measured and predicted auto-ignition delay times as a function of inverse temperature for mixtures with $\varphi = 0.25$ at various pressures. Recall that the error bars on the experimental data represent the limits of the definition of the auto-ignition delay time and the error bars on the predictions represent the effects of known uncertainty in reactions R1, R16, and R3214. The results indicate excellent agreement between the measurements and predictions across the complete range of temperature and pressure conditions for both observed ignition behaviors (strong and mixed). Furthermore, excellent agreement is evidenced between the results from the UM-RCF those from the TU-RCM. It is therefore clear that the accuracy of auto-ignition delay time predictions made using the typical zero-dimensional model described above and the Mehl 2011 mechanism are not significantly affected by inhomogeneous ignition behavior at these conditions for $\varphi = 0.25$. This is an indication that the energy released during the inhomogeneous ignition process does not significantly influence the subsequent homogeneous auto-ignition.

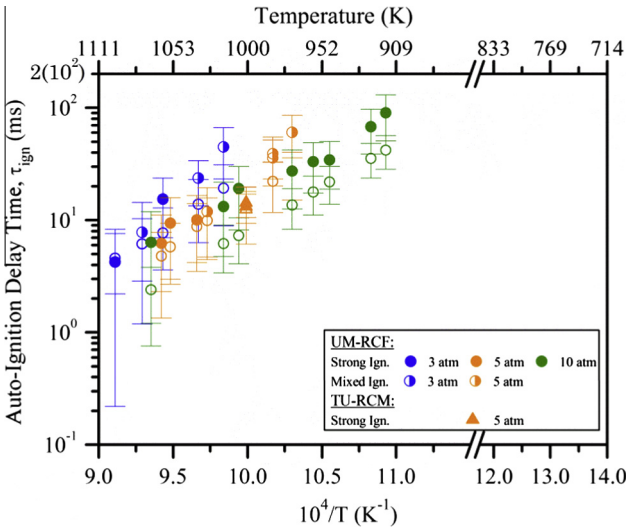

Fig. 6a. Measured and predicted auto-ignition delay time as a function of inverse temperature for mixtures with $\varphi = 0.25$, for $P = 3$, 5, and 10 atm. Solid markers represent experimental measurements and hollow markers represent corresponding model predictions. Uncertainty bounds of the predictions are the effects of the uncertainties in the rate coefficients of reactions R1, R16, R3214; whereas, uncertainty bounds of the measurements are the limits of the definition of the auto-ignition delay time.

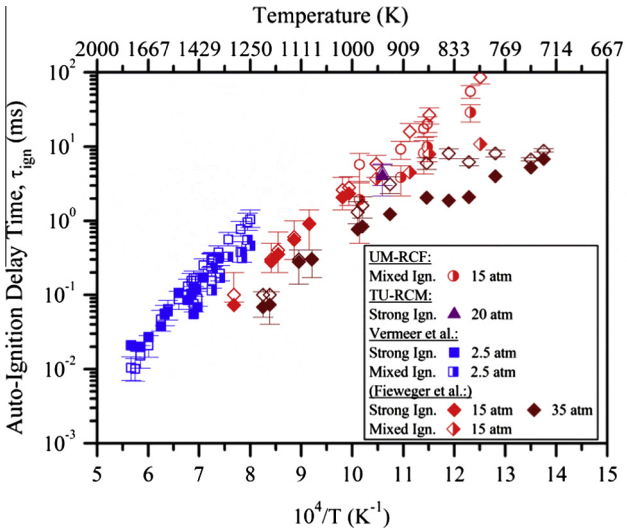

Fig. 7. Measured and predicted auto-ignition delay time as a function of inverse temperature, for mixtures with $\varphi = 1.0$. Results are from the present work, Fieweger et al. [3], and Vermeer and Oppenheim [4]. Solid markers represent experimental measurements and hollow markers represent corresponding model predictions. Uncertainty bounds of the predictions are the effects of the uncertainties in the rate coefficients of reactions R1, R16, R3214; whereas, uncertainty bounds of the measurements are the limits of the definition of the auto-ignition delay time.

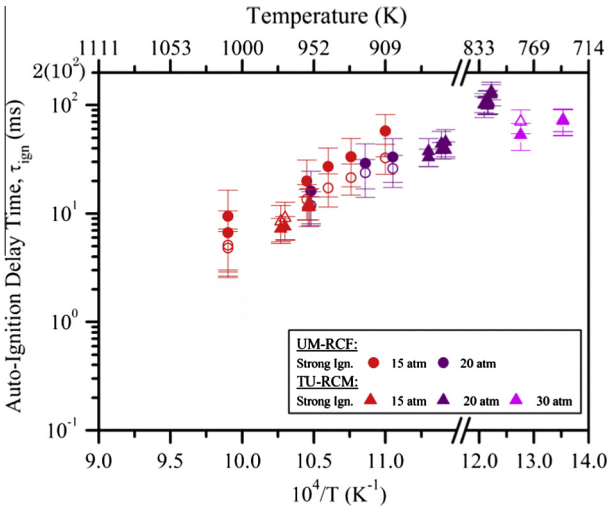

Fig. 6b. Measured and predicted auto-ignition delay time as a function of inverse temperature for mixtures with $\varphi = 0.25$, for $P = 15$, 20, and 30 atm. Solid markers represent experimental measurements and hollow markers represent corresponding model predictions. Uncertainty bounds of the predictions are the effects of the uncertainties in the rate coefficients of reactions R1, R16, R3214; whereas, uncertainty bounds of the measurements are the limits of the definition of the auto-ignition delay time.

Fig. 7 presents the measured and predicted auto-ignition delay times as a function of inverse temperature for mixtures with $\varphi = 1.0$ at various pressures. Overall the results indicate excellent agreement between all measurements and predictions for temperatures greater than 1000 K at all pressures; however, the agreement varies at temperatures less than this value. There is generally good agreement between the experimental results from the UM-RCF and those from Fieweger et al. [3] and Vermeer and Oppenheim [4], though the only significant overlap in initial conditions is for 15 atm. Regarding the results from Vermeer and Oppenheim [4] there is excellent agreement between the measurements and predictions for the experiments which exhibited strong ignition and good agreement for those which exhibited mixed ignition. While the nominal auto-ignition delay time measurements appear to be slightly less than the nominal predictions when mixed ignition behavior occurs, the uncertainty bounds in all cases have significant overlap indicating that the model is still accurate at these conditions. Regarding the results from Fieweger et al. [3] at 15 atm, there is excellent agreement between the measurements and predictions for the experiments which exhibited strong ignition (at temperatures above ~1000 K); however, after the onset of mixed ignition at lower temperatures the measurements are consistently lower than predictions with increasing discrepancy as the temperature is decreased. The results from the UM-RCF at 15 atm are in agreement with these findings, where the measurements are systematically lower than predicted times. This is consistent with behaviors seen previously for syngas and hydrogen fuels [6,19], which were linked to energy release during inhomogeneous ignition coupled with increasingly longer auto-ignition delay times. Regarding the results from Fieweger et al. [3] at 35 atm, all of which exhibited strong ignition, there is excellent agreement between the measurements and predictions for temperatures 1000–1250 and 725–750 K; while at temperatures between these ranges the measurements are up to an order of magnitude faster than predictions. As illustrated in Fig. 5 the NTC region lies between ~750 and 1000 K at this pressure, which suggests that this discrepancy is related to error in the Mehl 2011 mechanism and/or the CHEMKIN zero-dimensional reactor model in predicting auto-ignition delay times in the NTC region. This level of discrepancy is generally consistent with the benchmarking results of Mehl et al. [2] for the NTC region at high pressures, though limited experimental data was reported for those conditions.

Overall these results are an indication that the effect of ignition behavior on the predictive accuracy of auto-ignition delay times made using zero-dimensional modeling is strongly dependent on the equivalence ratio, where inhomogeneous behaviors have little impact for mixtures with $\varphi = 0.25$ and can cause significant reductions in delay times for $\varphi = 1.0$. This dependence on equivalence ratio is in excellent agreement with previous findings by Mansfield and Wooldridge [6], who found similar behavior for syngas fuel and related such behavior to the amount of energy released during inhomogeneous ignition. Furthermore, the results of Vermeer and

Oppenheim [4] at high temperatures indicate the effect of inhomogeneous ignition behavior on predictive accuracy is also dependent on the magnitude of the auto-ignition delay time itself, in that very short auto-ignition delay times (<1 ms) lead to a negligible effect of inhomogeneous behaviors even at high φ.

4. Conclusions

This work represents an important integration of results from diverse experimental platforms to describe common ignition behaviors of iso-octane, and further to provide a quantitative basis for predicting and interpreting data of ignition studies beyond the fuel and conditions studied here. Studies such as this are vital toward fundamental understanding of low-temperature combustion systems where prediction and control of chemically driven ignition phenomena is key to safety and performance. Importantly, the insights and tools developed in this work are relevant not only to systems which rely solely on chemically controlled ignition but also those which can be impacted by uncontrolled auto-ignition during an active ignition process, e.g., knock, pre-ignition, and super-knock in spark ignited internal combustion engine systems.

The comprehensive results of the present work clearly illustrate the existence of both inhomogeneous and homogeneous auto-ignition behaviors for stoichiometric and lean air-dilute iso-octane mixtures at thermodynamic conditions relevant to engines and other combustion systems. Analysis of patterns in the ignition behaviors revealed a dependence on temperature, pressure, and equivalence ratio with distinct thermodynamic regions in which the ignition behavior is consistent and repeatable. The strong ignition limit was identified for each equivalence ratio, indicating a transition in ignition behavior from homogeneous to inhomogeneous. The location of this limit was found to shift to higher temperatures as the equivalence ratio was increased, with the most significant change at pressures greater than 10 atm. Interestingly, proximity to the NTC region increased the propensity for homogeneous ignition, likely resulting from a decrease in thermal sensitivity of the auto-ignition delay time.

The location of the strong ignition limit for each equivalence ratio was predicted with remarkable accuracy using the Sankaran Criterion, which is a comparison of the laminar flame speed to the thermal gradient driven spontaneous propagation speed. For $\varphi = 0.25$ the prediction was most accurate for an assumed thermal gradient of 10 K/mm, whereas for $\varphi = 1.0$ this value was 5 K/mm. In conjunction with the previous findings for syngas fuels by Mansfield and Wooldridge [6], this is a strong indication that the Sankaran Criterion can be used to predict ignition behavior for a broad range of hydrocarbons and hydrogen based fuels. This validation of the Sankaran Criterion for a hydrocarbon fuel importantly broadens the use of this tool and is an indication that ignition processes in hydrocarbon and high hydrogen content fuels are fundamentally similar. Furthermore, the quantitative nature of this criterion uniquely describes the roles of chemical kinetics, transport phenomena, and thermal characteristics in determining auto-ignition behavior, allowing for a deeper understanding of these phenomena and facilitating a thoughtful extension to more complex systems which include turbulence and mixture inhomogeneity.

Auto-ignition delay time measurements were compared to zero-dimensional model predictions for all experiments considered in the present work, revealing the accuracy of predictions was strongly dependent on equivalence ratio and ignition behavior. The results indicate that the presence of inhomogeneous ignition behavior does not significantly affect the accuracy of auto-ignition delay time predictions for mixtures with $\varphi = 0.25$; whereas, for mixtures with $\varphi = 1.0$ the presence of inhomogeneous ignition behavior can significantly reduce the accuracy of predictions at the conditions studied here. This inaccuracy at higher φ is likely the result of increased energy release during the inhomogeneous event, causing a significant shift in the thermodynamic state of the yet unburned gas mixture and a subsequent violation of the isobaric/isothermal assumptions in the zero-dimensional model. These results are an important indication that while inhomogeneous ignition behavior may still be present at lean conditions, the subsequent effect on the auto-ignition delay time may be reduced or eliminated. Furthermore, it is evident that ignition behavior must be appropriately classified in any future experimental work for near stoichiometric mixtures of iso-octane at temperatures below ~1000 K to ensure proper interpretation of the results.

Acknowledgements

The authors acknowledge the generous support of the U.S. DOE NETL Award Number DE-FE0007465 and the Department of Mechanical Engineering at the University of Michigan. The authors thank Dimitris Assanis for sharing his insight and iso-octane data.

Appendix A. Supplementary material

Supplementary data associated with this article can be found, in the online version, at http://dx.doi.org/10.1016/j.fuel.2014.08.019.

References

[1] Richards G, McMillian M, Gemmen R, Rogers W, Cully S. Issues for low-emission, fuel-flexible power systems. Prog Energy Combust Sci 2001;27:141–69.
[2] Mehl M, Pitz WJ, Westbrook CK, Curran HJ. Kinetic modeling of gasoline surrogate components and mixtures under engine conditions. Proc Combust Inst 2011;33:193–200.
[3] Fieweger K, Blumenthal R, Adomeit G. Shock-tube investigations on the self-ignition of hydrocarbon-air mixtures at high pressures. Symp Combust 1994;25:1579–85.
[4] Vermeer DJ, Oppenheim AK. Auto-ignition of hydrocarbons behind reflected shock waves. Combust Flame 1972;18:327–36.
[5] Meyer JW, Oppenheim AK. On the shock-induced ignition of explosive gases. Symp Combust 1971;13:1153–64.
[6] Mansfield AB, Wooldridge MS. High-pressure low-temperature ignition behavior of syngas mixtures. Combust Flame 2014;161:2242–51.
[7] Sankaran R, Im HG, Hawkes ER, Chen JH. The effects of non-uniform temperature distribution on the ignition of a lean homogeneous hydrogen–air mixture. Proc Combust Inst 2005;30:875–82.
[8] Donovan MT, He X, Zigler BT, Palmer TR, Wooldridge MS, Atreya A. Demonstration of a free-piston rapid compression facility for the study of high temperature combustion phenomena. Combust Flame 2004;137:351–65.
[9] Di H, He X, Zhang P, Wang Z, Wooldridge MS, Law CK, et al. Effects of buffer gas composition on low temperature ignition of iso-octane and n-heptane. Combust Flame 2014. http://dx.doi.org/10.1016/j.combustflame.2014.04.01.
[10] Reaction design. CHEMKIN 10101 2010.
[11] Middleton RJ, Martz JB, Lavoie GA, Babajimopoulos A, Assanis DN. A computational study and correlation of premixed isooctane air laminar reaction fronts diluted with EGR. Combust Flame 2012;159:3146–57.
[12] Strozzi C, Sotton J, Mura A, Bellenoue M. Characterization of a two-dimensional temperature field within a rapid compression machine using a toluene planar laser-induced fluorescence imaging technique. Meas Sci Technol 2009;20:125403.
[13] Lee D, Hochgreb S. Hydrogen autoignition at pressures above the second explosion limit. Int J Chem Kinet 1998;30:385–406.
[14] Walton SM, He X, Zigler BT, Wooldridge MS. An experimental investigation of the ignition properties of hydrogen and carbon monoxide mixtures for syngas turbine applications. Proc Combust Inst 2007;31:3147–54.
[15] Einecke S, Schulz C, Sick V. Measurement of temperature, fuel concentration and equivalence ratio fields using tracer LIF in IC engine combustion. Appl Phys B 2014;71:717–23.
[16] Kalghatgi GT, Bradley D. Pre-ignition and "super-knock" in turbo-charged spark-ignition engines. Int J Eng Res 2012;13:399–414.
[17] Pal P, Mansfield AB, Wooldridge MS, Im HG. Characteristics of syngas auto-ignition at high pressure and low temperature conditions with thermal inhomogeneities. In: 12th Int. conf. combust. energy util; 2014.
[18] Bansal G, Im HG. Autoignition and front propagation in low temperature combustion engine environments. Combust Flame 2011;158:2105–12.
[19] Chaos M, Dryer FL. Syngas combustion kinetics and applications. Combust Sci Technol 2008;180:1053–96.

Combustion and Flame 162 (2015) 2286–2295

Contents lists available at ScienceDirect

Combustion and Flame

journal homepage: www.elsevier.com/locate/combustflame

The effect of impurities on syngas combustion

Andrew B. Mansfield [a,*], Margaret S. Wooldridge [a,b]

[a] Department of Mechanical Engineering, University of Michigan, Ann Arbor, MI 48109, USA
[b] Department of Aerospace Engineering, University of Michigan, Ann Arbor, MI 48109, USA

ARTICLE INFO

Article history:
Received 25 January 2015
Received in revised form 27 January 2015
Accepted 27 January 2015
Available online 2 March 2015

Keywords:
Syngas
Impurity
Trimethylsilanol
Methane
Rapid compression facility

ABSTRACT

The effects of chemical impurities on the combustion of syngas were investigated, focusing on CH_4, a common component of syngas, and trimethylsilanol (TMS), an unstudied impurity related to those common to landfill-based syngas. Ignition properties were systematically investigated at high-pressure low-temperature conditions relevant to gas turbine combustor operation using the University of Michigan Rapid Compression Facility. Pressure time history measurements and high-speed imaging of the ignition process in this facility were used to determine auto-ignition delay times and observe ignition behaviors. The four simulated syngas mixtures used were (1) pure syngas: 30% H_2, 70% CO fuel volume, (2) syngas with CH_4: 27% H_2, 67% CO, 6% CH_4, (3 & 4) pure syngas with 10 or 100 ppm TMS, all with fuel-to-O_2 equivalence ratios (φ) of 0.1 at air dilution (i.e. molar O_2 to inert gas ratio of 1:3.76), and N_2 as the primary diluent gas. The pressures after compression were 5 & 15 atm with temperatures of ~1010–1110 K respectively. The results uniquely illustrated the occurrence of two-step ignition behavior at higher pressures, with two distinct regions of heat release and pressure rise. First and second auto-ignition delay times were therefore defined and interestingly the times were affected differently by the addition of impurities. The addition of CH_4 consistently increased auto-ignition delay times up to 40% at 15 atm, while increasing delay times at 5 atm by up to a factor of three. Conversely, the addition of 10 ppm TMS impurity addition caused a consistent decrease of ~10–30% delay times at 15 atm with insignificant impact at 5 atm, and 100 ppm TMS impurity caused consistent decreases of 50–70% at 15 atm and 20–30% decreases at 5 atm. The marked pressure dependence of the auto-ignition delay time, typical for syngas at these conditions, was virtually eliminated for the 100 ppm TMS mixture. Kinetic modeling suggests that the promoting effects of TMS are related to enhanced consumption and/or reduced production of HO_2. The impact of TMS is remarkably similar to that for SiH_4 in pure H_2, suggesting a possible trend for poorly understood Si-based species to promote auto-ignition in syngas and hydrogen mixtures.
© 2015 The Combustion Institute. Published by Elsevier Inc. All rights reserved.

1. Introduction

Synthesized gas, or syngas, is a fuel mixture composed primarily of hydrogen and carbon monoxide, which can be produced via gasification or decomposition of carbonaceous feedstock such as coal, biomass, or landfill wastes. This fuel can be used directly in transportation or stationary combustion devices, enabling both a diversification of fuel sources and a reduction in pollutant emissions such as SO_x, NO_x, particulate matter, and heavy metals [1]. As this is a high-hydrogen-content fuel, increased NO_x emission is a concern and the application of abatement schemes focusing on low-temperature, lean, and/or pre-mixed conditions are currently under strong consideration, e.g. dry low-NO_x strategies in gas turbines and homogeneous charge compression ignition in internal combustion engines [2,3]. Given that the performance and safety of these combustion schemes are highly dependent on the chemical kinetics of fuel oxidation, it is imperative that these kinetics be well understood at relevant combustion device conditions ($P \sim 1$–40 atm, $T < 1100$ K) for air-dilute mixtures over a range of equivalence ratios [4–6]. Additionally, the high variability in syngas fuel composition and its potential effects on syngas combustion must be considered, as diverse combinations of H_2, CO, CH_4, CO_2, N_2, and other trace species such as Si, N, and S-based compounds are known to exist in real mixtures [7–9]. This variation is detailed in Table 1, which illustrates typical syngas composition in real industrial applications. As indicated by Glarborg [10], these impurities have the potential to drastically alter the reactivity and dominant chemical kinetic pathways of the fuel oxidation process.

* Corresponding Author at: 2350 Hayward St., Room 2293 G.G. Brown Building, Ann Arbor, MI 48109. USA.
E-mail addresses: amansfld@umich.edu (A.B. Mansfield), mswool@umich.edu (M.S. Wooldridge).

http://dx.doi.org/10.1016/j.combustflame.2015.01.026
0010-2180/© 2015 The Combustion Institute. Published by Elsevier Inc. All rights reserved.

While the chemical kinetics of basic syngas mixtures (hydrogen and carbon monoxide only) have been well studied, see Chaos and Dryer [4] and the references therein, there are few experimental investigations on the effects of impurities and constituent variation on the combustion of syngas mixtures. Mathieu et al. [12] measured the effects of variations in CH_4, CO_2, H_2O, and NH_3 content on auto-ignition delay using a shock tube at ~98% Ar dilution, $\varphi = 0.5$, $P = 2$–32 atm, $T = \sim 960$–1860 K. The results indicated that the addition of up to 0.16% CO_2, 0.22% H_2O, or 0.02% NH_3 by total mixture volume had negligible effect at all conditions, while the addition of up to 0.08% CH_4 increased the auto-ignition delay time by up to an order of magnitude. Additionally, Mathieu et al. [13] investigated the effects of several compounds on syngas auto-ignition delay time using numerical methods, considering the addition of up to 15% CH_4, 1.7% C_2H_6, 5.3% C_2H_4, 0.7% C_2H_2, 21.8% H_2O, and 15% CO_2 by total fuel volume for mixtures at air-dilution, $\varphi = 0.5$ and 1.0, $P = 1$–35 atm, $T = 900$–1400 K. The results of this work indicated that for all hydrocarbon (HC) species except C_2H_2 an increase in the auto-ignition delay time by a factor of two or more is expected, with the most significant magnitude change for $T > 1000$ K. Gersen et al. [14] measured the effects of variations in H_2, CO, and CH_4 content on auto-ignition delay times using a rapid compression machine at approximately air-dilution, $\varphi = 0.5$ and 1.0, $P = \sim 20$–80 bar, $T = \sim 900$–1100 K. The mole fraction of CH_4 in the fuel was varied from 0 to 1, for H_2 from 0 to 1, and for CH_4 from 0 to 0.5. The results showed that while the relative concentration of CO had minimal effect, increasing the concentration of H_2 significantly decreased auto-ignition delay time and increasing the concentration of CH_4 significantly increased this time at all conditions.

In addition to these studies, the effects of impurities on the combustion of pure hydrogen have been evaluated for several compounds. As syngas combustion chemistry is dominated by hydrogen kinetic pathways [4], it is likely that effects similar to these would also be observed for syngas mixtures. Mueller et al. [15] measured the effects of NO and NO_2 addition to pure hydrogen fuel on species mole fraction profiles in a flow reactor at ~1% fuel dilution, $\varphi = 1$–2, $P = \sim 0.5$–14 atm, $T = \sim 750$–850 K. The experimental results, as well as those from subsequent kinetic modeling, illustrated a promoting effect of both NO and NO_2, with order of magnitude decreases in "characteristic reaction times" predicted for 10–1000 ppm concentrations. Mathieu et al. [16] studied the effects of up to 1600 ppm H_2S addition by total mixture volume on auto-ignition delay times in a shock tube at ~98% Ar dilution, $\varphi = 0.5$, $P = 2$–35 atm, $T = \sim 960$–1860 K. The findings of that study illustrated an inhibiting effect, with increases in auto-ignition delay time of up to a factor of six. Petersen et al. [17] measured the effects of up to 0.046% silane (SiH_4) addition by total mixture volume on the auto-ignition delay times of pure hydrogen in a shock tube at ~98% Ar dilution, $\varphi = 1.0$, $P = \sim 1$ atm, $T = \sim 1000$–2250 K. The results indicate that the addition of ~1% SiH_4 to the fuel volume led to decreases in the auto-ignition delay time by a factor of two or more. This finding is in agreement with the previous study by McClain et al. [18] which indicated that increasing concentration of SiH_4 in an H_2 mixture significantly decreased auto-ignition delay times in a shock tube with ~air-dilution, $\varphi = 1.0$ and 0.5, for $P = \sim 1.5$ atm and $T = 800$–1050 K.

Overall, previous studies of the effects of impurities on syngas and hydrogen combustion are limited to a select few species and the results indicate that different species indeed yield varying ignition promoting and inhibiting effects. While the effects of an individual impurity vary, it is probable that impurities consisting of compounds with similar structures may lead to similar effects. This hypothesis is supported by the almost universal ignition inhibiting behavior of similar HC species, illustrated by the experimental and computational work of Mathieu et al. discussed above. With this in mind, the significant promoting effect of SiH_4 in H_2 mixtures is particularly interesting, considering the substantial and increasing concentrations of organic Si compounds in syngas derived from waste (landfills, waste digesters, or water treatment facilities) [9,19]. As detailed in Rasi et al. [9] and Pierce et al. [20] syngas from these sources contains both silanol {...Si–OH} and siloxane {...Si–O–Si...} species at up to 10–100 ppm concentrations. Common compounds include trimethylsilanol and decamethylcyclopentasiloxane, which make up a majority of the organic Si content within syngas from waste sources [9]. While the fouling tendencies of these and other organic Si species in combustion devices is well documented [19,20], their effect on combustion chemistry has not been investigated in any capacity. Considering the significant ignition promoting effects observed for a chemically similar compound, i.e. SiH_4, and the increasing concentrations of Si-based species in syngas, this lack of knowledge presents a significant barrier to the safe and effective implementation of this fuel.

The objective of the current study was to advance the understanding of the effects of impurities on the chemical kinetics of syngas oxidation, focusing on CH_4 and trimethylsilanol (TMS) impurities at thermodynamic and mixture conditions relevant to practical device operation. This objective was accomplished through an experimental investigation of auto-ignition delay times at lean, low-temperature, high-pressure conditions, using the University of Michigan Rapid Compression Facility (UM-RCF). Uniquely, high-speed imaging was utilized for each experiment, ensuring that only ideal homogeneous ignition behaviors were exhibited for the data reported here. This important diagnostic enabled testing at lower temperatures and pressures not possible in previous experimental studies by other investigators, thereby expanding knowledge of impurity effects to more practical conditions. The auto-ignition delay time and pressure time history measurements were compared to predictions made using typical zero-dimensional homogeneous reactor ignition modeling and the formaldehyde oxidation mechanism of Li et al. [21] (Li 2007 mechanism), used frequently to successfully predict syngas combustion [4,12,22]. This model was then used to interpret and analyze observed pressure time histories and impurity effects, in order to describe behavior trends and connect these with potential underlying chemical kinetic pathways.

Table 1
Typical syngas composition [7–9,11].

Component	% by Volume
H_2	25–30
CO	30–60
CO_2	5–15
H_2O	2–30
CH_4	0–5
N_2	0–4
Ar, N_2, H_2S, COS, NH_3, Ash	0–1
Trace Impurities (Fe, Cl, Si – species, Metals, etc.)	<100 ppm

2. Methods

2.1. Experimental methods

Ignition experiments were conducted for realistic syngas mixtures with fuel-to-oxygen equivalence ratio of $\varphi = 0.1$ and were air-dilute with N_2, i.e. molar O_2 to inert gas ratio of 1:3.76. In some cases, small amounts of the N_2 diluent gas were replaced by Ar and/or CO_2 to modify the test temperature. Four fuel mixtures were used, (1) pure syngas: 30% H_2, 70% CO fuel volume, (2) syngas with CH_4: 27% H_2, 67% CO, 6% CH_4, (3) pure syngas with 10 ppm TMS, and (4) pure syngas with 100 ppm TMS. Mixtures were designed to represent lean syngas mixtures used in the power

industry while spanning typical CH_4 concentrations [1,11] and typical TMS impurity concentrations observed by Rasi et al. [9] (~5 ppm). Considering the upward trend in organic Si species in waste-based syngas reported by Rasi et al. [9], the mixture containing 100 ppm TMS was selected to represent potential future concentrations. Ignition experiments were conducted at 5 and 15 atm for the broadest range of temperatures allowable in the UM-RCF for these mixtures (~1010–1110 K, based on experimental test times and associated uncertainties). While it was desirable to increase the equivalence ratio beyond the value chosen here, $\varphi = 0.1$, it was not possible to achieve homogeneous ignition behavior at the thermodynamic conditions of interest for higher values of φ. Please see Mansfield and Wooldridge [22] for a discussion of the state and syngas mixture conditions associated with homogeneous versus inhomogeneous ignition. A detailed tabulation of the gas mixture composition and thermodynamic state corresponding to each auto-ignition delay time measurement is given in the Supplemental material section.

Regarding the experimental apparatus, the UM-RCF is designed to create a gas volume with uniform thermodynamic conditions through an isentropic compression process. A detailed description of the UM-RCF and results of studies characterizing its performance can be found in Donovan et al. [23] and He et al. [24]. Briefly, the apparatus consists of a long cylinder, the Driven Section, in which a gas mixture is rapidly compressed by the motion of a free piston (Sabot). Prior to compression, the test volume is evacuated with a pump and then filled with a specific test gas mixture. Upon firing, the Sabot travels the length of the Driven Section compressing the test gas mixture into the Test Section – a small cylindrical volume located at the end of the Driven Section (~50 mm length and 50 mm diameter). As the Sabot reaches its final position near the Test Section, the Sabot achieves an annular interference fit, thereby sealing the test gas mixture in the Test Section. At this point, the Test Section is filled with a uniform and isentropically compressed test gas mixture at the desired initial thermodynamic condition. For this study, the Test Section was instrumented with a piezoelectric transducer (6125B Kistler, Amherst, NY) and charge amplifier (5010 Kistler, Amherst, NY) for pressure measurements, and a transparent polycarbonate end-wall to permit high-speed imaging of the ignition process. During each experiment the pressure time history was recorded using the pressure transducer at 100 kHz sampling frequency. The uncertainty in the pressure measurements is estimated as ⩽1% (~0.1 atm) considering both the signal-to-noise ratio in the post-ignition pressure time history data and the non-linearity limits defined by the manufacturer during the calibration process. High-speed color imaging was recorded using a digital video camera (V711-8G-MAG-C, Vision Research, Phantom) with a Navitar 50 mm lens (F0.95), a Hoya 62 mm lens (+2 zoom), and a Hoya 62 mm UV(0) filter. Video sequences were recorded at 25,000 frames/s with the CMOS array with resolution of 512 × 512 pixels, resulting in an exposure time of 39.3 μs.

All test gas mixtures were made using a dedicated stainless steel tank and the mixture composition was determined by measurement of the relative partial pressures of the components. After filling, the tank was continuously stirred by an internal mechanism and was left to mix for at least one hour before use. Error in the mixture composition is assumed to be negligible and have negligible effect on the ignition results, considering ~80–95% (mole basis) of the mixture is comprised of N_2 and O_2.

2.2. Computational methods

Auto-ignition delay time and pressure time history predictions were made using the constant volume adiabatic zero-dimensional homogeneous reactor model in the CHEMKIN software suite [25] with the Li 2007 chemical kinetic mechanism. This mechanism was used given previous success in predicting syngas ignition behavior [4,21,22] and because it includes CH_4 oxidation chemistry. Using this auto-ignition model, a corresponding auto-ignition delay time prediction was calculated for each ignition experiment in this study using the initial thermodynamic condition and mixture composition of the experiments. The auto-ignition delay time from the model predictions was defined as the time from the start of the calculation to the time when $dT(t)/dt$ was maximized. In some cases two inflection points were predicted in the temperature time history, indicating two "steps" of energy release during ignition. The occurrence of two-step auto-ignition corresponds well to the experimental observations and is discussed in detail below. Important to note is that TMS is not included in the Li 2007 mechanism and the authors are aware of no oxidation model which includes this species and associated combustion products. Therefore auto-ignition delay time predictions are presented only for experiments which used the pure syngas or syngas with CH_4 mixtures. For each prediction, quantified uncertainty bounds were calculated using the known uncertainty in the "A-factor" of the Arrhenius reaction rates for the four most sensitive reactions, $CO + O_2 = CO_2 + O$ (R21), $HO_2 + H = H_2 + O_2$ (R10), $H + O_2 = OH + O$ (R1) and $H + O_2 (+M) = HO_2 (+M)$ (R9). These were identified using OH sensitivity analysis conducted in the CHEMKIN software suite for the pure syngas mixture at $P = 15$ atm, and $T = 1066$ K. The results of the sensitivity analysis and the rate coefficients used are listed in Supplemental material.

3. Results

For each experiment in the UM-RCF, a pressure time history and a high-speed imaging video were recorded, allowing for the determination of auto-ignition delay times and direct observation of the auto-ignition behavior. A typical pressure time history during an ignition experiment for initial pressures of 15 and 5 atm can be seen in Figs. 1 and 2, respectively. Similar trends are observed for both experiments. The pressure initially increases during the compression stroke until the Sabot is seated at the end-of-compression (EOC) event, followed by a slight decrease in pressure due to heat transfer from the test gas volume into the cool Test Section walls, followed by a large and rapid increase in pressure during the ignition. For each experiment, the time and pressure were noted at the three distinct events: end-of-compression, minimum pressure (P_{min}), and maximum pressure (P_{max}), highlighted in Fig. 1. After filtering the pressure time history with a 75-point smoothing algorithm to reduce signal noise, the pressure and time value for each event were defined mathematically as a local maximum or mini-

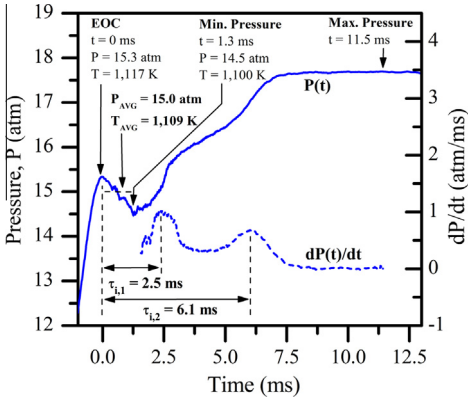

Fig. 1. Typical pressure time history, P(t), and time derivative of the pressure time history, dP(t)/dt, for experimental conditions exhibiting two-step ignition behavior; P = 15.0 atm, T = 1,109 K, φ = 0.1 for a pure syngas mixture; where $\tau_{i,1}$ and $\tau_{i,2}$ are the first and second auto-ignition delay times respectively.

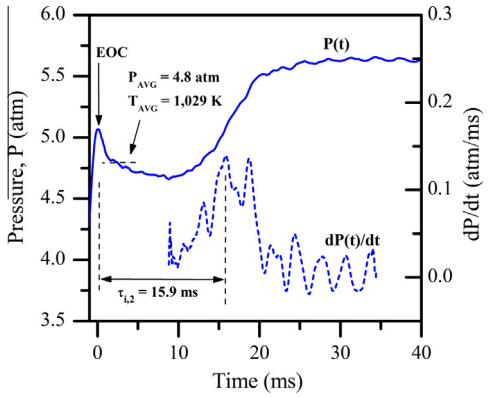

Fig. 2. Typical pressure time history, P(t), and time derivative of the pressure time history, dP(t)/dt, for experimental conditions exhibiting one-step ignition behavior; P = 4.8 atm, T = 1,029 K, φ = 0.1 for pure syngas mixture; where $\tau_{i,2}$ is the auto-ignition delay time.

mum respectively. The pressure data ($P(t)$) between P_{min} and P_{max} was then filtered a second time with a 100-point smoothing algorithm to further reduce signal noise, and the numerical derivative of the pressure time history ($dP(t)/dt$) was calculated using a center differencing scheme.

For each auto-ignition experiment a thermodynamic state was assigned representing the unburned isothermal isobaric condition at which the experiment was conducted. The gas temperature within the Test Section was calculated using thermodynamic relations as this temperature was not measured directly. As suggested by Lee and Hochgreb [26] and experimentally verified by Donovan et al. [23], the initial compression stroke and the post-compression expansion of the adiabatic core region in the UM-RCF are well represented as an isentropic compression process. Therefore, the initial uncompressed thermodynamic conditions were used in conjunction with isentropic state relations to calculate the temperature at both EOC and P_{min}. Propagation of the pressure measurement uncertainty of $\leqslant$1% through the isentropic state relations yields an uncertainty of $\leqslant$0.4% in the assigned temperature ($\sim$5 K). In most cases, there was no appreciable decrease in temperature between the EOC event and the ignition event (i.e. <10 K change from EOC to P_{min}), and so the EOC thermodynamic state represented the experiment well, and was assigned to the auto-ignition delay time measurement. For experiments with appreciable decrease in temperature (i.e. >10 K) between EOC and P_{min}, an average thermodynamic state was assigned in order to incorporate the effects of post-compression heat transfer. The average pressure was defined mathematically as the arithmetic mean of the pressure measured from EOC to P_{min} and the average temperature was calculated thereafter assuming an isentropic expansion from the thermodynamic state at the EOC event to the average pressure. Assignment of an average state in this manner has been successfully applied in numerous past experiments using the UM-RCF for similar syngas fuels [22,27]. As discussed in detail in Mansfield and Wooldridge [22], assignment of an average state allows for accurate incorporation of heat transfer effects while retaining critical clarity in reporting, vastly improving the archival value of the results as compared to the assignment of the EOC condition only.

For experiments with an initial pressure of 15 atm, seen in Fig. 1, trends in the dP/dt time history exhibited two peaks for all mixtures; one corresponding to each "step" of pressure rise during the ignition event. As evidenced, each step represents a region of rapid pressure rise and the two steps observed are separated by a region with a reduced rate of pressure rise. Two ignition delay times were therefore determined for each experiment that exhibited these features ($\tau_{i,1}$ and $\tau_{i,2}$) as the time from EOC to each peak in the dP/dt time history. The definitions are illustrated in Fig. 1.

For experiments with an initial pressure of 5 atm, as presented in Fig. 2, a single peak in dP/dt was observed for all mixtures and correspondingly one ignition delay time, $\tau_{i,2}$, was determined from each of these experiments. The most significant source of uncertainty associated with these auto-ignition delay time measurements is from the selection of the smoothing algorithm in the data filtering process. Uncertainty for each measurement was quantified by varying the number of points included in the initial filtering algorithm by ±50% and defining bounds for each measurement which spanned the resulting range of auto-ignition delay times calculated. In the vast majority of cases the uncertainty in the measured auto-ignition delay time was <1%; though, in a few select cases 20–35% uncertainty was observed, likely the result of a convolution of the auto-ignition event with an artifact in the pressure time history. Uncertainty bounds in the assigned temperature values were also calculated in this manner, as variation in the smoothing algorithm parameters affects the selection of key pressure values (EOC, P_{min}, P_{max}) used to calculate the temperature. While in most cases the temperature uncertainty was less than the previously defined value of $\sim$5 K, in certain cases the uncertainty exceeded this value. A tabulated list of all experimental results, including calculated uncertainty bounds for the auto-ignition delay time measurements and assigned temperatures, is provided in the Supplemental material section.

A frame from the typical high-speed imaging results of chemiluminescence during syngas auto-ignition is shown in Fig. 3. As seen, homogeneous ignition is indicated by the spatial uniformity of the chemiluminescence emission. For each experiment the high-speed imaging results were reviewed to confirm that only homogeneous ignition occurred. This ensured that all characteristics of the pressure time history correspond to global phenomena (chemical kinetics and heat transfer), which are well represented by a zero-dimensional homogeneous reactor model. As illustrated in detail by Mansfield and Wooldridge [22], the effects of localized ignition phenomena can significantly impact the accurate interpretation of pressure time history results for syngas fuel and so avoiding these behaviors was critical in the present work.

3.1. Auto-ignition delay times at 5 and 15 atm

Figures 4a and 4b illustrate the auto-ignition delay time measurement results for the second ($\tau_{i,2}$) and first ($\tau_{i,1}$) steps of the ignition at 15 atm. Overall the results for both steps illustrate

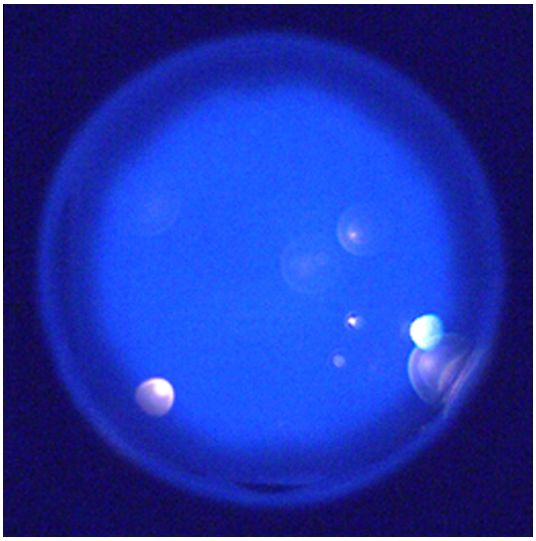

Fig. 3. Single frame from high-speed imaging of typical ignition behavior within Test Section, illustrating homogeneous chemilluminescence, for the pure syngas mixture at experimental conditions P = 4.6 atm, T = 1052 K, φ = 0.1.

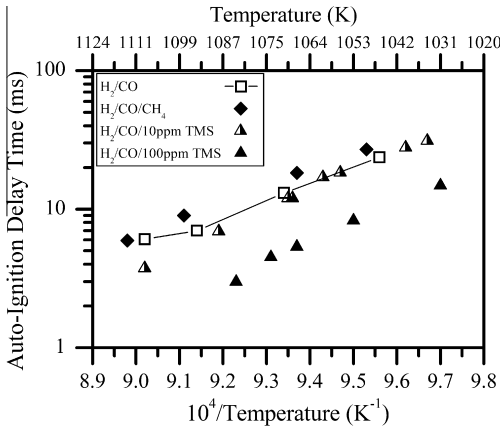

Fig. 4a. Measured auto-ignition delay time of the second step of ignition ($\tau_{i,2}$) as a function of inverse temperature for P = 15 atm. The solid line is provided for visual reference to the pure syngas data. Uncertainty bounds of the auto-ignition measurements and temperatures are the limits of the post-processing algorithm filtering parameters, and are not visible on this scale.

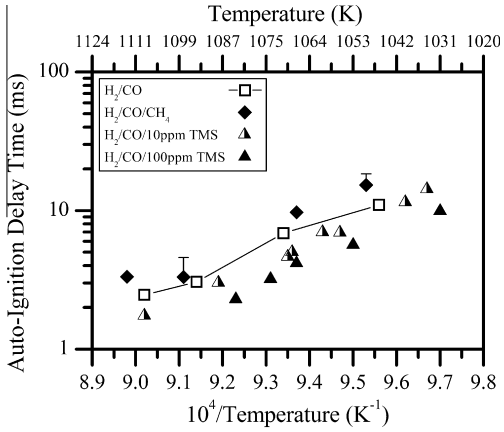

Fig. 4b. Measured auto-ignition delay time of the first step of ignition ($\tau_{i,1}$) as a function of inverse temperature for P = 15 atm. Uncertainty bounds of the auto-ignition measurements and temperatures are the limits of the post-processing algorithm filtering parameters. The solid line is provided for visual reference to the pure syngas data.

excellent repeatability and consistent trends throughout the temperature range evaluated. The data demonstrate TMS can be added to the syngas mixtures in a controlled and consistent manner in the present experimental system, an important verification considering that this compound has not been tested in any known previous combustion experiment. The effects of CH_4 and TMS impurity addition are in trend wise agreement between the first and second auto-ignition delay times, generally with CH_4 inhibiting and TMS promoting ignition, though the magnitude of the impact is more pronounced for $\tau_{i,2}$. The generally observed inhibiting effects for the syngas with CH_4 mixture are in agreement with previous findings by Gersen et al. [14] and Mathieu et al. [12] who also observed this outcome.

Regarding the results for $\tau_{i,2}$ shown in Fig. 4a, it is apparent that the addition of CH_4 consistently increases the auto-ignition delay time relative to the pure syngas mixtures by ~40%. Conversely, the addition of TMS causes a decrease in the auto-ignition delay times, with magnitude dependent on both the concentration and the initial temperature. For 10 ppm TMS addition, significant effects are only observed at $T > 1060$ K, at which point the auto-ignition delay time is reduced by ~30%. For 100 ppm TMS addition, there is a drastic impact on the measurements, with consistent 50–70% decrease in the auto-ignition delay time across all temperatures. Regarding the results for $\tau_{i,1}$ shown in Fig. 4b, it is apparent that the addition of CH_4 consistently increases the auto-ignition delay time measurement by 40–50%. Again, the addition of TMS results in a reduction in measured auto-ignition delay times; where 10 ppm addition leads to a consistent 10–30% reduction, and 100 ppm leads to a consistent 45–50% reduction. As the effect of 10 ppm and 100 ppm TMS addition was similar for $\tau_{i,1}$, but drastically different for $\tau_{i,2}$, this suggests that the second step of the ignition process is more sensitive to this impurity. Conversely, the difference between $\tau_{i,1}$ and $\tau_{i,2}$ remains approximately constant at ~5 ms for both pure syngas and syngas with CH_4 across all conditions.

Figure 5 illustrates the auto-ignition delay time measurement results ($\tau_{i,2}$) for 5 atm initial pressure. Again, the results indicate excellent repeatability and consistent trends throughout the temperature range. Recall that the uncertainty bounds of the temperature assignments are the limits of the post-processing filtering algorithm parameters. The effects of CH_4 and TMS generally agree with those at 15 atm, with CH_4 inhibiting and TMS promoting ignition, but the magnitudes of the impact differ. It is apparent that the addition of CH_4 has minimal impact below 1050 K, though at higher temperatures the auto-ignition delay time is increased by up to a factor of 3. While the apparent activation energy (the slope of the auto-ignition delay time as a function of the inverse temperature) decreases as temperature decreases for all other mixtures, the apparent activation energy for the syngas with CH_4 mixture does not change as a function of temperature. For 10 ppm TMS addition, there is no significant effect on the auto-ignition delay time; whereas for 100 ppm TMS addition, there is a consistent 20–30% decrease in the auto-ignition delay time. Interestingly, as the temperature increases to ~1070 K, the auto-ignition delay time appears to be increasingly less sensitive to addition of 100 ppm of TMS or CH_4, suggesting that the effects of these impurities at these mole fraction levels are negligible at temperatures above this value. This may be the result of reductions in the magnitude of the auto-ignition delay times at these conditions, as compared to lower temperatures and higher pressures.

3.2. Pressure dependence

As demonstrated in the figures above, the effect of TMS addition on the auto-ignition delay time is highly pressure dependent, with significantly larger magnitude impact at 15 atm. Figure 6 illustrates the auto-ignition delay time measurements for the second step of the ignition process ($\tau_{i,2}$) at both 5 and 15 atm for the pure syngas and syngas with TMS mixtures. Regarding the

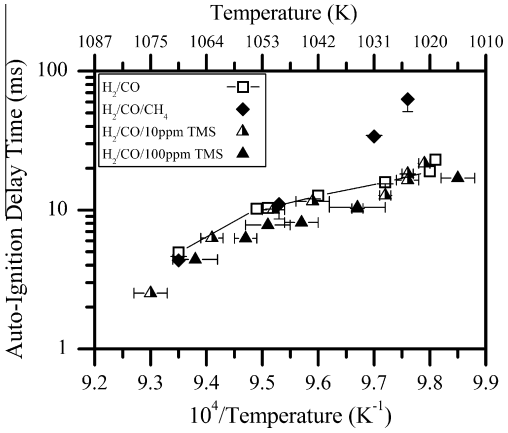

Fig. 5. Measured auto-ignition delay time ($\tau_{i,2}$) as a function of inverse temperature for P = 5 atm. Uncertainty bounds of the auto-ignition measurements and temperatures are the limits of the post-processing algorithm filtering parameters. The solid line is provided for visual reference to the pure syngas data.

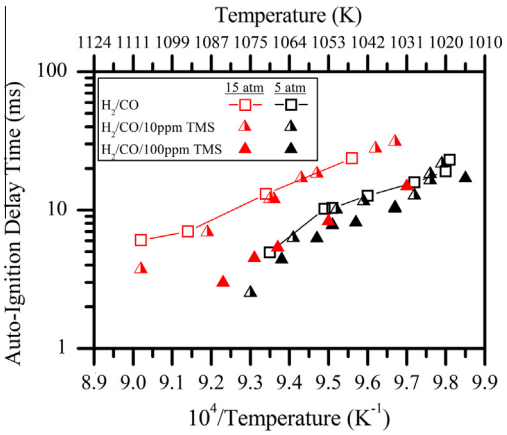

Fig. 6. Measured auto-ignition delay time of the second step of ignition ($\tau_{i,2}$) as a function of inverse temperature for P = 5 and 15 atm for pure syngas and syngas with TMS mixtures. The solid lines are provided for visual reference to the pure syngas data. Uncertainty bounds of the auto-ignition measurements and temperatures are the limits of the post-processing algorithm filtering parameters, and are not visible on this scale.

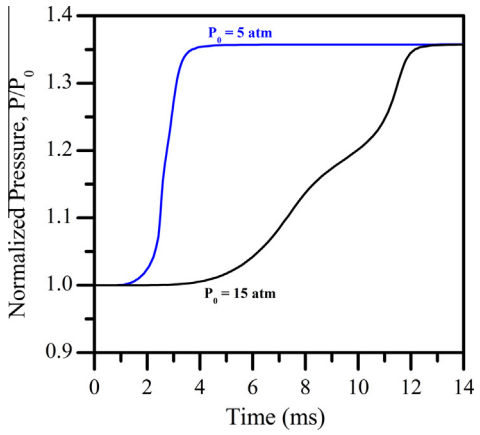

Fig. 7. Typical predicted pressure time histories, normalized by the initial pressure, for P = 5 atm and 15 atm, T = 1066 K, and the pure syngas mixture.

pressure dependence of the auto-ignition delay time, there is a dependence for the pure syngas mixture illustrated in Fig. 6, with increases in ignition delay time of up to 100% as the pressure is increased from 5 to 15 atm at the same temperature. This behavior is indeed expected as the increase in pressure corresponds to a shift to slower HO_2 and H_2O_2 dominated chemical kinetic pathways [28]. While 10 ppm TMS addition has minimal impact on this pressure dependence, it is evident that 100 ppm TMS addition reduces the pressure dependence of the auto-ignition delay time to nearly zero. As this pressure dependence is likely closely related to HO_2 and H_2O_2 dominant chemistry, this suggests that the promoting effect of TMS is related to interaction with these species.

Remarkably, similar significant reduction in both auto-ignition delay times and the pressure dependence of the auto-ignition delay time was reported by both Petersen et al. [17] and McLain et al. [18] for SiH_4 addition to pure H_2 mixtures. Jachimowski and McLain [29] postulated that this decrease in pressure dependence was due to HO_2 radical scavenging by SiH_4, promoting H_2O_2 and subsequently OH formation, though these claims have not been evaluated experimentally.

3.3. Comparison with kinetic model predictions

As previously mentioned, predictions for auto-ignition delay times of pure syngas and syngas with CH_4 were made using the Li 2007 mechanism and the homogeneous reactor model in CHEMKIN. For all 15 atm experiments, the kinetic model accurately predicted the existence of a two-step ignition process; whereas, for 5 atm the kinetic model predicted single step ignition in most cases, though two-step ignition in rapid succession (<1 ms separation) was predicted for some conditions. This is not in disagreement with the measurements at 5 atm however, as the resolution of the experiment, due to the data smoothing process, is insufficient to accurately observe two ignition steps in such immediate occurrence. Typical pressure time history results (normalized by the initial pressure for clarity in the comparison) from simulations with initial conditions $P = 5$ and 15 atm, $T = 1066$ K, using the pure syngas mixture are seen in Fig. 7. These results demonstrate the relationship between the initial pressure and the time between first and second ignition steps; where for 15 atm the ignition steps are separated by ~4 ms, and for 5 atm, the separation is <1 ms.

Figures 8 and 9 illustrate the measured and predicted auto-ignition delay times for 15 and 5 atm, respectively. Recall the uncertainty bounds of the predictions are the effect of the uncertainty

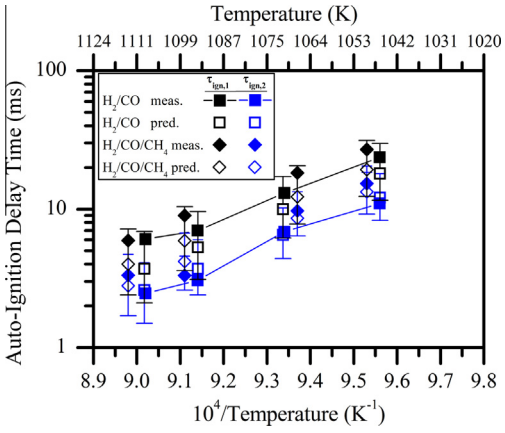

Fig. 8. Measured and predicted auto-ignition delay times ($\tau_{i,1}$ and $\tau_{i,2}$) as a function of inverse temperature for P = 15 atm, for pure syngas and syngas with CH_4. Uncertainty bounds of the predictions are the effect of the uncertainty in the rate coefficient of reactions R1 and R9 add two.

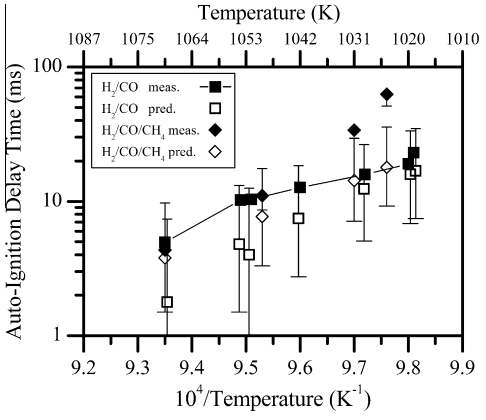

Fig. 9. Measured and predicted auto-ignition delay time ($\tau_{i,2}$) as a function of inverse temperature for P = 5 atm, for pure syngas and syngas with CH_4. Uncertainty bounds of the predictions are the effect of the uncertainty in the rate coefficient of reactions R1 and R9 add two.

in the rate coefficient of reactions R21, R10, R1, and R9. As seen in Fig. 8, predictions for all temperatures, both mixtures, and both $\tau_{i,1}$ and $\tau_{i,2}$, are in excellent agreement with the measurements at 15 atm. Likewise, as illustrated in Fig. 9, predictions for both mixtures for all temperatures at 5 atm are in very close agreement with the experimental data except for the syngas with CH_4 mix-

ture. Predictions for this mixture at temperatures below ~1040 K are faster than the measurements and outside the uncertainty bounds. While this may suggest error in the Li 2007 kinetic mechanism, these data correspond to the lowest temperatures and longest auto-ignition delay times, therefore it is possible that the slight disagreement is the result of more pronounced heat transfer effects not sufficiently captured by the model. Overall the evidence in Figs. 7–9 shows the system is well represented by the Li 2007 chemical kinetic reaction mechanism and a homogeneous reactor physical model, importantly allowing for more the detailed chemical kinetic analysis discussed below.

4. Discussion

4.1. Two-step ignition behavior

The experimental results of the present work illustrates the existence of a two-step ignition process for experiments with 15 atm initial pressure, embodied by two distinct regions of heat release and corresponding pressure rise. Furthermore, model predictions indicate that near 5 atm, two-step ignition is likely occurring though the steps are in such rapid succession that it is not possible to observe a separation in time experimentally. The existence of this two-step ignition behavior for syngas fuel mixtures has not been previously reported, although similar behavior is evident in the pressure time history results of Kéromnès et al. [30] and Kalitan et al. [31]. As the auto-ignition delay time is often defined as the time where dP/dt is maximized, it is possible that in these and other previous studies multi-step ignition behavior was observed but only a single auto-ignition delay time was reported. Additionally, given that historical combustion experiments were conducted primarily near atmospheric pressures, according to Chaos and Dryer [4] and the references therein, it is possible that significant two-step ignition was not exhibited for a majority of these lower pressure studies.

As demonstrated above, the two-step nature of the ignition process was well predicted by the Li 2007 kinetic mechanism in the CHEMKIN reactor model. It was therefore possible to use this model in more detail, to probe trends in two-step behavior across various conditions as well as its chemical kinetic foundations. Of particular interest was the dependence of this behavior on initial pressure. Additionally, given the highly variable nature of syngas mixture composition, understanding how this two-step ignition behavior is affected by constituent variation, e.g. the ratio of H_2:CO, is also important. In order to evaluate the effects of these factors, simulations were conducted for a range of initial thermodynamic state and mixture conditions. Illustrated in Fig. 10 are predicted pressure time histories for syngas mixtures with P = 5 and 15 atm, T = 1066 K, for air-dilute mixtures with φ = 0.1, and variable H_2:CO (molar ratio) of 1:3, 1:1, 3:1, 1:0. Note that the pressure values are normalized by the initial unburned value for comparative clarity. Considering these predictions, it is evident that the occurrence of two-step ignition behavior is strongly dependent on both the initial pressure and the molar ratio of H_2 to CO. Noticeably, significant two-step ignition behavior is not apparent at 5 atm for these conditions; however, the addition of CO does impact the rate of pressure rise during the ignition event, with increasing amounts of CO yielding lower pressure rise rates. This is in excellent agreement with the experimental findings of the present work, and indeed supports the notion that previous studies of syngas near atmospheric conditions would likely not observe two-step ignition behavior. In contrast, at 15 atm two-step ignition behavior, indicated by two distinct regions of differing rate of pressure rise, is apparent for all mixtures except pure H_2. At this higher pressure both the relative magnitude of pressure rise from the second step and the time separation between first and second steps of the ignition process are increased with CO. Remarkably, at 15 atm and the highest CO concentration there is a marked increase in the time of energy release during both first and second steps of the ignition process as compared to the other conditions evaluated. For example, at 5 atm and H_2:CO = 1:1, the heat release and corresponding pressure rise from initial to final states occurs over <1 ms; whereas, for 15 atm and H_2:CO = 1:3 the same relative pressure rise occurs over more than 10 ms. In a practical application, two-step heat release and ignition behavior of this significance could have a marked impact on system performance if not appropriately considered.

The effect of equivalence ratio on two-step ignition behavior was also investigated computationally, in order to assess the impact of such behaviors at a mixture condition more directly relevant to combustor operation. Illustrated in Fig. 11 are simulated pressure time histories for syngas mixtures with P = 15 atm, T = 1066 K, for air-dilute mixtures with φ = 0.1–1.0, and H_2:CO (-molar ratio) of 3:1. The pressure, temperature and H_2:CO conditions were selected for further study as they exhibited the most pronounced two-step behavior in Fig. 10. As in Fig. 10 the pressure values in Fig. 11 are normalized by the initial unburned value for comparative clarity. It is evident that the magnitude of two-step ignition behavior is strongly related to the equivalence ratio, with pronounced separation between first and second stages for φ = 0.1–0.15, and negligible separation for higher values. This is further support of the notion that two-step ignition behaviors were not observed in previous studies, as previous studies tended to focus on higher equivalence ratio conditions.

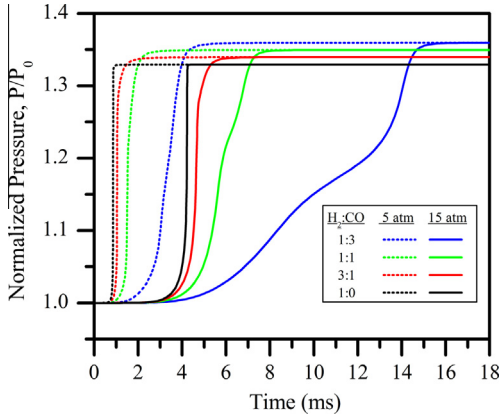

Fig. 10. Predicted pressure time histories, for P = 5 and 15 atm, T = 1066 K, and syngas at φ = 0.1, H_2:CO (molar ratio) = 0:1, 1:3, 1:1, 3:1, 1:0, air-dilute with N_2.

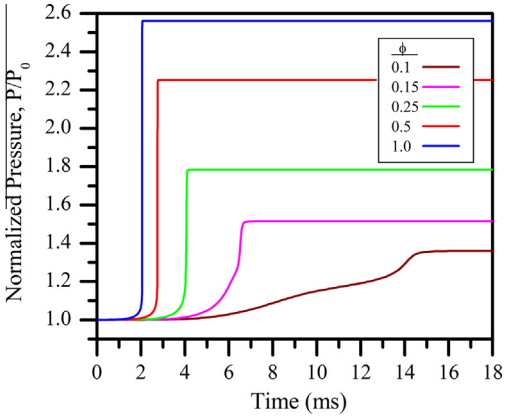

Fig. 11. Predicted pressure time histories, for P = 15, T = 1066 K, and syngas at φ = 0.1–1.0, H_2:CO (molar ratio) = 3:1, air-dilute with N_2.

The relationship between two-step ignition behavior and both the initial pressure and molar ratio of H_2:CO for syngas mixtures implies that these factors are important to the chemical kinetic foundations of this behavior. Regarding these foundations, it was desirable to develop an understanding of the root causes of two-step ignition behavior in syngas fuels. To accomplish this, the kinetic model was once more utilized to predict mole fraction time histories for both major and radical species during the ignition process. This simulation was conducted for the pure syngas mixture used in the present experimental work at $P = 15$ atm, $T = 1066$ K; a condition which exhibits significant two-step ignition. Illustrated in Fig. 12 are predicted mole fraction time histories at this condition, which reveal the stepped behavior in the pressure time history is reflected in the mole fraction time histories of both major and radical species. As evidenced in Fig. 12a, during the first step of the ignition process both H_2 and CO are consumed, correspondingly forming H_2O and CO_2. When the H_2 supply is essentially exhausted, the rate of pressure rise decreases and the rate of CO consumption remains nearly constant. This reduction in pressure rise rate is expected, as the total rate of fuel consumption decreases when H_2 is no longer significantly available. The rate of pressure rise continues at this reduced magnitude until after some time the remaining CO is rapidly consumed and a significantly larger rate of pressure rise occurs. This second rapid rise in pressure forms the second step in the pressure time history. Shown in Fig. 12b are the major radical species formed during the two-step ignition process. The simulation indicates H_2O_2 and HO_2 radicals dominate the first step of the ignition process, as predicted by Chaos et al. [28] and mentioned earlier; however, OH and O radicals dominate the second step of the ignition process.

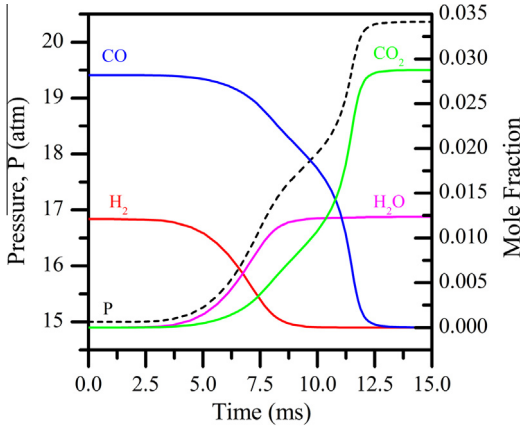

Fig. 12a. Predicted pressure and major species mole fraction time histories for P = 15 atm, T = 1066 K, and the pure syngas mixture.

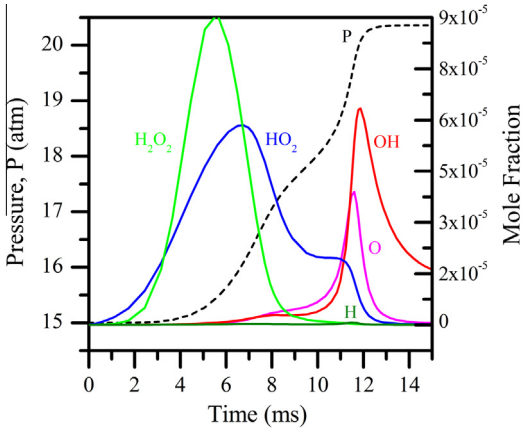

Fig. 12b. Predicted pressure and radical species mole fraction time histories for P = 15 atm, T = 1066 K, and the pure syngas mixture.

As to the chemical kinetic foundation for two-stepped ignition behavior, the question is therefore what causes the delay in rapid CO oxidation characteristic of the second step of the ignition process? Rate-of-production analysis for CO at this condition, shown in the Supplemental material, importantly indicates that nearly all CO is consumed via the reaction $CO + OH = CO_2 + H$ (R23). This finding, in addition to the radical mole fraction time history results in Fig. 12b, suggests that the delay in rapid CO oxidation is likely related to a corresponding delay in the formation of OH. Rate-of-production analysis was therefore performed for OH, which is also shown in the Supplemental material. Results of that analysis indicate that $H_2O_2 (+M) = OH + OH (+M)$ (R15) dominates the formation of OH during the first step of the ignition process. Once the H_2 supply is nearly exhausted at the end of the first step of the ignition, the dominant formation reactions then change to primarily $H + O_2 = OH + O$ (R1) and $O + H_2O = OH + OH$ (R4). As discussed in detail by Chaos et al. [28] and Mansfield and Wooldridge [22], $H + O_2 = OH + O$ (R1) is in direct competition with $H + O_2 (+M) = HO_2 (+M)$ (R9), and the corresponding formation rate of OH is highly dependent on both pressure and temperature. Considering the competition of these reactions, as pressure is increased and/or temperature decreased the rate of OH production diminishes significantly. It is therefore likely that the pressure dependence of OH production from reactions R1 and R13 during the time after the first step of the ignition is the underlying foundation for the dependence of two-step ignition behavior on pressure. In other words, when pressure is increased, the rate of OH production after the first step of the ignition process is slowed and more time is required to build the OH radical pool to a sufficient level for rapid CO oxidation. This results in a more pronounced two-step ignition behavior as the first and second steps are separated by more time. Competition between reactions R1 and R13 can also explain the dependence of two-step ignition behavior on the H_2:CO molar ratio. This ratio will affect the temperature at the end of the first step of the ignition process, with more H_2 yielding a higher temperature. The increased temperature will lead to an increased rate of OH formation and correspondingly will decrease the time between first and second steps of the ignition. Furthermore, the dependence of two-step ignition behavior on equivalence ratio can be related to these reactions, as an increase in fuel concentration will also increase the availability of OH radicals.

Overall the results of both the experimental investigation and chemical kinetic analysis of the present work illustrate an important yet often overlooked characteristic of syngas mixtures: features of multi-stage heat release. With this in mind, the method of reporting a single auto-ignition delay time, as traditionally done for syngas mixtures, misses information important to understanding the combustion kinetics of these fuels. The approach of reporting both the first and second auto-ignition delay times is an important improvement in capturing this multi-stage behavior. Other methods for reporting could include more characteristics such as magnitude and rates of pressure rise, which may further increase the value and accuracy of similar experimental data. Note the magnitude of the effects of multi-stage heat release is convolved with the volume and heat transfer characteristics of the test section of the experimental apparatus. The amount of energy transferred to the test gases during the combustion process is directly affected by the amount of energy lost to the cool test section walls and/or expended in compressing the cool boundary layer gas volume. Consequently, care should be used when comparing multi-step ignition data from different facilities.

4.2. Inhibiting effect of CH_4

The experimental results of the present work illustrate a pressure dependent inhibiting effect of CH_4 on the auto-ignition of syngas, which is well predicted by the Li 2007 kinetic mechanism and the CHEMKIN reactor model. The inhibition effect and the trend in pressure dependence are both in excellent agreement with the findings by Mathieu et al. [12], who suggested that $CH_4 + OH = CH_3 + H_2O$ (R49) was the primary reaction through which CH_4 inhibits syngas auto-ignition (identified using sensitivity analysis). Uniquely, experimental results in the present work indicate that while $\tau_{i,1}$ and $\tau_{i,2}$ are increased by the addition of CH_4, the magnitude of their difference is consistent with that for pure syngas. This suggests that the CH_4 acts primarily on the kinetics during the first step of the ignition at the present concentration. In order to evaluate this hypothesis, the CHEMKIN reactor model was once more utilized. Illustrated in Fig. 13 are predicted mole fraction time histories for the syngas with CH_4 mixture at $P = 15$ atm, $T = 1066$ K for the major species. Additionally, the predicted pressure traces for both the pure syngas and syngas with CH_4 are included for comparison. As seen in the figure, the ignition proceeds in a very similar manner as predicted for pure syngas. Interestingly though, CH_4 is consumed completely along with H_2 during the first step of the ignition. Furthermore, OH rate-of-production analysis for this mixture, shown in the Supplemental material, indicates that CH_4 scavenges OH during the first step of the ignition process via $CH_4 + OH = CH_3 + H_2O$ (R49) and $CH_2O + OH = CHO + H_2O$ (R38). After the first step of ignition, however, there is no major consumption of OH by CH_4 or related intermediates. The predicted pressure time history results also indeed illustrate a lengthening in the time of the first step of the ignition process by ~2 ms for the mixture with CH_4, though the time from the end of the first step to the second step remains approximately constant at ~3 ms. Therefore, the modeling results strongly support the notion that the effect of CH_4 impurity addition at this concentration is to directly increase $\tau_{i,1}$ through OH scavenging while minimally affecting the kinetics of the second step of the ignition process. The experimentally observed effect on $\tau_{i,2}$ is therefore likely the result of delayed heat release from the first step of the ignition process. It is possible that by increasing the relative concentration of CH_4 that its inhibition effects would extend to the second step of the ignition process, though that was not evaluated here. Overall these results again highlight the importance of comprehensively considering the multi-step ignition process, as impurities can affect the driving chemical kinetics of each step differently.

Comparison of predicted pressure time history results for each mixture illustrates a decrease in the maximum post-combustion pressure by ~0.15 atm for the mixture with CH_4. This can be explained by a reduction in the total heat of reaction (H_R) from 2.61 to 2.38 kcal/mol for the total mixture when changing from the pure syngas to the mixture with CH_4. The specific heat capacity values are not significantly different between the two mixtures.

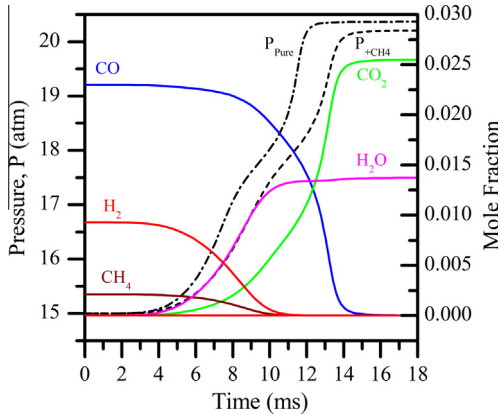

Fig. 13. Predicted pressure and major species mole fraction time histories, for P = 15 atm, T = 1066 K, and the syngas with CH_4 mixture. The predicted pressure time history for the pure syngas mixture is also included, to illustrate the predicted effect of CH_4 addition.

4.3. Promoting effect of TMS

As previously mentioned, no chemical kinetic mechanism currently exists which includes trimethylsilanol and the expected intermediate species during its oxidation. In order to evaluate the possible chemical kinetic foundations of the observed effects of TMS addition, a perturbation study was conducted using the CHEMKIN reactor model with a pure syngas fuel mixture. The perturbations were designed to explore the potential effects of the TMS impurity on the high pressure formation pathways of OH. Both Jachimowski and McLain [29] and Petersen et al. [17] suggested that SiH_4 disrupts the formation and/or enhances the consumption of HO_2 thus boosting OH production rates at high pressures. Given the effects of TMS closely resemble those of SiH_4 addition, it is possible that the kinetic foundations of the ignition promoting effect for TMS are related to changes in the same reaction pathways.

In the current work, two perturbations to the computational model were considered, which was conducted at $P = 5$ and 15 atm, $T = 1066$ K, for the pure syngas mixture. In the first, HO_2 consumption was boosted by increasing the A-factor of the reaction $HO_2 + HO_2 = H_2O_2 + O_2$ (R14) by up to 10^2 times, and in the second perturbation, HO_2 formation was inhibited by decreasing the A-factor of $H + O_2 (+M) = HO_2 (+M)$ (R9) by up to 10^{-3} times. The ranges were chosen to encompass limiting behaviors in the predicted trends of the auto-ignition delay times. Results of the model analysis, shown in the Supplemental material, indicate that indeed reductions in both auto-ignition delay time ($\tau_{i,2}$) and in the pressure dependence of the auto-ignition delay time can be achieved by modifying these reactions in the manner described. However, the magnitude of the decrease in the pressure dependence and the precise trends in the auto-ignition delay times observed experimentally are not well captured. This is expected because replicating the precise trends would likely require accurate inclusion of TMS and several additional Si-based intermediate species in the chemical kinetic mechanism. While the creation of such a mechanism may improve quantitative accuracy of the prediction of auto-ignition delay time, mechanism development was beyond the scope of the present work. Regardless, the modeling results presented here are important in that they support the notion that the effect of TMS is indeed likely related to HO_2 kinetic pathways, in good qualitative agreement with previous assertions for the similar Si-based impurity, SiH_4.

5. Conclusions

This work represents a unique investigation on the effects of common yet understudied impurities on the combustion of syngas fuel at thermodynamic conditions relevant to practical combustion devices, providing not only the first direct observations of sometimes drastic effects, but also highlighting trends in behavior that may extend beyond the specific compounds evaluated in the present work. Studies such as this are vital to the safe and effective application of real syngas or other high-hydrogen content fuels, especially when used in modern high-pressure low-temperature combustion strategies like dry low-NO_x.

The results of the present experimental work uniquely illustrate the occurrence of two-step ignition behavior at higher pressures, with two distinct regions of heat release and pressure rise. First

and second auto-ignition delay times ($\tau_{i,1}$ and $\tau_{i,2}$) were therefore defined and interestingly the times were affected differently by the addition of CH_4 and TMS impurities. Modeling results suggest the occurrence and magnitude of two-step ignition behavior can be explained by highly pressure and temperature dependent OH kinetics, which can cause a delay between H_2 and CO oxidation thus creating two distinct steps in the ignition process. Trends identified using this model illustrate that two-step ignition behavior becomes more prominent with increasing pressure, increasing relative concentration of CO, and decreasing equivalence ratio.

The addition of CH_4 consistently increased both $\tau_{i,1}$ and $\tau_{i,2}$ up to 40% at 15 atm, while increasing delay times at 5 atm by a factor of 3 only for $T < \sim 1050$ K. Model analysis suggests this inhibiting effect is due to OH scavenging primarily via the $CH_4 + OH = CH_3 + H_2O$ (R49) reaction, which acts to slow the first step of the ignition process. Conversely, the addition of TMS consistently decreased the auto-ignition delay times, with the magnitude of the effect related to the TMS concentration and the initial pressure. 10 ppm TMS impurity addition caused a minimal effect on $\tau_{i,2}$ at both 5 and 15 atm and a consistent decrease of ~10–30% in $\tau_{i,1}$ at 15 atm. The effect of 100 ppm TMS impurity addition was much more drastic, with consistent decreases of 50–70% in $\tau_{i,2}$ and 45–50% in $\tau_{i,1}$ at 15 atm and 20–30% reduction in $\tau_{i,2}$ at 5 atm. Furthermore, the pressure dependence of the auto-ignition delay time, typically causing up to 100% increase as pressure increased from 5 to 15 atm, was virtually eliminated for the 100 ppm TMS mixture. Kinetic modeling suggests that these ignition promoting effects are related to enhanced consumption and/or reduced production of HO_2, though the precise chemical kinetic effects cannot be resolved with existing kinetic mechanisms. The drastic effects of TMS have significant safety implications, as pronounced early ignition can lead to catastrophic failures. Furthermore, the upward trend in organic Si content in syngas mixtures and the current movement toward higher pressure combustion systems means consideration of these effects is of increasing importance.

The impact of TMS addition observed here is remarkably similar to that for SiH_4 in pure H_2 made in previous investigations. This suggests a possible trend for Si-based species to promote auto-ignition in syngas and hydrogen mixtures. Such a trend may facilitate an extension of the findings in the present results beyond SiH_4 and TMS, to other Si-based species commonly present in syngas fuel. Important to note, however, is that this extension is limited by the lack of understanding as to the exact mechanism for ignition promotion. Because of this, it is not immediately apparent if siloxane compounds, for instance, will necessarily have a promoting effect due to their Si content alone, or whether their alternative structure will lead to other effects. Therefore, the evaluation of siloxanes impurities in syngas mixtures is an excellent opportunity for future work.

Acknowledgments

The authors acknowledge the generous support of the U.S. Department of Energy via the National Energy Technology Laboratory, Award Number DE-FE0007465 and the Department of Mechanical Engineering at the University of Michigan.

Appendix A. Supplementary material

Supplementary data associated with this article can be found, in the online version, at http://dx.doi.org/10.1016/j.combustflame.2015.01.026.

References

[1] United States Department of Energy, "Hydrogen from Coal Program – Research, Development, and Demonstration Plan," 2014. <http://www.netl.doe.gov/research/coal/energy-systems/fuels/hydrogen-rd>.
[2] US Department of Energy, "Advanced Turbine Research Program, <http://www.netl.doe.gov/research/coal/energy-systems/turbines/advanced-research>," 2014. <http://www.netl.doe.gov/research/coal/energy-systems/turbines/advanced-research>.
[3] G.A. Richards, M.M. McMillian, R.S. Gemmen, W.A. Rogers, S.R. Cully, Prog. Energy Combust. Sci. 27 (2001) 141–169.
[4] M. Chaos, F.L. Dryer, Combust. Sci. Technol. 180 (2008) 1053–1096.
[5] G.A. Lavoie, J. Martz, M. Wooldridge, D. Assanis, Combust. Flame 157 (2010) 1106–1110.
[6] T. Lieuwen, V. McDonell, D. Santavicca, T. Sattelmayer, Combust. Sci. Technol. 180 (2008) 1169–1192.
[7] C.L. Miller, D.C. Cicero, M.A. Ackiewicz, Hydrogen from coal program: research, development, and demonstration plan for the period 2007 through 2016, Department of Energy, National Energy Technology Laboratory, 2007.
[8] J. Ciferno, J. Marano, Benchmarking biomass gasification technologies for fuels, chemicals and hydrogen production, Department of Energy, National Energy Techology Laboratory, 2002.
[9] S. Rasi, J. Lehtinen, J. Rintala, Renew. Energy 35 (2010) 2666–2673.
[10] P. Glarborg, Proc. Combust. Inst. 31 (2007) 77–98.
[11] R. Jones, N. Shilling, IGCC Gas Turbines for Refinery Applications, GE Power Syst., Schenectady, NY, 2003.
[12] O. Mathieu, M.M. Kopp, E.L. Petersen, Proc. Combust. Inst. 34 (2012) 3211–3218.
[13] O. Mathieu, E.L. Petersen, A. Heufer, N. Donohoe, W. Metcalfe, H.J. Curran, F. Güthe, G. Bourque, J. Eng. Gas Turbines Power 136 (2013).
[14] S. Gersen, H. Darmeveil, H. Levinsky, Combust. Flame 159 (2012) 3472–3475.
[15] M. Mueller, R. Yetter, F. Dryer, Int. J. Chem. Kinet. 31 (1999) 705–724.
[16] O. Mathieu, F. Deguillaume, E.L. Petersen, Combust. Flame 161 (2013) 23–36.
[17] E. Petersen, D. Kalitan, M.A. Rickard, J. Propuls, Power 20 (2004) 665–674.
[18] A. McLain, C. Jachimowski, R. Rogers, Ignition of SiH4-H2-O2-N2 behind reflected shock waves, NASA Technical Paper 2114, February, 1983.
[19] E. Wheless, J. Pierce, Siloxanes in landfill and digester gas update, in: Proc. 27th SWANA Landfill Gas Symp. San Antonio, TX, 2004.
[20] J. Pierce, Siloxane quantification, removal, and impact on landfill gas utilization facilities, in: 8th Annual LMOP Conference and Project Expo, 2005.
[21] J. Li, Z. Zhao, A. Kazakov, M. Chaos, F.L. Dryer, J.J. Scire, Int. J. Chem. Kinet. 39 (2007) 109–136.
[22] A.B. Mansfield, M.S. Wooldridge, Combust. Flame 161 (2014) 2242–2251.
[23] M.T. Donovan, X. He, B.T. Zigler, T.R. Palmer, M.S. Wooldridge, A. Atreya, Combust. Flame 137 (2004) 351–365.
[24] X. He, B.T. Zigler, S.M. Walton, M.S. Wooldridge, A. Atreya, Combust. Flame 145 (2006) 552–570.
[25] CHEMKIN 10101. Reaction Design, San Diego, 2010.
[26] D. Lee, S. Hochgreb, Int. J. Chem. Kinet. 30 (1998) 385–406.
[27] S.M. Walton, X. He, B.T. Zigler, M.S. Wooldridge, Proc. Combust. Inst. 31 (2007) 3147–3154.
[28] M. Chaos, M.P. Burke, Y. Ju, F.L. Dryer, in: T. Lieuwen, V. Yang, R. Yetter (Eds.), Gas Synthesis Combustion, Fundamentals and Applications, CRC Press, Boca Raton, FL, 2009, pp. 29–70.
[29] C. Jachimowski, A. McLain, A chemical kinetic mechanism for the ignition of silane/hydrogen mixtures, NASA Technical Paper 2129, 1983.
[30] A. Kéromnès, W.K. Metcalfe, K.a. Heufer, N. Donohoe, A.K. Das, C.-J. Sung, J. Herzler, C. Naumann, P. Griebel, O. Mathieu, M.C. Krejci, E.L. Petersen, W.J. Pitz, H.J. Curran, Combust. Flame 160 (2013) 995–1011.
[31] D.M. Kalitan, J.D. Mertens, M.W. Crofton, E.L. Petersen, J. Propuls, Power 23 (2007) 1291–1303.

This article was downloaded by: [141.212.136.175]
On: 13 May 2015, At: 06:34
Publisher: Taylor & Francis
Informa Ltd Registered in England and Wales Registered Number: 1072954 Registered office: Mortimer House, 37-41 Mortimer Street, London W1T 3JH, UK

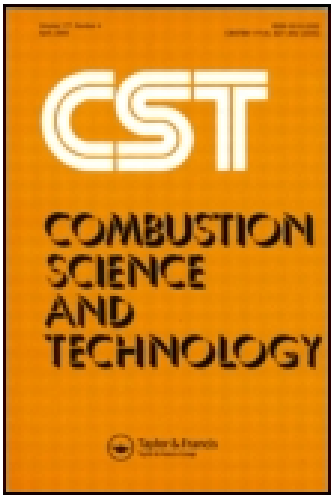

CrossMark
Click for updates

Combustion Science and Technology
Publication details, including instructions for authors and subscription information:
http://www.tandfonline.com/loi/gcst20

A Regime Diagram for Autoignition of Homogeneous Reactant Mixtures with Turbulent Velocity and Temperature Fluctuations

Hong G. Im[a], Pinaki Pal[b], Margaret S. Wooldridge[bc] & Andrew B. Mansfield[b]

[a] Clean Combustion Research Center, King Abdullah University of Science and Technology, Thuwal, Saudi Arabia

[b] Department of Mechanical Engineering, University of Michigan, Ann Arbor, Michigan, USA

[c] Department of Aerospace Engineering, University of Michigan, Ann Arbor, Michigan, USA

Accepted author version posted online: 02 Apr 2015.

To cite this article: Hong G. Im, Pinaki Pal, Margaret S. Wooldridge & Andrew B. Mansfield (2015) A Regime Diagram for Autoignition of Homogeneous Reactant Mixtures with Turbulent Velocity and Temperature Fluctuations, Combustion Science and Technology, 187:8, 1263-1275, DOI: 10.1080/00102202.2015.1034355

To link to this article: http://dx.doi.org/10.1080/00102202.2015.1034355

PLEASE SCROLL DOWN FOR ARTICLE

Taylor & Francis makes every effort to ensure the accuracy of all the information (the "Content") contained in the publications on our platform. However, Taylor & Francis, our agents, and our licensors make no representations or warranties whatsoever as to the accuracy, completeness, or suitability for any purpose of the Content. Any opinions and views expressed in this publication are the opinions and views of the authors, and are not the views of or endorsed by Taylor & Francis. The accuracy of the Content should not be relied upon and should be independently verified with primary sources of information. Taylor and Francis shall not be liable for any losses, actions, claims, proceedings, demands, costs, expenses, damages, and other liabilities whatsoever or howsoever caused arising directly or indirectly in connection with, in relation to or arising out of the use of the Content.

This article may be used for research, teaching, and private study purposes. Any substantial or systematic reproduction, redistribution, reselling, loan, sub-licensing, systematic supply, or distribution in any form to anyone is expressly forbidden. Terms &

Conditions of access and use can be found at http://www.tandfonline.com/page/terms-and-conditions

Downloaded by [] at 06:34 13 May 2015

Combust. Sci. Technol., 187: 1263–1275, 2015
Copyright © Taylor & Francis Group, LLC
ISSN: 0010-2202 print / 1563-521X online
DOI: 10.1080/00102202.2015.1034355

Taylor & Francis
Taylor & Francis Group

A REGIME DIAGRAM FOR AUTOIGNITION OF HOMOGENEOUS REACTANT MIXTURES WITH TURBULENT VELOCITY AND TEMPERATURE FLUCTUATIONS

Hong G. Im,[1] Pinaki Pal,[2] Margaret S. Wooldridge,[2,3] and Andrew B. Mansfield[2]

[1]*Clean Combustion Research Center, King Abdullah University of Science and Technology, Thuwal, Saudi Arabia*

[2]*Department of Mechanical Engineering, University of Michigan, Ann Arbor, Michigan, USA*

[3]*Department of Aerospace Engineering, University of Michigan, Ann Arbor, Michigan, USA*

A theoretical scaling analysis is conducted to propose nondimensional criteria to predict weak and strong ignition regimes for a compositionally homogeneous reactant mixture with turbulent velocity and temperature fluctuations. This leads to a regime diagram that provides guidance on expected ignition behavior based on the thermo-chemical properties of the mixture and the flow/scalar field conditions. The analysis extends the original Zeldovich's theory by combining the turbulent flow and scalar characteristics in terms of the characteristic Damköhler and Reynolds numbers of the system, thereby providing unified and comprehensive understanding of the physical and chemical mechanisms controlling autoignition. Estimated parameters for existing experimental measurements in a rapid compression facility show that the regime diagram predicts the observed ignition characteristics with good fidelity.

Keywords: Ignition regimes; Scaling analysis; Temperature fluctuations; Weak/strong ignition

Downloaded by [] at 06:34 13 May 2015

INTRODUCTION

Towards clean and efficient energy utilization, new strategies in combustion devices for both automotive and stationary applications operate using lean, nearly homogeneous reactant mixtures at boosted pressure and preheated conditions. These include aircraft engines operating at higher inlet temperatures (Lieuwen and Yang, 2013), low temperature combustion engines (Lavoie et al., 2010), and stationary gas turbines using lean premixed combustion (US DOE, 2009), among many examples. Under these conditions, autoignition often becomes a dominant process for burning. As such, accurate prediction of autoignition characteristics—the ignition delay times as well as the entire evolution of

Received 17 December 2014; revised 11 February 2015; accepted 23 March 2015.

Address correspondence to Hong G. Im, Clean Combustion Research Center, Al-Kindi (West), Thuwal 23955-6900, Saudi Arabia. E-mail: hong.im@kaust.edu.sa

Color versions of one or more of the figures in the article cn be found online at www.tandfonline.com/gcst.

the fuel consumption behavior—is of paramount importance in successful implementation of the combustion systems.

Historically, the subject of autoignition and slow versus rapid combustion has been extensively studied in the context of detonation and explosion research. Earlier experimental studies of shock-induced ignition reported distinct ignition behavior, referred to as the "weak" and "strong" ignition regimes, for which the importance of the ignition delay time sensitivity, $d\tau_{ig}/dT$, was recognized (Meyer and Oppenheim, 1971; Oran and Boris, 1982; Oran et al., 1982). It was found that the $d\tau_{ig}/dT$ iso-lines serve as a rational criterion to distinguish the different ignition regimes. A theoretical study by Zeldovich (1980) proposed criteria for ignition regimes, classified as detonation, spontaneous propagation, and normal flame. The issue of premature ignition by local hot spots within a shock tube has also been revisited in recent studies (Javed et al., 2015; Uygun et al., 2014).

Recognizing the general interest in fundamental characterization of autoignition phenomena, the present study was further motivated by the recent research activities on combustion of coal-derived syngas in gas turbines as a new strategy for clean utilization of coal (US DOE, 2009). Due to the high flame temperatures and NO_x emissions associated with high hydrogen content fuels like syngas, a common combustion strategy is to operate in the lean premixed mode (Richards et al., 2001). In such conditions, combustion stability depends more highly on autoignition characteristics (Lieuwen et al., 2008). As for the autoignition characteristics of syngas mixtures at typical gas turbine operating conditions (20 bar and above), a compilation of recent experimental and computational studies was reported in Petersen et al. (2007), showing a wide range of discrepancies between measurements and predictions based on homogeneous adiabatic calculations with detailed chemistry, especially at low temperature ($<$1000 K) conditions.

Subsequently, a number of studies followed in order to identify the main cause of such discrepancies. Experimental studies using rapid compression facilities (RCF) reported a possibility that the discrepancies may be attributed to the non-uniform temperature and mixture fields arising from wall heat loss and flow vortex generation (Mittal et al., 2006; Walton et al., 2007). A recent study by Mansfield and Wooldridge (2014) conducted imaging experiments of syngas autoignition within an RCF, and reported an early phase front propagation, called the "weak" ignition regime, at low temperature conditions. They also confirmed that the ignition delay in such conditions is significantly shorter, by several factors, than the corresponding homogeneous ignition delay prediction. A pressure-temperature diagram was provided to distinguish between the weak and strong ignition regimes. Moreover, several criteria to identify the transition between weak and strong ignition regimes were evaluated, including the criterion by Zeldovich (1980). The modified formula proposed by Sankaran et al. (2005), based (in part) on the ignition delay time sensitivity, $d\tau_{ig}/dT$, was found to reproduce the experimentally observed trends very well. To corroborate experimental findings, Ihme and co-workers (Ihme, 2012; Wu and Ihme, 2014) used simple one- and two-dimensional models to demonstrate that the presence of turbulent fluctuations can lead to significant ignition advancement. These recent series of findings have led to a consensus in the community that scalar non-uniformities are the likeliest causes of the discrepancies between zero-dimensional modeling and the experimental autoignition delay time data (Dryer et al., 2014).

Considering the established significance of thermal and compositional nonuniformities on autoignition characteristics, the main objective of the present work is to extend the understanding to develop a rational criterion to predict the conditions associated with the different autoignition regimes for general turbulent mixing conditions. To this end,

Downloaded by [] at 06:34 13 May 2015

the diagrams shown in the experimental studies (Mansfield and Wooldridge, 2014; Meyer and Oppenheim, 1971), which focused on a regime criterion solely based on chemical characteristics of the ignition sensitivity, are not sufficient; such a criterion lacks other potentially important information about the level of scalar fluctuations that trigger the front initiation and propagation.

To elaborate further, the Zeldovich criterion (Zeldovich, 1980), which was further refined and demonstrated by Sankaran et al. (2005), defines the nondimensional number, Sa, as:

$$\mathrm{Sa} = \beta \frac{S_L}{S_{sp}} = \beta S_L \left| \frac{d\tau_{ig}}{dT} \nabla T \right|, \quad \beta = 0.5 \tag{1}$$

where S_L is the laminar flame speed, $S_{sp} = \left| \frac{d\tau_{ig}}{dT} \nabla T \right|^{-1}$ is the spontaneous ignition front propagation speed, and τ_{ig} is the ignition delay time for the homogeneous mixture at the average or bulk temperature. The factor $\beta < 1$ reflects the fact that sufficiently rapid spontaneous front propagation is needed in order to ensure strong ignition. Hereinafter, Eq. (1) will be referred to as the Zeldovich–Sankaran criterion. The ignition regime criterion predicts a weak ignition if $\mathrm{Sa} > 1$, as the deflagration front dominates the ignition behavior, and strong ignition if $\mathrm{Sa} < 1$, in which case the spontaneous ignition process dominates. Therefore, it is evident that the ignition regimes are determined by the ignition delay sensitivity ($d\tau_{ig}/dT$) and the temperature distribution (∇T), which is determined by the scalar field distribution. In RCF and shock tube autoignition studies of syngas, thermal gradients on the order of 5 K/mm are expected (Mansfield and Wooldridge, 2014); however, systematic studies of the effects of flow and scalar field fluctuations are needed to expand the predictive regime diagram to realistic combustion devices where much larger temperature gradients can be expected.

This study presents a theoretical scaling analysis to extend the regime criterion in terms of nondimensional parameters that are commonly used in characterizing turbulent combustion systems. In the following, the relevant physical quantities are identified and simplifying assumptions are introduced. Subsequent derivations of relevant scaling relations then lead to the ignition regime criterion with turbulent combustion parameters. The predicted regime diagram is then validated by the evaluation of the conditions encountered in experimental measurements.

PROBLEM DEFINITION AND ASSUMPTIONS

Figure 1 shows a schematic of the problem under consideration and important characteristic quantities. The length scales include the chamber length, L, the integral eddy scale, ℓ, the Taylor microscale, λ, and the deflagration flame thickness, δ_f. In general, ℓ is considered a fraction of L, and λ/ℓ scales with the turbulent Reynolds number as will be discussed later. The laminar flame speed, S_L, and the root mean square (RMS) turbulent velocity fluctuation at the integral scale, u', are important velocity scales that will be compared to the other relevant velocities to be determined later. For the scaling analysis, the following simplifications and assumptions are made:

1. Weak ignition is primarily caused by front propagation originating from small-scale local temperature fluctuations, with a length scale typically of an order of mm or less,

Downloaded by [] at 06:34 13 May 2015

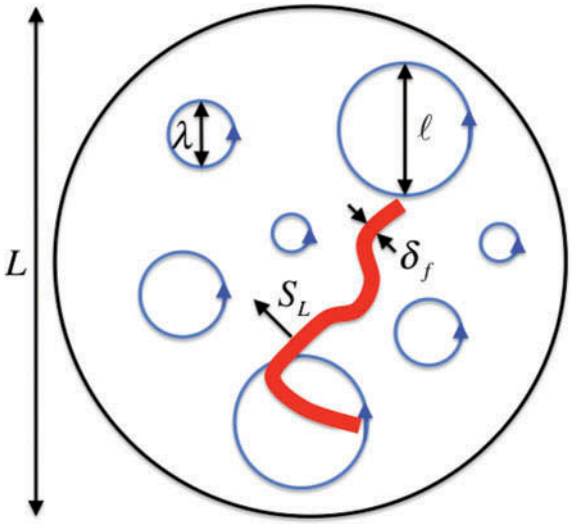

Figure 1 A schematic of a combustion chamber with various physical length scales.

Downloaded by [] at 06:34 13 May 2015

such as local hot spots, and the effects of large scale bulk temperature gradients, such as gradients caused by wall heat losses, are not considered. This is based on the experimental observations that early stage ignition kernels are often generated in the interior of the combustor, not necessarily near the wall region.

2. The mixture composition is homogeneous, and only the temperature fluctuations are considered. The scales of initial temperature and velocity fluctuations are comparable and correlated.
3. The Prandtl number of the mixture is unity, so that combined with assumption 2, the dissipation of temperature fluctuations is mainly driven by turbulent flows. This implies that the time and length scales for turbulent velocity and scalar fields are the same (i.e., the Batchelor scale is identical to the Kolmogorov scale).

To characterize the turbulent velocity and scalar fields, key nondimensional parameters are introduced. Following the framework of Liñán and Williams (1993), a rational way to characterize turbulent combustion systems is to use the turbulent Reynolds number, which represents the intensity of turbulence, and the characteristic turbulent Damköhler number, which represents the intensity of chemical reaction. For the integral scale eddy whose velocity, length, and time scales are characterized by u', ℓ, $\tau_\ell = \ell/u'$, respectively, the turbulent Reynolds number is defined as:

$$\mathrm{Re}_\ell = \frac{u'\ell}{\nu} \tag{2}$$

where ν is the kinematic viscosity of the bulk mixture gas. As for the measure of the chemical intensity, two ignition Damköhler numbers are defined as:

$$\mathrm{Da}_\ell = \frac{\tau_\ell}{\tau_{ig}} \tag{3}$$

which is referred to as the *integral* Damköhler number, and

$$\mathrm{Da}_\lambda = \frac{\tau_{\lambda_T}}{\tau_{ig}} \tag{4}$$

is referred to as the *mixing* Damköhler number, where τ_{ig} is the ignition delay time for the homogeneous reactant mixture at the bulk temperature, τ_{λ_T} is the mixing time scale associated with the Taylor microscale for the temperature field, λ_T. The mixing time scale and the Taylor microscale are determined in terms of the RMS temperature fluctuation, T', and the mean temperature dissipation rate, $2\alpha\widetilde{|\nabla T|^2}$, written as:

$$\tau_{\lambda_T} = \frac{T'^2}{\alpha\widetilde{|\nabla T|^2}}, \quad \lambda_T^2 = \frac{T'^2}{\widetilde{|\nabla T|^2}} \tag{5}$$

In analogy with those of the Taylor microscales for velocities:

$$\tau_\lambda = \frac{u'^2}{\nu\widetilde{\left|\partial u_j/\partial x_j\right|^2}}, \quad \lambda^2 = \frac{u'^2}{\widetilde{\left|\partial u_j/\partial x_j\right|^2}} \tag{6}$$

Based on assumption 3, it follows that the mixing time and length scales for temperature are interchangeable with those for turbulent velocities, such that:

$$\tau_{\lambda_T} = \tau_\lambda, \quad \lambda_T = \lambda \tag{7}$$

SCALING ANALYSIS

The main objective of the scaling analysis is to derive an expression for the Zeldovich–Sankaran criterion in terms of the characteristic Reynolds and Damköhler numbers. Recalling from the theory of homogeneous turbulence (Tennekes and Lumley, 1972), the scaling relation yields:

$$\frac{\lambda}{\ell} = \mathrm{Re}_\ell^{-1/2}, \quad \frac{\tau_\lambda}{\tau_\ell} = \frac{\lambda/u'_\lambda}{\ell/u'} = \frac{\lambda}{\ell}\frac{u'}{u'_\lambda} = \left(\frac{\lambda}{\ell}\right)^{2/3} = \mathrm{Re}_\ell^{-1/3} \tag{8}$$

It follows that

$$\mathrm{Da}_\lambda = \frac{\tau_{\lambda_T}}{\tau_{\mathrm{ig}}} = \frac{\tau_\lambda}{\tau_{\mathrm{ig}}} = \frac{\tau_\ell}{\tau_{\mathrm{ig}}}\frac{\tau_\lambda}{\tau_\ell} = \mathrm{Da}_\ell\,\mathrm{Re}_\ell^{-1/3} \tag{9}$$

The significance of Da_λ is that it is the ratio of the characteristic temperature dissipation time to the characteristic ignition delay time at the bulk mean temperature. Therefore, if $\mathrm{Da}_\lambda < 1$, the temperature fluctuations are dissipated before ignition occurs, thus it is unlikely to exhibit the weak ignition behavior triggered by reaction front propagation.

The next step is to extend the Zeldovich–Sankaran criterion, Eq. (1), to turbulent conditions. To this end, it is assumed that the occurrence of the hot-spot-induced pre-ignition is proportional to the statistical mean temperature gradient, such that

Downloaded by [] at 06:34 13 May 2015

$$\mathrm{Sa} \approx \beta S_L \left| \frac{d\tau_{ig}}{dT} \right| |\widetilde{\nabla T}| \tag{10}$$

where it is estimated that

$$|\widetilde{\nabla T}| \approx \frac{T'}{\lambda_T} \approx \frac{T'}{\lambda} = \frac{T'}{\ell \mathrm{Re}_\ell^{-1/2}} \tag{11}$$

Therefore, Eq. (10) is written as:

$$\mathrm{Sa} \approx \beta S_L \left| \frac{d\tau_{ig}}{dT} \right| \frac{T'}{\ell} \mathrm{Re}_\ell^{1/2} = \beta \left(\frac{S_L}{\delta_f} \right) \left(\frac{\delta_f}{\ell} \right) T' \left| \frac{d\tau_{ig}}{dT} \right| \mathrm{Re}_\ell^{1/2} \tag{12}$$

which includes the length scale ratio, δ_f/ℓ, where δ_f is the characteristic flame thickness. Following Liñán and Williams (1993):

$$\begin{aligned} \frac{\delta_f}{\ell} &= \mathrm{Re}_\ell^{-1/2} \mathrm{Da}_{\ell,f}^{-1/2} = \mathrm{Re}_\ell^{-1/2} \left(\frac{\tau_\ell}{\tau_f} \right)^{-1/2} = \mathrm{Re}_\ell^{-1/2} \left(\frac{\tau_\ell}{\tau_{ig}} \right)^{-1/2} \left(\frac{\tau_{ig}}{\tau_f} \right)^{-1/2} \\ &= \mathrm{Re}_\ell^{-1/2} \mathrm{Da}_\ell^{-1/2} \left(\frac{\tau_{ig}}{\tau_f} \right)^{-1/2} \end{aligned} \tag{13}$$

where it is noted that the integral Damköhler number in Liñán and Williams (1993) was defined differently from Eq. (3) above, and was based on the flame time scale, $\tau_f = \delta_f/S_L$. Therefore, the factor τ_{ig}/τ_f must be included. Combining Eqs. (12) and (13), the turbulent ignition regime criterion can be written as:

$$\mathrm{Sa} = K \mathrm{Da}_\ell^{-1/2}, \quad K = \beta \left(\frac{T'}{\left(\tau_f \tau_{ig}\right)^{1/2}} \right) \left| \frac{d\tau_{ig}}{dT} \right| \tag{14}$$

where K is referred to as the normalized thermal ignition sensitivity. In comparison with the laminar version in Eq. (1), $S_L |\nabla T|$ has now been expressed as $\left(T'/\tau^*\right) \mathrm{Da}_\ell^{-1/2}$ through the dimensional scaling, with a *reduced* time scale, $\tau^* = \left(\tau_f \tau_{ig}\right)^{1/2}$. The final ignition regime criterion becomes:

$$\begin{cases} \mathrm{Da}_\ell < K^2 : \text{ weak ignition} \\ \mathrm{Da}_\ell > K^2 : \text{ strong ignition} \end{cases} \tag{15}$$

As discussed with Eq. (9), an additional condition of $\mathrm{Da}_\lambda = \mathrm{Da}_\ell \, \mathrm{Re}_\ell^{-1/3} > 1$ needs to be satisfied to ensure weak ignition, since otherwise the temperature fluctuations are likely to dissipate away before the front forms. Finally, $\mathrm{Da}_\ell < 1$ would ensure an even stronger mixing scenario, since eddies at all scales would have time scales shorter than the ignition delay time, such that all temperature fluctuations would be dissipated and only strong ignition would be expected.

Downloaded by [] at 06:34 13 May 2015

THE REGIME DIAGRAM AND DISCUSSION

Compiling the above scaling analysis leads to the regime diagram as shown in Figure 2. The autoignition processes in nearly homogeneous mixtures with turbulent fluctuations are characterized in the Da–Re space, to represent the relative chemical and turbulence intensities determined by the chemistry, thermodynamics, and turbulent transport in the gas mixture. It is shown that the primary factor to determine the ignition regime is Da_ℓ, while Re_ℓ modifies the conditions further.

First, for a given Re_ℓ, the Zeldovich–Sankaran criterion indicates that the weak/mixed ignition regime is possible for $1 < \mathrm{Da}_\ell < K^2$. If $\mathrm{Da}_\ell > K^2$, then the reactant mixture is either too reactive (small τ_{ig}) or the mixture ignition characteristics are not sensitive to the temperature fluctuations (small $d\tau_{ig}/dT$), such that the entire mixture ignites almost at the same time despite some level of temperature fluctuations. This is referred to as the *reaction–dominant* strong ignition regime. On the other hand, if $\mathrm{Da}_\ell < 1$, then the turbulent mixing is rapid (small τ_ℓ), such that the temperature fluctuations are dissipated before the local ignition takes place. In contrast to the $\mathrm{Da}_\ell > K^2$ case, this is referred to as the *mixing–dominant* strong ignition regime. Note that the K parameter includes the ignition delay sensitivity, which is more than just a time-scale characterization, and depends strongly on the ignition chemistry of the specific fuel.

Between the limits $1 < \mathrm{Da}_\ell < K^2$, weak ignition is possible; however, the mixing Damköhler number, Da_λ, provides an additional criterion for this region of the regime diagram. Considering that the dynamics of turbulent mixing and dissipation are commonly

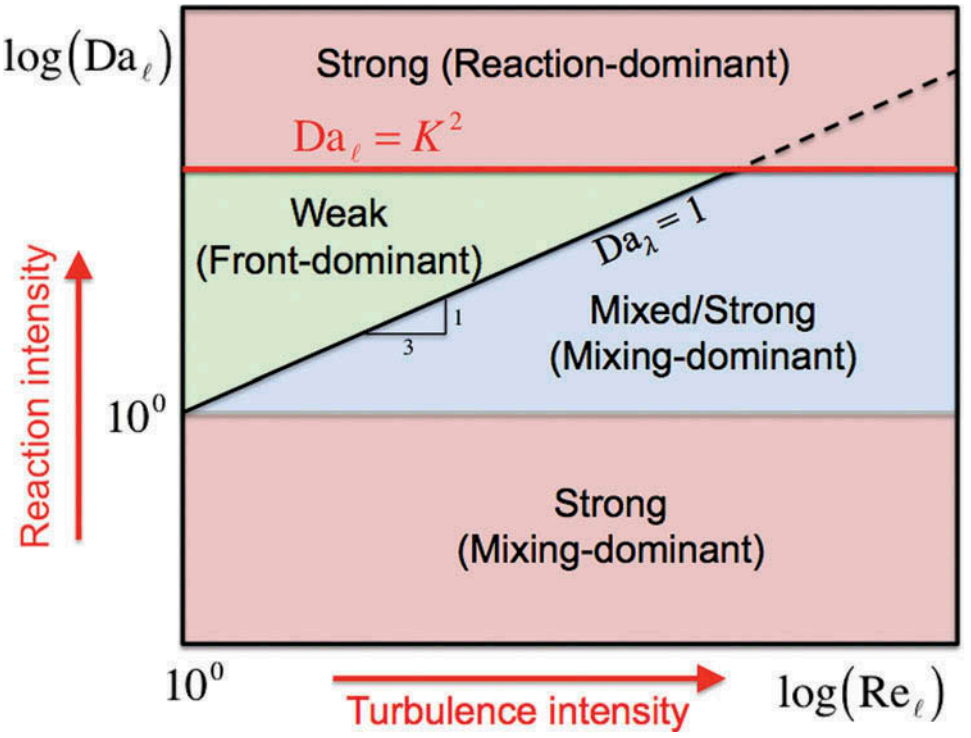

Figure 2 Regime diagram for strong and weak ignition for nearly homogeneous reactant mixture with temperature fluctuations.

Downloaded by [] at 06:34 13 May 2015

characterized by the Taylor scale, λ, a proper criterion to determine the mixing–dominant strong ignition would be the ratio of the Taylor mixing time, τ_λ, to the ignition time, τ_{ig}. Therefore, the $\mathrm{Da}_\lambda = 1$ condition serves as a more refined criterion within the limits of $1 < \mathrm{Da}_\ell < K^2$ to further identify the boundary between the weak and strong ignition regimes. Considering Eq. (9), this line appears on the regime diagram with a slope of 1/3, indicating that the occurrence of weak ignition phenomena will become less likely as the turbulent Reynolds number of the mixture increases. Still, the conditions between $\mathrm{Da}_\lambda < 1$ and $\mathrm{Da}_\ell > 1$ are a "grey" zone, in that some mixed mode ignition in which a mild level of front propagation followed by a strong ignition may occur. This is denoted as the *mixing–dominant mixed/strong* ignition regime.

The regime diagram serves as a qualitative guidance to the expected ignition behavior. The appropriate autoignition regime can be identified given the knowledge of the thermo-chemical properties of the mixture (e.g., pressure, temperature, reaction chemistry, etc.), and the characteristic turbulent flow parameters (e.g., Reynolds number, turbulence/scalar fluctuation intensity, etc.). If the initial condition of the mixture falls into the weak ignition or mixed/strong ignition regimes, then large discrepancies in the ignition delay prediction against the measured data can be expected and must be treated carefully.

To validate that the proposed regime diagram predicts the ignition characteristics in actual systems, the experimental data for syngas autoignition by Mansfield and Wooldridge (2014) are processed and plotted on the regime diagram, as shown in Figure 3. The homogeneous ignition delay times are computed using CHEMKIN (Kee et al., 1989) calculations with the detailed reaction mechanism by Li et al. (2007). The experimental conditions, the types of the observed ignition behavior, and the corresponding regime diagram parameters are provided in Table 1. The turbulence parameter estimation was difficult, as no detailed measurements of flow field fluctuations were available, as is often the case with many ignition experiments. Therefore, estimations were made based on the reported mean velocity and a presumed level of turbulence intensity at 1%, turbulence integral length scale, $\ell \sim 0.4L$ (where L is the dimension of the combustion chamber), and a temperature fluctuation, $T' \sim 10$ K. Since the K^2 line also depends on the physicochemical parameters of the mixture, each experimental data point yields a separate horizontal line on the regime diagram.

Figures 3a and 3b show a compilation of selected data points corresponding to the strong and weak ignition behavior, respectively. Although not all available data points are shown for clarity, it was confirmed that most of the data points represented ignition behavior consistent with the regime diagram. While there are some uncertainties in the parameter estimations (especially those related to turbulent fluctuations), the experimental data points mapped on the regime diagram are found to be in very good agreement with the proposed theory. More experimental data with detailed flow field measurements will be needed to validate the theoretical prediction for a wide range of device and mixture conditions.

CONCLUDING REMARKS

A theoretical scaling analysis was conducted to develop a regime diagram to predict weak and strong ignition regimes for a compositionally homogeneous reactant mixture with turbulent temperature fluctuations. The diagram provides guidance on expected ignition behavior based on the thermo-chemical properties of the mixture and the flow/scalar field conditions. The analysis is an extension of the previous studies by Zeldovich (1980) and Sankaran et al. (2005) to combine the turbulent flow and scalar characteristics in terms

Downloaded by [] at 06:34 13 May 2015

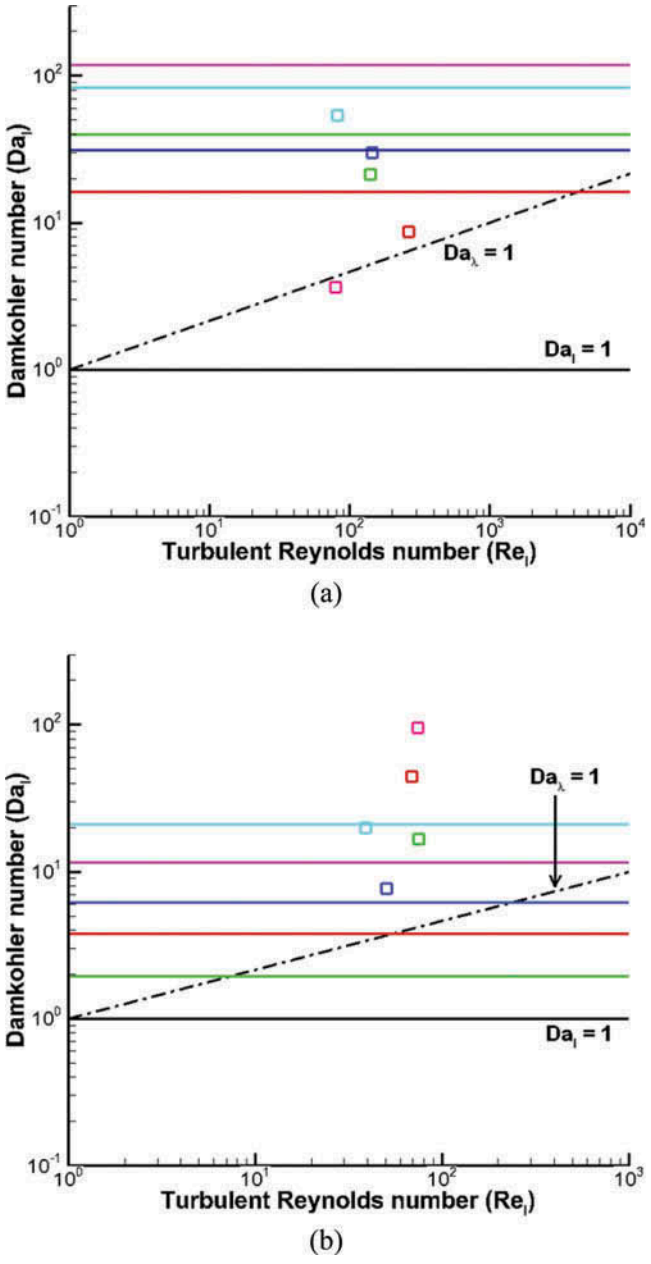

Figure 3 Location of (a) weak/mixed ignition cases 1–5 and (b) strong ignition cases 6–10 in red, green, dark blue, sky blue, pink, respectively, on the turbulent regime diagram.

of the characteristic Damköhler and Reynolds numbers of the system. The results of this work provided a more unified and comprehensive understanding of the physical and chemical mechanisms controlling ignition characteristics compared to the existing experimental maps in previous studies (Mansfield and Wooldridge, 2014; Meyer and Oppenheim, 1971), which were solely based on the ignition delay sensitivity.

Downloaded by [] at 06:34 13 May 2015

Downloaded by [] at 06:34 13 May 2015

Table 1 Details of the experimental cases of Mansfield and Wooldridge (2014) and corresponding regime diagram parameters

Mixture composition[a] (vol%)					Assigned thermo. state		Ignition behavior[b]	0D ignition delay, τ_{ig} (msec)	Ignition delay sensitivity, $\lvert d\tau_{ig}/dT \rvert$ (ms/K)	Flame time scale, τ_f (μs)					
H_2	CO	O_2	N_2	CO_2	P (atm)	T (K)					K^c	$Da_l{}^c$	K^2/Da_l	Re_l	Da_λ
5.1	7.3	12.5	63.0	12.0	15.5	983	M	23.0	0.57	21.40	4.04	8.69	1.88	263.16	1.35
5.1	7.3	12.7	73.8	1.1	9.2	1020	M	9.4	0.25	4.21	6.3	21.27	1.87	140.84	4.09
5.1	7.3	12.6	73.8	1.2	9.7	1033	M	6.7	0.18	3.76	5.58	29.85	1.04	144.92	5.68
5.1	7.3	12.7	73.8	1.1	5.5	1043	M	3.7	0.14	1.50	9.13	54.05	1.54	80.96	12.50
5.1	7.3	12.6	63.1	11.9	4.4	962	W	55.0	1.63	10.15	10.9	3.64	32.5	78.72	0.85
1.7	2.4	20.8	70.4	4.7	4.4	1043	S	4.5	0.25	92.0	1.94	44.44	0.085	68.96	10.83
1.7	2.5	20.9	73.3	1.7	4.7	1012	S	12.0	0.63	425.0	1.39	16.67	0.12	75.18	3.95
1.7	2.4	20.8	69.9	5.2	3.0	995	S	26.0	1.03	166.0	2.48	7.69	0.8	50.37	2.08
1.7	2.4	20.8	74.8	0.3	2.4	992	S	10.0	0.86	87.30	4.59	20.0	1.05	39.21	5.89
1.7	2.6	20.8	74.8	0	3.1	1029	S	2.1	0.17	30.0	3.39	95.23	0.12	74.07	22.68

[a]Balance Ar.
[b]Experimentally observed. M: mixed, W: weak, S: strong ignition.
[c]Assumed quantities: $T' \sim 10$ K, $u' \sim 0.1$ m/s, $l \sim 2$ cm.

It was recognized that the Zeldovich–Sankaran criterion includes the ignition delay sensitivity, $d\tau_{ig}/dT$, as a critical factor. Therefore, the traditional regime characterization based on the Damköhler and Reynolds numbers (such as those for turbulent premixed combustion regimes), which were based on time scales only, was not sufficient to describe the transitions between weak and strong ignition phenomena, and the introduction to the sensitivity parameter, K, was necessary. The regime diagram further showed how turbulence characteristics would affect the Zeldovich–Sankaran criterion based on the Kolmogorov theory of homogeneous isotropic turbulence.

The Zeldovich–Sankaran criterion indicates that there is a region where mixtures with high K values or high thermal sensitivity are more susceptible to weak ignition. Such conditions are reached with hydrogen/oxygen mixtures at low temperatures and high pressures. Therefore, the theory serves as a reasonable argument that the ignition delay discrepancies observed in syngas mixtures at low temperatures may be attributed to the ignition front propagation triggered by the local temperature peaks.

As for the turbulent combustion modeling implications, the proposed ignition regime diagram serves as a general guideline to identify whether the combustion processes are ignition controlled or flame-propagation controlled. Many turbulent premixed combustion closure models inherently assume a flame-dominant combustion mode, and it is hoped that the present study provides a metric to assess the validity of these models, as a supplement to the commonly-used Borghi diagram (Peters, 2000).

As a final remark, for higher hydrocarbon fuels that are known to exhibit the negative temperature coefficient (NTC) behavior, there is a broad range of intermediate temperature conditions at which the K value is expected to be low, thus promoting strong ignition. Weak ignition and associated front propagation behavior at NTC conditions have recently been studied (Gupta et al., 2013; Kim et al., 2015; Mansfield et al., 2015; Yoo et al., 2011). Further work is needed in order to validate the proposed regime diagram and ignition criterion for such complex fuels. Moreover, the sensitivity of the ignition characteristics to different uniform mixture compositions as well as the level of composition fluctuations would introduce further complexities to the problem. Additional detailed computational investigations using direct numerical simulations are underway.

Downloaded by [] at 06:34 13 May 2015

ORCID

Hong G. Im http://orcid.org/0000-0001-7080-1266
Pinaki Pal http://orcid.org/0000-0002-8630-5731
Margaret S. Wooldridge http://orcid.org/0000-0003-1754-180X

FUNDING

This work was sponsored by King Abdullah University of Science and Technology and the U.S. Department of Energy via NETL award DE-FE0007456.

REFERENCES

Dryer, F.L., Wooldridge, M.S., Peterson, E.L., McDonell, V.G., and Im, H.G. 2014. Panel discussion: Ignition delay issue. Presented at the United States Department of Energy University Turbine Systems Research (UTSR) meeting, October 21, 2014.

Gupta, S., Im, H.G., and Valorani, M. 2013. Analysis of *n*-heptane auto-ignition characteristics using computational singular perturbations. *Proc. Combust. Inst*., **34**, 1125–1133.

Ihme, M. 2012. On the role of turbulence and compositional fluctuations in rapid compression machines: Autoignition of syngas mixtures. *Combust. Flame*, **159**, 1592–1604.

Javed, T., Es-sebbar, E., Jaasim, M., Badra, J., Im, H.G., and Farooq, A. 2015. Interpreting low-temperature shock tube ignition delay data. Presented at the 7th European Combustion Meeting, Budapest, Hungary, March 30–April 2.

Kee, R., Rupley, F., and Miller, J. 1989. CHEMKIN-II: A fortran chemical kinetics package for the analysis of gas-phase chemical kinetics. SAND89-8009, Sandia National Laboratories.

Kim, S.O., Luong, M.B., Chen, J.H., and Yoo, C.S. 2015. A DNS study of the ignition of lean PRF/air mixtures with temperature inhomogeneities under high pressure and intermediate temperature. *Combust. Flame*, **162**(3), 717–726.

Lavoie, G.A., Martz, J.B., Wooldridge, M.S., and Assanis, D.N. 2010. A multi-mode combustion diagram for spark assisted compression ignition. *Combust. Sci. Tech*., **157**(6), 1106–1110.

Li, J., Zhao, Z., Kazakov, A., Chaos, M., Dryer, F.L., and Scire, J.J. 2007. A comprehensive kinetic mechanism for CO, CH_2O and CH_3OH combustion. *Int. J. Chem. Kinet*., **39**, 109–136.

Lieuwen, T., McDonell, V., Santavicca, D., and SattelMayer, T. 2008. Burner development and operability issues associated with steady flowing syngas fired combustors. *Combust. Sci. Technol*., **180**(6), 1169–1192.

Lieuwen, T.C., and Yang, V. (Eds). 2013. *Gas Turbine Emissions*, Cambridge Aerospace Series, Book 38, Cambridge University Press, Cambridge, UK, Ch. 1–2.

Linan, A., and Williams, F.A. 1993. *Fundamental Aspects of Combustion*, Oxford University Press, New York.

Mansfield, A.B., and Wooldridge, M.S. 2014. High-pressure low-temperature ignition behavior of syngas mixtures. *Combust. Flame*, **161**(9), 2242–2251.

Mansfield, A.B., Wooldridge, M.S., Di, H., and He, X. 2015. Low-temperature ignition behavior of iso-octane. *Fuel*, **139**, 79–86.

Meyer, J.W., and Oppenheim, A.K. 1971. On the shock-induced ignition of explosive gases. *Proc. Combust. Inst*., **13**, 1153–1164.

Mittal, G., Sung, C.J., and Yetter, R.A. 2006. Autoignition of H_2/CO at elevated pressures in a rapid compression machine. *Int. J. Chem. Kinet*., **38**, 516–529.

Oran, E.S., and Borris, J.P. 1982. Weak and strong ignition. II. Sensitivity of the hydrogen-oxygen system. *Combust. Flame*, **48**, 149–161.

Peters, N. 2000. *Turbulent Combustion*, Cambridge University Press, Cambridge, UK, Ch. 2.

Petersen, E.L., Kalitan, D.M., Barrett, A.B., Reehal, S.C., Mertens, J.D., Beerer, D.J., Hack, R.L., and McDonell, V.G. 2007. New syngas/air ignition data at low temperature and elevated pressure and comparison to current kinetic models. *Combust. Flame*, 149, 244–247.

Richards, G.A., McMillian, M.M., Gemmen, R.S., Rogers, W.A., and Cully, S.R. 2001. Issues for low-emission, fuel-flexible power systems. *Prog. Energy Combust*., **27**(2): 141–169.

Sankaran, R., Im, H.G., Hawkes, E.R., and Chen, J.H. 2005. The effects of non-uniform temperature distribution on the ignition of a lean hydrogen-air mixture. *Proc. Combust. Inst*., **30**, 875–882.

Tennekes, H., and Lumley, J.L. 1972. *A First Course in Turbulence*, MIT Press, Cambridge, MA.

United States Department of Energy. 2009. Hydrogen from Coal Program—Research, Development and Demonstration Plan. Available at: http://fossil.energy.gov/programs/fuels/publications/ programplans/2009_Draft_H2fromCoal_Sept30_web.pdf

Uygun, Y., Ishihara, S., and Olivier, H. 2014. A high pressure ignition delay time study of 2-methylfuran and tetrahydrofuran in shock tubes. *Combust. Flame*, **161**, 2519–2530.

Walton, S.M., He, X., Zigler, B.T., and Wooldridge, M.S. 2007. An experimental investigation of the ignition properties of hydrogen and carbon monoxide mixtures for syngas turbine applications. *Proc. Combust. Inst*., **31**, 3147–3154.

Wu, H., and Ihme, M. 2014. Effects of flow-field and mixture inhomogeneities on the ignition dynamics in continuous flow reactors. *Combust. Flame*, **161**, 2317–2326.

Downloaded by [] at 06:34 13 May 2015

Yoo, C.S., Lu, T., Chen, J.H., and Law, C.K. 2011. Direct numerical simulations of ignition of lean *n*-heptane/air mixture with temperature inhomogeneities at constant volume: Parametric study. *Combust. Flame*, **158**, 1727–1741.

Zeldovich, Y.B. 1980. Regime classification of an exothermic reaction with nonuniform initial conditions. *Combust. Flame*, **39**, 211–214.

Downloaded by [] at 06:34 13 May 2015

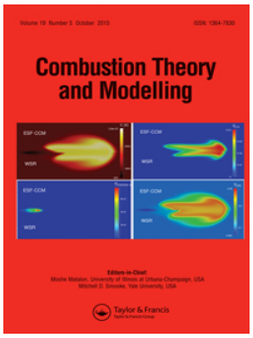

Taylor & Francis
Taylor & Francis Group

Combustion Theory and Modelling

ISSN: 1364-7830 (Print) 1741-3559 (Online) Journal homepage: http://www.tandfonline.com/loi/tctm20

A computational study of syngas auto-ignition characteristics at high-pressure and low-temperature conditions with thermal inhomogeneities

Pinaki Pal, Andrew B. Mansfield, Paul G. Arias, Margaret S. Wooldridge & Hong G. Im

To cite this article: Pinaki Pal, Andrew B. Mansfield, Paul G. Arias, Margaret S. Wooldridge & Hong G. Im (2015) A computational study of syngas auto-ignition characteristics at high-pressure and low-temperature conditions with thermal inhomogeneities, Combustion Theory and Modelling, 19:5, 587-601, DOI: 10.1080/13647830.2015.1068373

To link to this article: http://dx.doi.org/10.1080/13647830.2015.1068373

Published online: 30 Jul 2015.

Submit your article to this journal

Article views: 190

View related articles

View Crossmark data

Full Terms & Conditions of access and use can be found at
http://www.tandfonline.com/action/journalInformation?journalCode=tctm20

Download by: [University of Michigan] **Date:** 29 February 2016, At: 10:19

Combustion Theory and Modelling, 2015
Vol. 19, No. 5, 587–601, http://dx.doi.org/10.1080/13647830.2015.1068373

Taylor & Francis
Taylor & Francis Group

A computational study of syngas auto-ignition characteristics at high-pressure and low-temperature conditions with thermal inhomogeneities

Pinaki Pal [a], Andrew B. Mansfield[a], Paul G. Arias[b], Margaret S. Wooldridge [a,c] and Hong G. Im [b*]

[a]*Department of Mechanical Engineering, University of Michigan, Ann Arbor, USA;* [b]*Clean Combustion Research Center, King Abdullah University of Science and Technology, Thuwal, Kingdom of Saudi Arabia;* [c]*Department of Aerospace Engineering, University of Michigan, Ann Arbor, USA*

(*Received 16 February 2015; accepted 15 June 2015*)

A computational study was conducted to investigate the characteristics of auto-ignition in a syngas mixture at high-pressure and low-temperature conditions in the presence of thermal inhomogeneities. Highly resolved one-dimensional numerical simulations incorporating detailed chemistry and transport were performed. The temperature inhomogeneities were represented by a global sinusoidal temperature profile and a local Gaussian temperature spike (hot spot). Reaction front speed and front Damköhler number analyses were employed to characterise the propagating ignition front. In the presence of a global temperature gradient, the ignition behaviour shifted from spontaneous propagation (strong) to deflagrative (weak), as the initial mean temperature of the reactant mixture was lowered. A predictive Zel'dovich–Sankaran criterion to determine the transition from strong to weak ignition was validated for different parametric sets. At sufficiently low temperatures, the strong ignition regime was recovered due to faster passive scalar dissipation of the imposed thermal fluctuations relative to the reaction timescale, which was quantified by the mixing Damköhler number. In the presence of local hot spots, only deflagrative fronts were observed. However, the fraction of the reactant mixture consumed by the propagating front was found to increase as the initial mean temperature was lowered, thereby leading to more enhanced compression-heating of the end-gas. Passive scalar mixing was not found to be important for the hot spot cases considered. The parametric study confirmed that the relative magnitude of the Sankaran number translates accurately to the quantitative strength of the deflagration front in the overall ignition advancement.

Keywords: auto-ignition; syngas; flames; numerical simulation; ignition regimes

Downloaded by [University of Michigan] at 10:19 29 February 2016

1. Introduction

In view of growing environmental concerns and limited petroleum reserves, the utilisation of coal-derived synthetic gas (syngas) is considered an attractive alternative for power generation applications [1, 2]. Syngas offers considerable opportunity for clean use of coal with potential for near-zero pollutant emissions, including greenhouse gases, when combined with carbon capture and sequestration methods.

Despite the promises, however, successful implementation of syngas combustion in gas turbines faces many technical challenges associated with the high level of hydrogen content,

*Corresponding author. Email: hong.im@kaust.edu.sa; Tel: 966-12-808-4726 (office): 966-54-470-0186 (mobile)

© 2015 Taylor & Francis

such as high flame speeds, extended flammability limits, flashback and blowout, primarily due to the unique thermo-diffusive properties of hydrogen. In addition, these gas turbines are typically operated at high-pressure (up to 30 bar) and low-temperature (<1000 K) conditions, at which the ignition and combustion characteristics of syngas are not well understood. Recent experimental investigations [3–7] reported large discrepancies between measurements and homogeneous chemical kinetic modelling predictions in the ignition delay times at these conditions, with the experimental values being orders of magnitude less than the corresponding model predictions.

A number of potential contributing factors were proposed to explain the observed discrepancies, such as uncertainties in the kinetic rate constants of certain key elementary reactions, for example, $CO + HO_2 = CO_2 + OH$, the effects of gas impurities and surface-catalytic processes [5,6,8,9]. In addition, it was recognised that the presence of thermal inhomogeneities at high pressures and low temperatures may also contribute to the overall ignition advancement in comparison with the homogeneous prediction, by way of early flame kernel growth and front propagation. For example, Medvedev *et al.* [10] analysed the ignition delay data reported by various experimental facilities [3,11,12] and reported that, at relatively low temperatures, the measured ignition delays were close to the timescales of deflagrative flame propagation, which were much shorter than the corresponding homogeneous ignition delays. In a recent experimental study using syngas in the rapid compression facility (RCF), Mansfield and Wooldridge [13] demonstrated a transition in the auto-ignition behaviour from the strong (characterised by nearly homogeneous ignition) to the weak (initiated by localised reaction sites and followed by front propagation) regime as the initial mean temperature was lowered.

These observed trends were qualitatively similar to earlier shock tube studies of hydrogen–oxygen ignition [14–17], in which localised ignition at an early stage led to a significant acceleration in the ignition delay times. Meyer and Oppenheim [15] reported that the boundary between strong and weak ignition coincided with an iso-line of the sensitivity of homogeneous ignition delay time to temperature, $\mathrm{d}\tau_{ig}/\mathrm{d}T$, in the pressure–temperature space. Consistent behaviour was found in the RCF study [13], where a $\mathrm{d}\tau_{ig}/\mathrm{d}T =$ constant line served as a reasonable criterion for differentiating the strong and weak ignition regimes. Recently, reduced order modelling was also attempted [18,19] to demonstrate that turbulent fluctuations can also result in a significant reduction in the ignition delay times.

Considering the significance of different ignition regimes in determining the net ignition delay times, the ultimate practical goal is to obtain a rational criterion to predict whether a given mixture will ignite in the strong or weak regime. To this end, it is evident that a constant $\mathrm{d}\tau_{ig}/\mathrm{d}T$ criterion is not sufficient, as a perfectly homogeneous mixture must ignite in the strong regime regardless of the mixture's ignition sensitivity. An additional parameter to represent the local or global temperature distribution within the mixture must also be considered.

Further theoretical development has led to a unified criterion to identify various ignition regimes proposed by Zel'dovich [20], which was later modified and validated by Sankaran *et al.* [21] in two-dimensional direct numerical simulations of auto-igniting homogeneous mixtures in the presence of temperature fluctuations. However, since the Zel'dovich–Sankaran criterion is based on the local temperature gradient, it cannot readily be used as a predictive metric in practical devices in which only statistical mean quantities in turbulent fluctuations are available. Im *et al.* [22], by a scaling analysis, proposed a turbulent ignition regime diagram as an extension of the criterion to be applicable in bulk turbulent combustion systems.

Downloaded by [University of Michigan] at 10:19 29 February 2016

As a complementary work to the regime diagram, the objective of the present study is to validate the Zel'dovich–Sankaran criterion as a predictive indicator of the ignition regime of a reactant mixture. As a first step, extensive parametric studies are conducted using simple one-dimensional configurations with the level of initial temperature fluctuations being prescribed as the key parameter. The corresponding ignition behaviours are then characterised and the resulting ignition delay times are reported in comparison with the reference homogeneous mixture conditions.

2. Numerical setup and initial conditions

One-dimensional (1D) constant-volume simulations are performed using the direct numerical simulation (DNS) code S3D [23], which solves the compressible, Navier–Stokes, species continuity and total energy equations. A fourth-order explicit Runge–Kutta method and an eighth-order central differencing scheme are used for time integration and spatial discretisation, respectively [24]. A detailed H_2/CO mechanism with 12 species and 33 chemical reactions [25] is employed. The mechanism is linked with the CHEMKIN^{TM} [26] and TRANSPORT^{TM} [27] libraries for evaluating the reaction rates and thermodynamic and mixture-averaged transport properties, respectively. Periodic boundary conditions are imposed, such that heat release in the computational domain leads to pressure rise and compression heating of the reactants.

A number of parametric conditions are considered for initial pressures (P_0) of 10 and 20 atm, and the initial mean temperature (T_0) in the range 850–1100 K, as typically encountered in gas turbines. A uniform syngas/air mixture with an H_2:CO molar ratio of 0.7:1 and a fuel–air equivalence ratio of 0.5 is chosen. In addition, the mixture is diluted with twice the amount of nitrogen present in the air (i.e. a molar ratio of N_2:O_2 = 11.28), to ensure the pressure rise is sufficiently high to serve as an indicator of auto-ignition, but also to avoid shock wave formation [28,29]. A uniform grid size of 4.7 μm is used to allow sufficient resolution of the thin propagating fronts. The initial flow is quiescent.

Temperature non-uniformities are represented by two types of initial conditions. First, to represent moderate global temperature variations, a sinusoidal temperature profile is superimposed on the initial mean temperature, with a prescribed root-mean-square (RMS) fluctuation, T', and wavelength spanning the domain length, L. Alternatively, to represent a localised ignition source, a hot spot is represented by superimposing a Gaussian temperature profile, T_{hs}, onto the mean temperature:

$$T_{\mathrm{hs}}(s) = \frac{A}{\pi} \exp\left[\frac{-2n^2\left(x - L/2\right)^2}{L^2}\right] - \frac{A}{2.5n}, \tag{1}$$

where the factor n governs the size of the hot spot and A determines the amplitude. By definition, T_{hs} has a zero mean so that the mean of the total temperature distribution remains at T_0. The amplitude (ΔT), of the hot spot is varied in the range 25–100 K as observed in some syngas ignition experiments [30], while the size of the hot spot is kept constant at 0.6 cm. The value of $n = 16$ is chosen in order to keep the size of the incipient hot spot reasonably small (localised) as compared to the domain size, as has been typically observed in experiments [13]. It is noted that for fixed domain length, initial mean temperature (T_0) and hot spot magnitude (A), a decrease in n results in an increase in the size/strength of the hot spot, while the initial end-gas temperature becomes lower in order to maintain constant T_0. Consequently, this would lead to a higher propensity for deflagrative front

Downloaded by [University of Michigan] at 10:19 29 February 2016

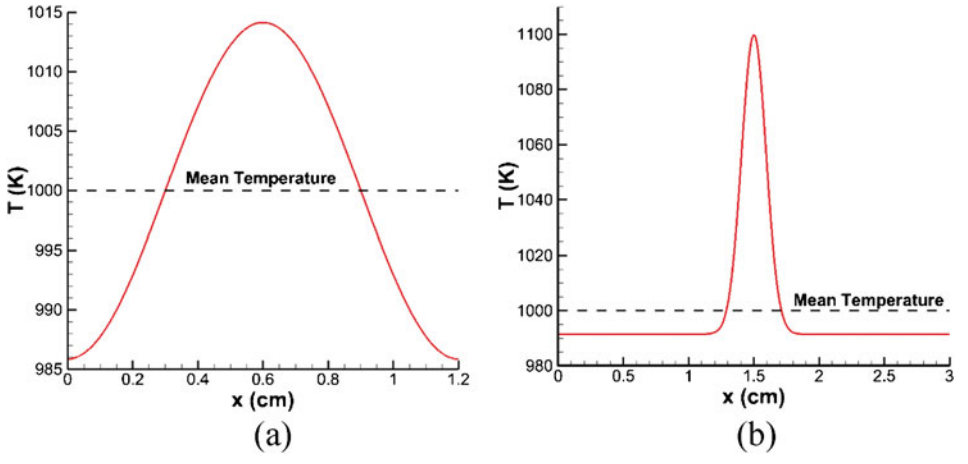

Figure 1. Sample initial temperature profiles with (a) global temperature gradient ($T' = 10$ K, $L = 1.2$ cm) and (b) local hot spot ($\Delta T = 100$ K), at T_0 of 1000 K.

propagation. In other words, the effect of solely decreasing n is qualitatively similar to the effect of solely increasing A (Section 3.2), and therefore is not discussed separately. The sensitivity to parameter n is directly reflected in the Sankaran number defined in Section 3.1.1, representing the changes in the RMS temperature. Figure 1 shows examples of initial temperature profiles for the two types of prescribed thermal inhomogeneities. In the present work, the ignition regime is classified as *weak* when most of the reactant mixture is consumed by deflagrative front propagation.

3. Results and discussion

3.1. *Effects of global temperature variations*

3.1.1 *Strong ignition limit: The Sankaran number*

To investigate the effect of global temperature variations, parametric tests are carried out at different thermodynamic conditions, for varying magnitudes of the RMS temperature

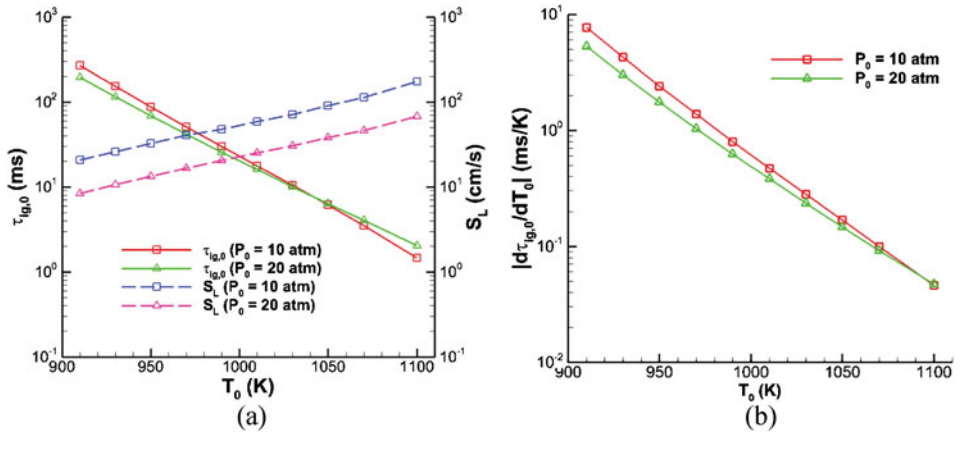

Figure 2. Homogeneous ignition delay and laminar flame speed versus initial mean temperature (a) and ignition delay sensitivity versus initial mean temperature (b), for all cases listed in Table 1.

Downloaded by [University of Michigan] at 10:19 29 February 2016

Table 1. Initial conditions for parametric cases.

Set #	P_0 (atm)	T_0 (K)	T' (K)	L (cm)
1	20	910–1100	10	1.2
2	10	910–1100	10	1.2
3	10	910–1100	10	2.4

fluctuation (T') and the associated wavelength (L), as listed in Table 1. The corresponding homogeneous ignition delay times ($\tau_{\mathrm{ig},0}$), laminar flame speeds (S_L), and temperature sensitivities of ignition delay ($|\mathrm{d}\tau_{\mathrm{ig},0}/\mathrm{d}T_0|$) at the mean initial conditions considered in the present work are plotted in Figures 2(a) and 2(b), respectively. The ignition delay time is defined as the time at which the maximum pressure rise rate occurs. Note that S_L decreases, whereas both $\tau_{\mathrm{ig},0}$ and $|\mathrm{d}\tau_{\mathrm{ig},0}/\mathrm{d}T_0|$ increase with a decrease in temperature, at a given pressure.

Figure 3 shows typical behaviour of temperature evolution for the overall progression of the ignition and combustion process for $T_0 = 1030$ K and $T' = 10$ K, corresponding to set #1. Ignition first occurs at the location of the highest temperature in the middle of the domain, and subsequently reaction fronts emanate from this ignition kernel, propagating towards the left and right ends of the domain. The propagating fronts heat the remaining charge by compression, thereby accelerating the ignition of the end-gas. Similar to Figure 3, for all other parametric cases listed in Table 1, the reactant mixture is completely consumed by ignition front propagation.

To determine the nature of the propagating front, the numerical results for the parametric cases are analysed based on two quantitative metrics. The first metric to distinguish between deflagrations and spontaneous propagation fronts is the density-weighted front propagation

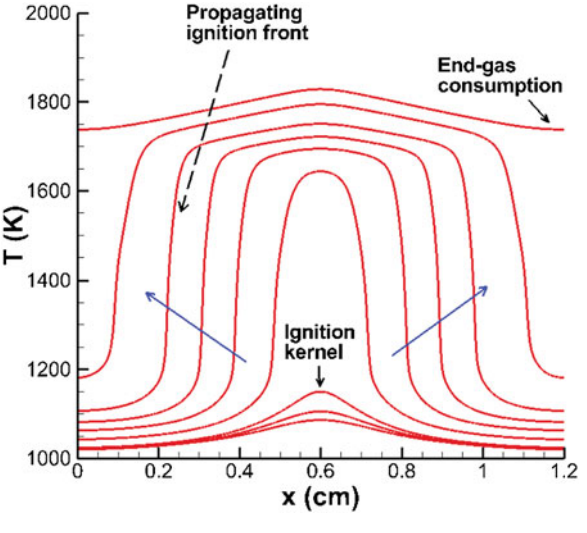

Figure 3. Temperature versus distance for a sequence of times, for $T_0 = 1030$ K, corresponding to set #1 in Table 1. The equally spaced time sequence starts from 7 ms with an increment of 0.25 ms. The arrows indicate the direction of increasing time.

Downloaded by [University of Michigan] at 10:19 29 February 2016

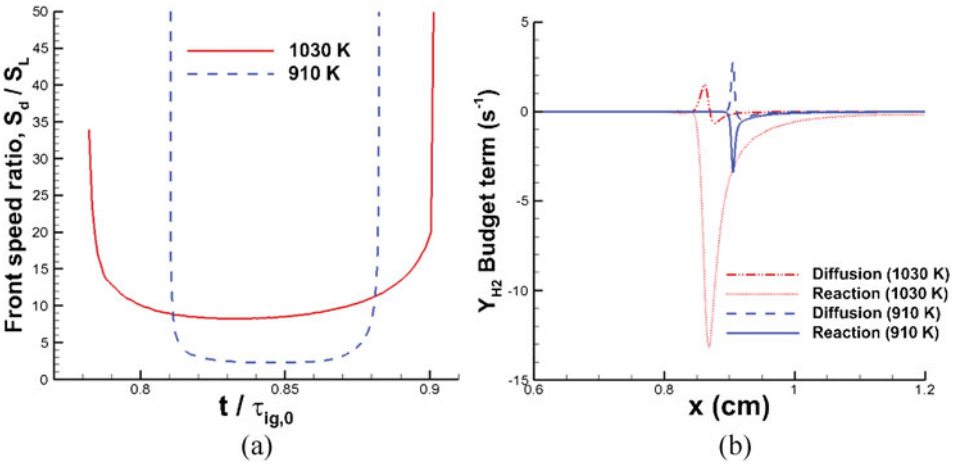

Figure 4. Evolution of normalised front propagation speed as a function of normalised time (a), and hydrogen reaction and diffusion budget terms at the time instant of lowest front propagation speed (b), for $T_0 = 1030$ K (red) and $T_0 = 910$ K (blue), corresponding to set #1 in Table 1.

speed [31, 32], S_d, defined as

$$S_d = \frac{1}{\rho_u |\nabla Y_k|} \left(\dot{w}_k - \frac{\partial}{\partial x_j} \left(\rho Y_k V_{j,k} \right) \right), \tag{2}$$

where Y_k, $V_{j,k}$ and w_k denote species mass fraction, species diffusion velocity in the j-direction, net production rate of species k, and ρ_u denotes the density of the unburned mixture, which is calculated from the local enthalpy and fresh reactant mixture condition based on the assumptions of constant pressure and enthalpy across the front [33]. S_d is computed at the location of maximum heat release and H_2 is chosen as the species k in the present work.

As the second metric to identify the nature of the propagating fronts, the reaction and diffusion budgets for the H_2 mass fraction at the time of minimum front propagation speed are examined. A characteristic front Damköhler number (Da_{fr}) is defined as the ratio of the peaks of reaction and diffusion of H_2 within the front:

$$\mathrm{Da_{fr}} = \frac{\max(|\dot{w}_{\mathrm{H_2}}|)}{\max(\nabla \cdot (-\rho D_{\mathrm{H_2}} \nabla Y_{\mathrm{H_2}}))}, \tag{3}$$

where the maximum values for the reaction and diffusion terms closest to the reaction zones are considered. H_2 is used for the calculations in the present study; it was found that the choice of other species such as OH and HO_2 yielded consistent results.

Figure 4(a) shows the computed temporal evolution of the front speed for two initial mean temperatures of 910 and 1030 K, corresponding to set #1 in Table 1. The x- and y-axes are normalised by the homogeneous ignition delay times ($\tau_{\mathrm{ig},0}$) and laminar flame speeds (S_L), respectively, at the corresponding initial mean conditions. Nominally, the curves exhibit a characteristic U-shape behaviour, representing a stabilised low speed front propagation between the initial ignition kernel development and final consumption points

Downloaded by [University of Michigan] at 10:19 29 February 2016

Downloaded by [University of Michigan] at 10:19 29 February 2016

where the speed becomes unbounded due to nearly zero fuel concentration gradient [33]. For $T_0 = 910$ K, S_d is almost equal to the laminar flame speed, whereas for $T_0 = 1030$ K, the ignition front propagates at a speed higher than the corresponding S_L by an order of magnitude. The final thermal runaway also occurs relatively faster for the lower T_0 case.

Figure 4(b) shows the spatial profiles of the diffusion and reaction terms in the H_2 species conservation equation for the two cases. As the configuration is symmetric, only the right half of the domain is shown. The time instants correspond to the minimum front propagation speed for the respective cases. For $T_0 = 1030$ K, the diffusion term is nearly negligible relative to the reaction term. On the other hand, for $T_0 = 910$ K, the two contributions are comparable. Figure 4 indicates that the higher temperature case exhibits spontaneous ignition behaviour whereas, for the lower temperature case, auto-ignition occurs via deflagrative front propagation.

The variation of $\mathrm{Da_{fr}}$ with T_0 for the three parametric sets listed in Table 1 is plotted in Figure 5 to capture the trend in auto-ignition behaviour. As T_0 decreases, transport effects become more important and the ignition regime transitions from spontaneous (strong) propagation to deflagration (weak), indicated by $\mathrm{Da_{fr}}$ approaching unity.

As an alternative metric to identify the nature of the front, the Zel'dovich–Sankaran criterion [21] predicts that strong ignition is encountered when

$$\mathrm{Sa} = \beta \frac{S_L}{S_{\mathrm{sp}}} = \beta S_L \left| \frac{\mathrm{d}\tau_{\mathrm{ig},\,0}}{\mathrm{d}T_0} \frac{\mathrm{d}T_0}{\mathrm{d}x} \right| \leq 1, \tag{4}$$

where Sa is called the Sankaran number and $S_{sp} = |(\mathrm{d}\tau_{\mathrm{ig},\,0}/\mathrm{d}T_0) \cdot (\mathrm{d}T_0/\mathrm{d}x)|^{-1}$ is the speed of a spontaneous ignition front. $\mathrm{d}T_0/\mathrm{d}x$ represents the initial temperature gradient in the mixture. β is chosen to be 0.5 following [21].

The variation of Sa with T_0 for the different parametric sets is also shown in Figure 5. The data shows the $\mathrm{Sa} = 1$ criterion coincides well with $\mathrm{Da_{fr}} \approx 1.4$, which is a reasonable

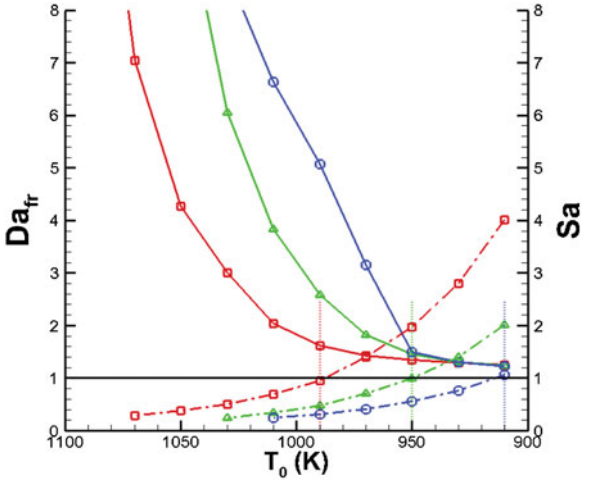

Figure 5. Variation of the front Damköhler number (solid lines) and Sankaran number (dash–dot lines) versus initial mean temperature (T_0) for parametric set #1 (circles), parametric set #2 (squares) and parametric set #3 (Δ 's) in Table 1. The dotted lines show the corresponding T_0 at which $\mathrm{Sa} = 1$ for each parametric set.

indicator to identify deflagrative fronts. For β in the range of 0.3–0.9, the strong ignition limit corresponding to Sa = 1 computed for each parametric set shifts by a maximum of $|\Delta T_0| =$ 20 K about the value computed for $\beta = 0.5$ and the corresponding $\mathrm{Da_{fr}}$ varied in the range 1.1–1.8, which is again a good indicator of deflagrative front propagation. This demonstrates that Equation (4) can serve as an appropriate non-dimensional criterion to predict the ignition regime. The magnitude of Sa quantitatively represents the net effect of chemistry, thermo-physical properties of the mixture and system-specific thermal characteristics on the auto-ignition behaviour.

3.1.2. Role of passive scalar mixing

In addition to transport within the flame front, the effect of diffusive transport can also modify the ignition characteristics. For example, rapid turbulent mixing within the bulk mixture may dissipate local temperature peaks before they can act as ignition kernels leading to front propagation. The impact of passive scalar mixing on auto-ignition can be quantified by the mixing Damköhler number ($\mathrm{Da_{mix}}$), defined as

$$\mathrm{Da_{mix}} = \tau_{\mathrm{mix}}/\tau_{\mathrm{ig,\,10\%}}, \tag{5}$$

where τ_{mix} is the mixing timescale determined by

$$\tau_{\mathrm{mix}} = \frac{T'^2}{2\alpha_0|\nabla T_0|^2} \tag{6}$$

and $\tau_{\mathrm{ig,\,10\%}}$ represents the shortest ignition timescale of the initial mixture [34] and is defined as the homogeneous ignition delay time at the temperature $T_{\mathrm{min}} + 0.9(T_{\mathrm{max}} - T_{\mathrm{min}})$, where T_{min} and T_{max} are the minimum and maximum initial temperatures in the domain; α_0 denotes the thermal diffusivity at the initial mean thermodynamic conditions.

When the $\mathrm{Da_{mix}}$ becomes less than O(1), the passive scalar dissipation effects are expected to become important. To substantiate this hypothesis, the parametric set #2 in Table 1 is expanded to include lower T_0 values at 880 and 860 K. The variation of the front and mixing Damköhler numbers with the initial mean temperature is shown in Figure 6(a). For $T_0 < 910$ K, as $\mathrm{Da_{mix}}$ becomes much lower than unity, $\mathrm{Da_{fr}}$ begins to increase, indicating a shift in the ignition regime from deflagration to spontaneous ignition. The time evolution of the temperature fluctuation (T') for a few parametric cases is shown in Figure 6(b). It is observed that the temperature fluctuations dissipate more significantly at lower T_0, as the mixing timescale becomes shorter relative to the reaction timescale, promoting strong ignition at sufficiently low initial mean temperatures and leading to non-monotonic ignition trend as shown in Figure 6(a).

Note that such a rapid scalar mixing scenario has not been observed in previous shock tube and RCF experiments [3] at lower temperatures. The present discussion of global temperature fluctuations applies to the conditions in which the temperature fluctuations are directly correlated with turbulent flows [35]. In the nearly quiescent conditions as encountered in shock tubes and RCF, local thermal stratification or hot spots are considered the primary mechanism to trigger early ignition and flame propagation. As such, the representative temperature gradient used in Equation (4) must be determined in a different way, which subsequently suppresses the possibility of $\mathrm{Da_{mix}} < 1$ observed in Figure 6(a).

Downloaded by [University of Michigan] at 10:19 29 February 2016

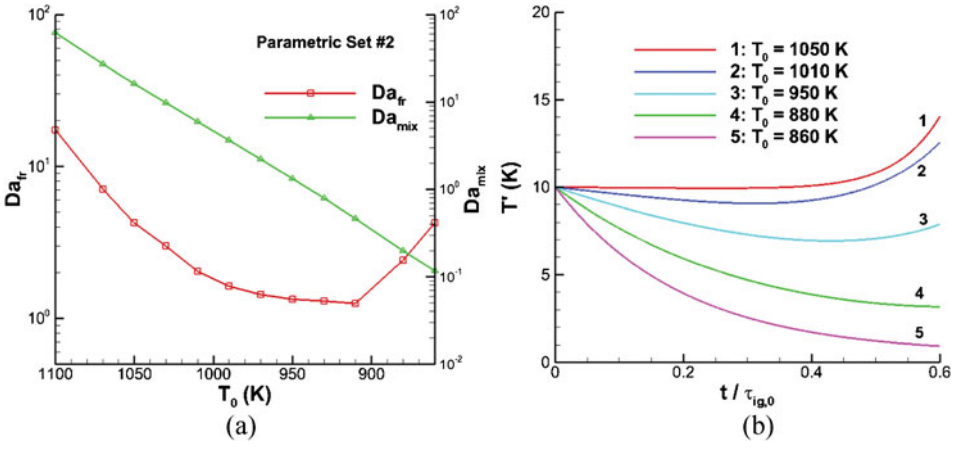

Figure 6. Variation of the front and mixing Damköhler numbers as a function of the initial mean temperature (a), and temporal evolution of temperature fluctuations for different initial mean temperatures (b), corresponding to parametric set #2 in Table 1.

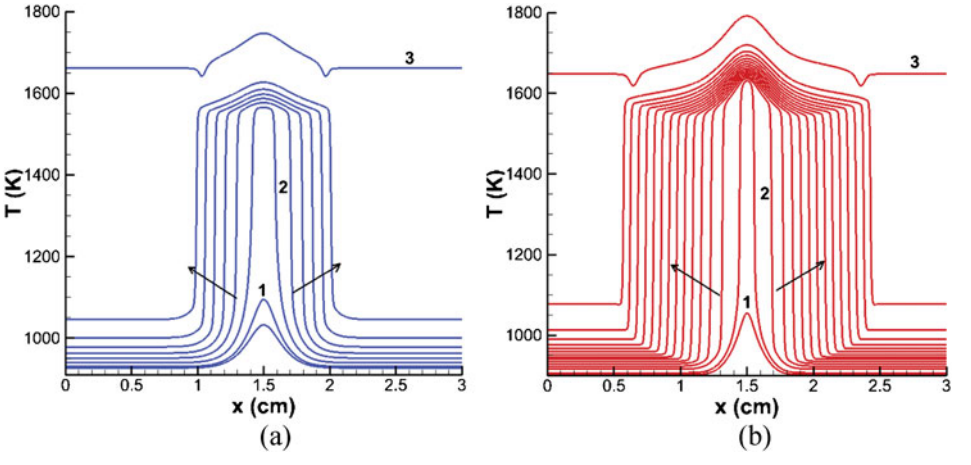

Figure 7. Temporal evolution of the temperature profiles during ignition for $T_0 = 910$ K, $P_0 = 20$ atm: $\Delta T = 25$ K starting at 146 ms (a); $\Delta T = 100$ starting at 24 ms (b), shown at an equal time increment of 4 ms. The arrows indicate the direction of increasing time. Numbers denote the ignition kernel (1), propagating front (2) and the end-gas auto-ignition (3) phase.

The characteristics of ignition caused by localised ignition sources are studied in the following section.

3.2. Effects of local hot spots

In this section, the influence of temperature inhomogeneities as highly localised temperature gradients, representing 'hot spots', on syngas auto-ignition characteristics are investigated. Parameters of interest are: (a) the hot spot strength (ΔT) for a given T_0; and (b) T_0 for a fixed value of ΔT. Details of the numerical setup are as described in Section 2.

Figure 7 shows the temporal evolution of the temperature field for $T_0 = 910$ K, $P_0 = 20$ atm, with two different hot spot strengths at (a) $\Delta T = 25$ K and (b) 100 K. For both

Downloaded by [University of Michigan] at 10:19 29 February 2016

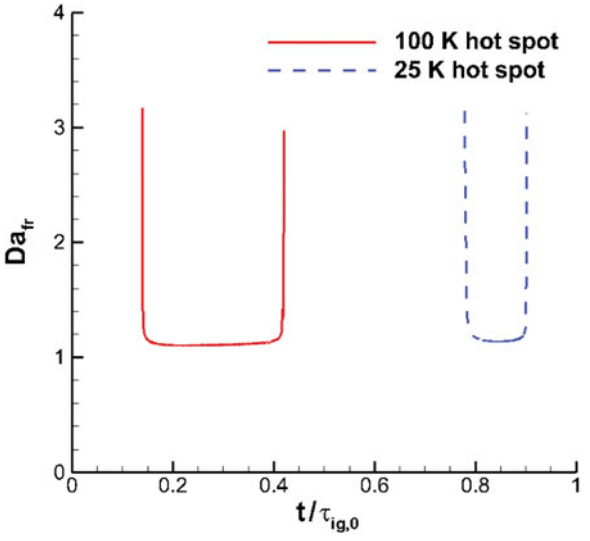

Figure 8. Front Damköhler number versus time (normalised by homogeneous ignition delay time at the mean initial mixture conditions) for $\Delta T = 25$ K and $\Delta T = 100$ K; $T_0 = 910$ K and $P_0 = 20$ atm.

cases, an ignition kernel first develops at the centre of the domain, leading to front propagation, followed by the end-gas auto-ignition. Temporal evolution of the corresponding front Damköhler numbers is shown in Figure 8. The pressure remains spatially uniform and varies with time only. For both cases, $\mathrm{Da_{fr}} \approx 1.15$ at the minimum plateau condition, indicating that the fronts are deflagrative in nature. Therefore, instead of $\mathrm{Da_{fr}}$, the percentage mass fraction burned by deflagration is employed to investigate the relative importance of deflagration versus end-gas self-ignition. It can be seen that the ignition front develops much earlier and travels much further into the unburned mixture for $\Delta T = 100$ K. As a result, the mass fraction burned by deflagration is found to be much higher for $\Delta T = 100$ K ($\approx 68\%$) as compared to that for $\Delta T = 25$ K ($\approx 33\%$).

To investigate the effect of the strength of the hot spot further, Figure 9 shows the evolution of (a) the mean and (b) the end-gas temperature for $T_0 = 910$ K and with ΔT ranging from 25 to 100 K. The time axis is normalised by $\tau_{\mathrm{ig},0}$, which is identical for all cases. As ΔT increases, the front propagation mode becomes more prominent (as shown in Figure 7), and the overall ignition delay time decreases. The earlier front establishment also leads to an earlier rise in the end-gas temperature as shown in Figure 9(b).

The hot spot ignition cases are now tested for the validity of the Zel'dovich–Sankaran criterion. Since Equation (4) is based on the bulk temperature gradient of the system, for the hot spot ignition condition a representative temperature gradient is defined as based on the initial root-mean-square (RMS) temperature and half of the domain size ($L/2$), similar to Section 3.1.1. Table 2 shows the mass fraction burned by deflagration and the computed Sankaran numbers for the four cases under study. It is clearly seen that Sa increases with increasing ΔT, thus capturing the quantitative contributions of the deflagrative front propagation in the overall ignition behaviour. For $\Delta T = 100$ K, Sa nearly reaches unity, at which a large fraction of the reactant mixture (nearly 70%) is consumed by the flame front. In addition to the test cases discussed above, additional parametric tests were also performed by varying the domain size for fixed ΔT and hot spot shape (not shown here). It was still observed that Sa = 1 coincided with a mass fraction burned by deflagration in the

Downloaded by [University of Michigan] at 10:19 29 February 2016

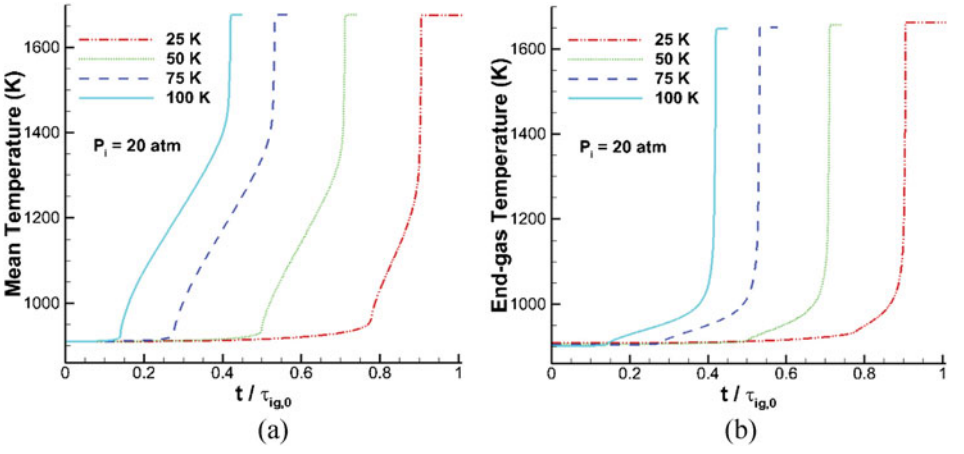

Figure 9. Evolution of the mean (a) and the end-gas temperature (b) versus time normalised by the homogeneous ignition delay time at T_0, for different values of ΔT; $T_0 = 910$ K and $P_0 = 20$ atm.

Table 2. Mass fraction burned by deflagration and Sankaran numbers for different parametric cases ($T_0 = 910$ K, $P_0 = 20$ atm).

ΔT (K)	Mass fraction burned by deflagration (%)	Sa
25	33	0.24
50	38	0.48
75	48	0.72
100	68	0.96

Table 3. Mass fraction burned by deflagration and Sankaran numbers for different parametric cases ($\Delta T = 100$ K, $P_0 = 20$ atm).

T_0 (K)	Mass fraction burned by deflagration (%)	Sa
1100	21	0.06
1050	27	0.12
910	68	0.96
890	73	1.82

range 60–70%. This indicates that the Zel'dovich–Sankaran criterion serves as a rational predictive criterion for identifying the transition from strong to weak ignition regime, and provides a quantitative estimate of the significance of the deflagration mode on the overall ignition characteristics. Note that passive scalar dissipation plays a negligible role here, as $\mathrm{Da_{mix}}$ for all parametric cases is found to be greater than unity.

The final set of the parametric study is carried out by varying T_0 from 890 to 1100 K, for fixed $P_0 = 20$ atm and $\Delta T = 100$ K. Although not shown here, it is observed that the propagating reaction front is in the deflagrative regime for all cases considered, similar to Figure 8. Table 3 summarises the corresponding mass fractions burned by deflagration and

Downloaded by [University of Michigan] at 10:19 29 February 2016

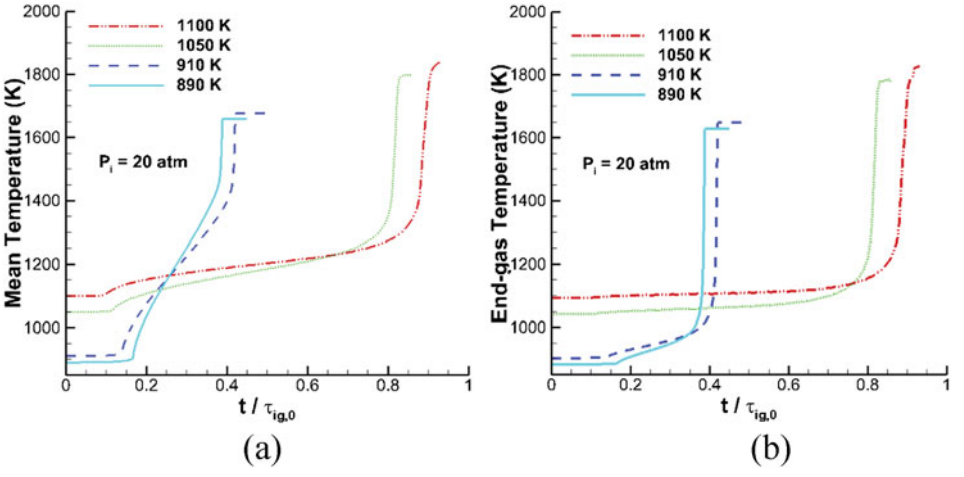

Figure 10. Evolution of the mean temperature (a) and the end-gas temperature (b), versus time (normalised by the homogeneous ignition delay time at the mean initial mixture conditions), for different magnitudes of T_0; $\Delta T = 100$ K and $P_0 = 20$ atm.

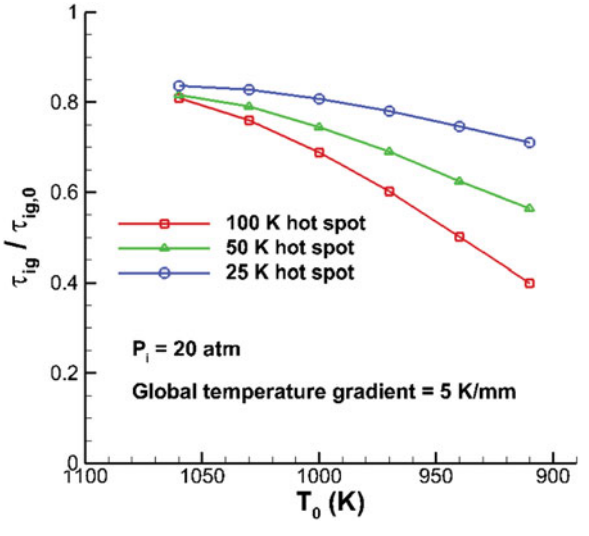

Figure 11. Variation of ignition delay timing (normalised by the homogeneous ignition delay at the corresponding initial mean temperature) with initial mean temperature for different hot spot strengths.

the corresponding Sankaran numbers. Based on the values of the mass fraction burned by deflagration, it is concluded that strong ignition is encountered for $T_0 = 1100$ K and $T_0 = 1050$ K, whereas weak ignition occurs at lower $T_0 = 910$ K and $T_0 = 890$ K. Again, the Zel'dovich–Sankaran criterion properly captures the ignition characteristics.

The evolutions of the mean and end-gas temperature for these cases are shown in Figures 10(a) and 10(b), respectively. The weak ignition regime results in significant advancement in the net ignition delay time as compared to its homogeneous counterpart.

The overall parametric effects for combinations of the variations in T_0 and ΔT are summarised in Figure 11, where the normalised ignition delay time is plotted versus T_0

Downloaded by [University of Michigan] at 10:19 29 February 2016

for different magnitudes of ΔT. In addition to the hot spot profiles, a global temperature gradient of 5 K/mm (similar to set #1 in Table 1) is also superimposed on the initial mean temperature. It is clearly observed that the sensitivity of auto-ignition phenomena to temperature inhomogeneities increases as the initial bulk temperature is lowered, leading to greater advancement in the net ignition delay time. As shown earlier, this trend directly reflects the transition from the strong to the weak ignition regime, resulting in greater influence of deflagrative front propagation. These findings are qualitatively in agreement with recent experimental findings based on detailed optical visualisations [13].

As a final remark, although the focus of the present work is on syngas auto-ignition, the Zel'dovich–Sankaran criterion is applicable to any reactant mixture in general, with known homogeneous ignition characteristics and deflagration front propagation speed. A recent experimental study using iso-octane confirms consistent behaviour [36]. Extension of the Zel'dovich–Sankaran criterion to predict weak versus strong ignition regimes in turbulent conditions has been proposed with a scaling analysis by Im *et al.* [22], and validation by multi-dimensional simulations is underway. Future work should also investigate the extension of the current theoretical framework to generalised turbulent mixing conditions including composition fluctuations.

Downloaded by [University of Michigan] at 10:19 29 February 2016

4. Conclusion

Auto-ignition characteristics of syngas fuel at high-pressure and low-temperature conditions were investigated by one-dimensional numerical simulations with detailed chemical kinetics and transport properties. Parametric tests were carried out over a wide range of thermodynamic conditions to study the effects of temperature inhomogeneities represented by global temperature gradients and localised hot spots. Front propagation speed and front Damköhler number analyses allowed detailed description of the propagating ignition front. It was observed that auto-ignition became more sensitive to the presence of temperature fluctuations as the bulk temperature was lowered, resulting in a transition from the strong to the weak ignition regime, accompanied by enhanced deflagrative front propagation. A larger strength of the hot spot was found to amplify the effects of weak ignition. Furthermore, the prevalence of weak ignition was found to yield a significant advancement of the net ignition delay time as compared to the corresponding homogeneous model predictions, by promoting end-gas compression-heating.

When the bulk mixture was not highly reactive, it was also observed that passive scalar dissipation could lead to very fast dissipation of the temperature fluctuations, when the mixing Damköhler number became much less than unity, thereby promoting strong ignition at sufficiently low temperatures. However, this effect was important only in cases of global temperature gradients, and not for local hot spots.

The numerical results were used to validate the Zel'dovich–Sankaran criterion, which takes into consideration the interplay of chemical kinetics, thermo-physical properties and device-dependent thermal characteristics, as a predictive metric to identify ignition regimes. It was demonstrated that $\mathrm{Sa} = 1$ adequately captures the boundary between the weak and strong ignition regimes. Furthermore, the relative magnitude of the Sankaran number translates accurately to the quantitative strength of the deflagration front in the overall ignition advancement.

Extension of the Zel'dovich–Sankaran criterion to turbulent conditions has been attempted and a regime diagram has been proposed [22]. Further validation of the concept in multi-dimensional simulations will be conducted in future work.

Funding

The authors acknowledge the financial support of the US Department of Energy via the National Energy Technology Laboratory [award number DE-FE0007465]; King Abdullah University of Science and Technology (KAUST).

ORCID

Pinaki Pal http://orcid.org/0000-0002-8630-5731
Margaret S. Wooldridge http://orcid.org/0000-0003-1754-180X
Hong G. Im http://orcid.org/0000-0001-7080-1266

Downloaded by [University of Michigan] at 10:19 29 February 2016

References

[1] R.A. Dennis and R. Harp, *Overview of the U.S. Department of Energy's office of fossil energy advanced turbine program for coal based power systems with carbon capture*, in Proceedings of ASME Turbo Expo 2007; Power for Land, Sea and Air, Paper GT2007-28338, 14–17 May 2007, Montreal, Canada.

[2] K.H. Casleton, R.W. Breault, and G.A. Richards, *System issues and tradeoffs associated with syngas production and combustion*, Combust. Sci. Technol. 180 (2008), pp. 1013–1052.

[3] E.L. Peterson, D.M. Kalitan, A.B. Barrett, S.C. Reehal, J.D. Mertens, D.J. Beerer, R.L. Hack, and V.G. McDonell, *New syngas/air ignition data at lower temperature and elevated pressure and comparison to current kinetic models*, Combust. Flame 149 (2007), pp. 244–247.

[4] C.-J. Sung, and C.K. Law, *Fundamental combustion properties of H_2/CO mixtures: Ignition and flame propagation at elevated pressures*, Combust. Sci. Technol. 180 (2008), pp. 1097–1116.

[5] F.L. Dryer and M. Chaos, *Ignition of syngas/air and hydrogen/air mixtures at low temperatures and high pressures: Experimental data interpretation and kinetic modelling implications*, Combust. Flame 152 (2008), pp. 293–299.

[6] M. Chaos and F.L. Dryer, *Syngas combustion kinetics and applications*, Combust. Sci. Technol. 180 (2008), pp. 1053–1096.

[7] D.J. Beerer and V.G. McDonell, *Autoignition of hydrogen and air inside a continuous flow reactor with application to lean premixed combustion*, J. Eng. Gas Turbines Power 130 (5) (2008), Paper No. 051507. Available at http://dx.doi.org/10.1115/1.2939007.

[8] D.M. Kalitan, J.D. Mertens, M.W. Crofton, and E.L. Peterson, *Ignition and oxidation of CO/H_2 fuel blends in air*, J. Propulsion & Power 23 (6) (2007), pp. 1291–1304.

[9] S.M. Walton, X. He, B.T. Zigler, and M.S. Wooldridge, *An experimental investigation of the ignition properties of hydrogen and carbon monoxide mixtures for syngas turbine applications*, Proc. Combust. Inst. 31 (2007), pp. 3147–3154.

[10] S.P. Medvedev, G.L. Agafonov, S.V. Khomik, and B.E. Gelfand, *Ignition delay in hydrogen–air and syngas–air mixtures: Experimental data interpretation via flame propagation*, Combust. Flame 157 (2010), pp. 1436–1438.

[11] R. Blumenthal, K. Fieweger, and K.H. Comp, *Self-ignition of H_2–air mixtures at high pressure and low temperature*, Proc. Int. Symp. Shock Waves 20 (1995), pp. 935–940.

[12] V.V. Martynenko, O.G. Penyaz'kov, K.A. Ragotner, and S.I. Shabunya, *High-temperature ignition of hydrogen and air at high pressures downstream of the reflected shock* wave, J. Eng. Phys. Thermophys. 77 (4) (2004), pp. 785–793.

[13] A.B. Mansfield and M.S. Wooldridge, *High-pressure low-temperature ignition behavior of syngas mixtures*, Combust. Flame 161 (9) (2014), pp. 2242–2251.

[14] V.V. Voevodsky and R.I. Soloukhin, *On the mechanism and explosion limits hydrogen–oxygen chain self-ignition in shock waves*, Proc. Combust. Inst. 10 (1965), pp. 279–283.

[15] J.W. Meyer and A.K. Oppenheim, *On the shock-induced ignition of explosive gases*, Proc. Combust. Inst. 13 (1971), pp. 1153–1164.

[16] E.S. Oran, T.R. Young, J.P. Boris, and A. Cohen, *Weak and strong ignition. I. Numerical simulations of shock tube experiments*, Combust. Flame 48 (1982), pp. 135–148.

[17] E.S. Oran and J.P. Borris, *Weak and strong ignition. II. Sensitivity of the hydrogen–oxygen system*, Combust. Flame 48 (1982), pp. 149–161.

[18] M. Ihme, *On the role of turbulence and composition fluctuations in rapid compression machines: Autoignition of syngas mixtures*, Combust. Flame 159 (2012), pp. 1592–1604.
[19] H. Wu and M. Ihme, *Effects of flow-field and mixture inhomogeneities on the ignition dynamics in continuous flow reactors*, Combust. Flame 161 (2014), pp. 2317–2326.
[20] Y.B. Zel'dovich, *Regime classification of an exothermic reaction with nonuniform initial conditions*, Combust. Flame 39 (1980), pp. 211–214.
[21] R. Sankaran, H.G. Im, E.R. Hawkes, and J.H. Chen, *The effects of non-uniform temperature distribution on the ignition of a lean homogeneous hydrogen–air mixture*, Proc. Combust. Inst. 30 (2005), pp. 875–882.
[22] H.G. Im, P. Pal, M.S. Wooldridge, and A.B. Mansfield, *A regime diagram for autoignition of homogeneous reactant mixtures with turbulent velocity and temperature fluctuations*, Combust. Sci. Technol. 187(8) (2015), pp. 1263–1275.
[23] J.H. Chen, A. Choudhary, B. de Supinski, M. DeVries, E.R. Hawkes, S. Klasky, W.K. Liao, K.L. Ma, J. Mellor-Crummey, N. Podhorszki, R. Sankaran, S. Shende, and C.S. Yoo, *Terascale direct numerical simulations of turbulent combustion using S3D*, Comput. Sci. Discov. 2 (2009), Paper No. 015001. Available at http://dx.doi.org/10.1088/1749-4699/2/1/015001.
[24] C.A. Kennedy and M.H. Carpenter, *A comparison of several new numerical methods for the simulation of compressible shear layers*, Appl. Numer. Math. 14 (1994), pp. 397–433.
[25] J. Li, Z. Zhao, A. Kazakov, M. Chaos, F.L. Dryer, and J.J. Scire, *A comprehensive kinetic mechanism for CO, CH_2O and CH_3OH combustion*, Int. J. Chem. Kinet. 39 (2007), pp. 109–136.
[26] R.J. Kee, F.M. Rupley, E. Meeks, and J.A. Miller, *CHEMKIN-III: a Fortran chemical kinetic package for the analysis of gas-phase chemical and plasma kinetics*, Tech. Rep. SAND96-8216, Sandia National Laboratories, 1996.
[27] R.J. Kee, G. Dixon-Lewis, J. Warnatz, M.E. Coltrin, and J.A. Miller, *A Fortran computer code package for the evaluation of gas-phase multicomponent transport properties*, Tech. Rep. SAND86-8246, Sandia National Laboratories, 1986.
[28] X.J. Gu, D.R. Emerson, and D. Bradley, *Modes of reaction front propagation from hot spots*, Combust. Flame 133 (2003), pp. 63–74.
[29] J.H. Chen, S.D. Mason, and J.C. Hewson, *The effect of temperature inhomogeneity on low-temperature autoignition of fuel-lean premixed hydrogen/air mixtures*, in: 16–19 March 2003, Chicago, IL.
[30] G. Mittal and C.-J. Sung, *Aerodynamics inside a rapid compression machine*, Combust. Flame 145 (2006), pp. 160–180.
[31] T. Echekki and J.H. Chen, *Analysis of the contribution of curvature to premixed flame propagation*, Combust. Flame 118 (1999), pp. 308–311.
[32] H.G. Im and J.H. Chen, *Structure and propagation of triple flames in partially premixed hydrogen–air mixtures*, Combust. Flame 119 (1999), pp. 436–454.
[33] J.H. Chen, E.R. Hawkes, R. Sankaran, S.D. Mason, and H.G. Im, *Direct numerical simulation of ignition front propagation in a constant volume with temperature inhomogeneities. I. Fundamental analysis and diagnostics*, Combust. Flame 145 (2006), pp. 128–144.
[34] S.O. Kim, M.B. Luong, J.H. Chen, and C.S. Yoo, *A DNS study of the ignition of lean PRF/air mixtures with temperature inhomogeneities under high pressure and intermediate temperature*, Combust. Flame 162 (3) (2014), pp. 717–726.
[35] G. Bansal and H.G. Im, *Autoignition and front propagation in low temperature combustion engine environments*, Combust. Flame 158 (2011), pp. 2105–2112.
[36] A.B. Mansfield, M.S. Wooldridge, H. Di, and X. He, *Low-temperature ignition behavior of iso-octane*, Fuel 139 (2015), pp. 79–86.

Downloaded by [University of Michigan] at 10:19 29 February 2016

Available online at www.sciencedirect.com
ScienceDirect
Proceedings of the Combustion Institute 000 (2016) 1–12
Proceedings of the Combustion Institute
www.elsevier.com/locate/proci

Computational characterization of ignition regimes in a syngas/air mixture with temperature fluctuations

Pinaki Pal [a], Mauro Valorani [b], Paul G. Arias [a], Hong G. Im [c,*], Margaret S. Wooldridge [a,d], Pietro P. Ciottoli [b], Riccardo M. Galassi [b]

[a] *Department of Mechanical Engineering, University of Michigan, Ann Arbor, MI 48109-2125, USA*
[b] *Departimento de Ingegneria Meccanica e Aerospaziale, University of Rome La Sapienza, Via Eudossiana 18, 00184 Rome, Italy*
[c] *Clean Combustion Research Center, King Abdullah University of Science and Technology (KAUST), Thuwal 23955-6900, Saudi Arabia*
[d] *Department of Aerospace Engineering, University of Michigan, Ann Arbor, MI 48109-2125, USA*

Received 3 December 2015; accepted 13 July 2016
Available online xxx

Abstract

Auto-ignition characteristics of compositionally homogeneous reactant mixtures in the presence of thermal non-uniformities and turbulent velocity fluctuations were computationally investigated. The main objectives were to quantify the observed ignition characteristics and numerically validate the theory of the turbulent ignition regime diagram recently proposed by Im et al. 2015 [29] that provides a framework to predict ignition behavior *a priori* based on the thermo-chemical properties of the reactant mixture and initial flow and scalar field conditions. Ignition regimes were classified into three categories: *weak* (where deflagration is the dominant mode of fuel consumption), *reaction-dominant strong,* and *mixing-dominant strong* (where volumetric ignition is the dominant mode of fuel consumption). Two-dimensional (2D) direct numerical simulations (DNS) of auto-ignition in a lean syngas/air mixture with uniform mixture composition at high-pressure, low-temperature conditions were performed in a fixed volume. The initial conditions considered two-dimensional isotropic velocity spectrums, temperature fluctuations and localized thermal hot spots. A number of parametric test cases, by varying the characteristic turbulent Damköhler and Reynolds numbers, were investigated. The evolution of the auto-ignition phenomena, pressure rise, and heat release rate were analyzed. In addition, combustion mode analysis based on front propagation speed and computational singular perturbation (CSP) was applied to characterize the auto-ignition phenomena. All results supported that the observed ignition behaviors were consistent with the expected ignition regimes predicted by the theory of the regime diagram. This work provides new high-fidelity data on syngas ignition characteristics over a broad range of conditions and demonstrates that the regime diagram serves as a predictive guidance in the

* Corresponding author.
E-mail address: hong.im@kaust.edu.sa (H.G. Im).

http://dx.doi.org/10.1016/j.proci.2016.07.059
1540-7489 © 2016 by The Combustion Institute. Published by Elsevier Inc.

Please cite this article as: P. Pal et al., Computational characterization of ignition regimes in a syngas/air mixture with temperature fluctuations, Proceedings of the Combustion Institute (2016), http://dx.doi.org/10.1016/j.proci.2016.07.059

understanding of various physical and chemical mechanisms controlling auto-ignition in thermally inhomogeneous and compositionally homogeneous turbulent reacting flows.
© 2016 by The Combustion Institute. Published by Elsevier Inc.

Keywords: Direct numerical simulation; Strong and weak ignition; Ignition regimes; Temperature fluctuations; Computational singular perturbation

1. Introduction

Low-temperature combustion (LTC) strategies have the potential to improve efficiency and reduce NO_x emissions in both transportation [1] and stationary power devices [2]. Reductions in combustion temperature can be achieved by operating at lean, nearly homogeneous, and/or diluted, conditions. However, issues related to combustion stability, safety and control may arise at these conditions, due to increased influence of abnormal ignition behaviors such as early ignition and flashback in gas turbines [2,3] or knock in reciprocating engines [4]. Improved understanding and better prediction of auto-ignition characteristics are therefore valuable for successful implementation of these advanced technologies.

Many experimental studies have been conducted to investigate auto-ignition of different fuels such as hydrogen [5–9], iso-octane [10,11] and syngas [12,13], at conditions relevant to practical combustion systems. Two types of auto-ignition regimes were commonly observed: strong (spatially homogeneous ignition) and weak (localized reaction sites and deflagration). Moreover, the boundary between strong and weak ignition regimes, known as the *strong ignition limit*, was found to coincide with an iso-line of the sensitivity of homogeneous ignition delay time to temperature, $d\tau_{ig}/dT$, in the pressure-temperature space [6,13]. Recent experimental investigations of syngas auto-ignition [14–18] at conditions relevant to gas turbine operation reported large discrepancies between measurements and homogeneous chemical kinetic modeling predictions of ignition delay times, with the former being orders of magnitude lower than the latter. Mansfield and Wooldridge [13] studied syngas auto-ignition in a rapid compression facility and demonstrated that the discrepancy was due to transition from strong to weak ignition regime as the initial mean temperature was lowered. In addition, a simple criterion proposed by Sankaran et al. [19] (referred to as the Sankaran criterion here), based on Zel'dovich's original theory [20] was found to capture the experimentally observed strong ignition limit *a priori*. This predictive criterion is defined as the ratio of laminar flame speed to the thermal gradient driven spontaneous propagation speed. Pal et al. [21] further numerically validated the Sankaran criterion as a predictive indicator of the ignition regime for homogeneous mixtures in the presence of thermal non-uniformities through parametric studies of syngas auto-ignition in a one-dimensional configuration.

In addition to thermal inhomogeneities, the presence of turbulence may also significantly influence auto-ignition phenomena in practical devices. Ihme and co-workers [22,23] demonstrated using a reduced order modeling approach that turbulent fluctuations could result in significant advancement of overall ignition. A number of DNS studies [24–28] have revealed that thermal stratification and turbulence can influence auto-ignition phenomena in LTC engines. More recently, Im et al. [29] conducted a theoretical scaling analysis and proposed non-dimensional criteria in terms of the characteristic Damköhler and Reynolds numbers of a system to predict the occurrence of strong and weak ignition regimes in thermally inhomogeneous turbulent reacting flows. The criteria formulated by extending the original Sankaran criterion [19] and taking into account the effects of passive scalar mixing due to turbulence, ultimately led to the development of a turbulent ignition regime diagram [29]. An alternative version of ignition regime diagram has also been proposed by Grogan et al. [30].

The present computational study investigates the effects of thermal inhomogeneities and turbulence on syngas auto-ignition behavior. 2D DNS of auto-ignition in a lean syngas/air mixture are performed at various parametric conditions. The high-fidelity simulations aim to provide additional insight into the range of ignition behaviors that can be expected under high-pressure low-temperature conditions, and also provide numerical validation of the turbulent ignition regime diagram [29]. In the next section, the ignition regime diagram is briefly reviewed. The numerical setup for simulations is presented next. The auto-ignition behaviors are subsequently characterized and the results are discussed in the context of the corresponding predictions of the regime diagram.

2. Turbulent ignition regime diagram

One of the non-dimensional parameters used as an ignition regime criterion is the Sankaran

Please cite this article as: P. Pal et al., Computational characterization of ignition regimes in a syngas/air mixture with temperature fluctuations, Proceedings of the Combustion Institute (2016), http://dx.doi.org/10.1016/j.proci.2016.07.059

number, Sa [19]:

$$\mathrm{Sa} \approx \beta S_L \left| \frac{d\tau_{ig}}{dT} \right| \widetilde{|\nabla T|} \tag{1}$$

where S_L and τ_{ig} are the laminar flame speed and homogeneous ignition delay corresponding to the initial bulk mixture conditions, $\widetilde{|\nabla T|}$ denotes the statistical mean temperature gradient [29] and β is a constant of order unity. In the present study, β is equal to 0.5 [19]. Scaling analysis yields the following expression for Sa [29]:

$$\mathrm{Sa} = K\mathrm{Da}_\ell^{-1/2}, \quad K = \beta \left(\frac{T'}{(\tau_f \tau_{ig})^{1/2}} \right) \left| \frac{d\tau_{ig}}{dT} \right| \tag{2}$$

Here, $\tau_f = \alpha / {S_L}^2$ is the flame time scale, where α is the thermal diffusivity of the initial bulk reactant mixture. T' represents the magnitude of thermal fluctuation. $\mathrm{Da}_\ell = \tau_t / \tau_{ig}$ is the integral scale Damköhler number, where τ_t is the turbulence time scale defined as the ratio of integral length scale (ℓ) to velocity fluctuation (u'). K is referred to as the normalized thermal ignition sensitivity [29].

The second ignition regime criterion is based on mixing Damköhler number, Da_λ, defined as the ratio of time scale associated with the Taylor microscale (τ_λ) to τ_{ig}:

$$\mathrm{Da}_\lambda = \frac{\tau_\lambda}{\tau_{\mathrm{ig}}} = \frac{\tau_\ell}{\tau_{\mathrm{ig}}} \frac{\tau_\lambda}{\tau_\ell} = \mathrm{Da}_\ell \mathrm{Re}_\ell^{-1/3} \tag{3}$$

where, $\mathrm{Re}_\ell = u'\ell/\nu$ is the turbulent Reynolds number, and ν is the kinematic viscosity of the bulk mixture gas.

Weak (W) ignition is expected if $\mathrm{Sa} > 1$, and strong ignition is expected if $\mathrm{Sa} < 1$ [19,21]. Therefore, Eq. (2) suggests that weak ignition is possible for $\mathrm{Da}_\ell < K^2$. If $\mathrm{Da}_\ell > K^2$, the reactant mixture ignites spontaneously despite some level of temperature fluctuations. This is referred to as the reaction-dominant strong (RD-S) ignition regime. In addition, $\mathrm{Da}_\ell < 1$ indicates that turbulent mixing is sufficiently rapid and the temperature fluctuations will be dissipated before local ignition kernels are formed. This is referred to as the mixing-dominant strong (MD-S) ignition regime. The conditions between $\mathrm{Da}_\lambda < 1$ and $\mathrm{Da}_\ell > 1$ represent a "grey" zone, in that some mixed mode ignition may occur. This is denoted as the *mixing-dominant* or *mixed/strong* (MXD) ignition regime. These different ignition criteria lead to the regime diagram as shown in Fig. 1.

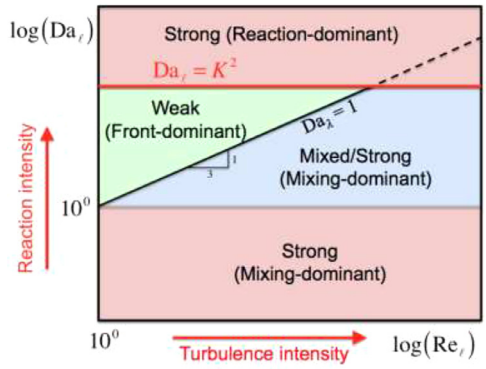

Fig. 1. Regime diagram for auto-ignition of homogeneous reactant mixture with temperature fluctuations and turbulence [29].

3. Numerical method and initial conditions

2D simulations were performed using the DNS code, S3D [31], which solves the compressible, Navier–Stokes, species and energy equations using a fourth-order explicit Runge–Kutta method for time integration and an eighth-order central differencing scheme for spatial discretization [32]. A detailed H_2/CO mechanism with 12 species and 33 chemical reactions from Li et al. [33] was linked with CHEMKIN [34] and TRANSPORT [35] libraries for evaluating the reaction rates and thermodynamic and mixture-averaged transport properties, respectively. Periodic boundary conditions were imposed in all directions to represent constant volume ignition.

A uniform syngas/air reactant mixture of equivalence ratio of 0.5, H_2:CO molar ratio of 0.7:1, an initial pressure of 20 atm, was chosen. In addition, the mixture was diluted with excess nitrogen equal

Table 1
Physical and regime diagram parameters for the DNS cases.

Case	T_0(K)	τ_{ig} (ms)	K^2	ℓ_e (mm)	u'(m/s)	τ_t (ms)	Da_ℓ	Re_ℓ	Da_λ	Ignition regime[a]
A	990	25.77	4.05	4.3	0.05	86.0	3.34	35.24	1.02	W
B	1100	2.07	2.51	4.3	0.05	86.0	41.6	29.40	13.5	RD-S
C	990	25.77	4.05	4.3	1.50	2.87	0.11	1057.4	0.01	MD-S
D	1100	2.07	2.51	1.4	0.325	4.31	2.08	62.2	0.6	MXD
E	1020	12.7	3.28	4.0	0.3	13.33	1.05	185.0	0.2	MXD
F	1100	2.07	2.51	6.0	0.2	30.0	14.5	164.0	2.65	RD-S
G	990	25.77	4.05	6.0	0.2	30.0	1.16	197.0	0.2	MXD
H	970	41.26	4.41	6.0	0.05	120.0	2.91	50.0	0.8	MXD

[a] Predicted ignition regime based on the combustion theory developed and presented by Im et al. [29].

Please cite this article as: P. Pal et al., Computational characterization of ignition regimes in a syngas/air mixture with temperature fluctuations, Proceedings of the Combustion Institute (2016), http://dx.doi.org/10.1016/j.proci.2016.07.059

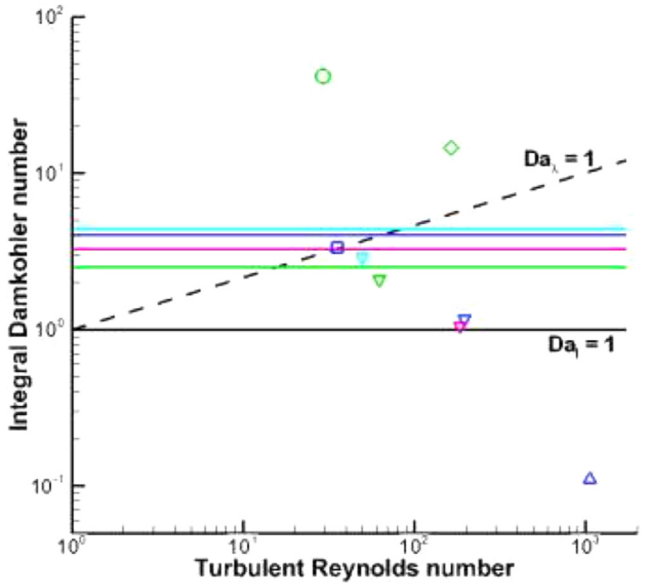

Fig. 2. Parametric cases A (blue square), B (green circle), C (blue triangle), D (green diamond), E (pink delta), F (green diamond), G (blue delta) and H (sky blue delta) on the ignition regime diagram. The solid lines with the same colors as the symbols correspond to the respective Sa = 1 lines for those cases. (For interpretation of the references to color in this figure legend, the reader is referred to the web version of this article).

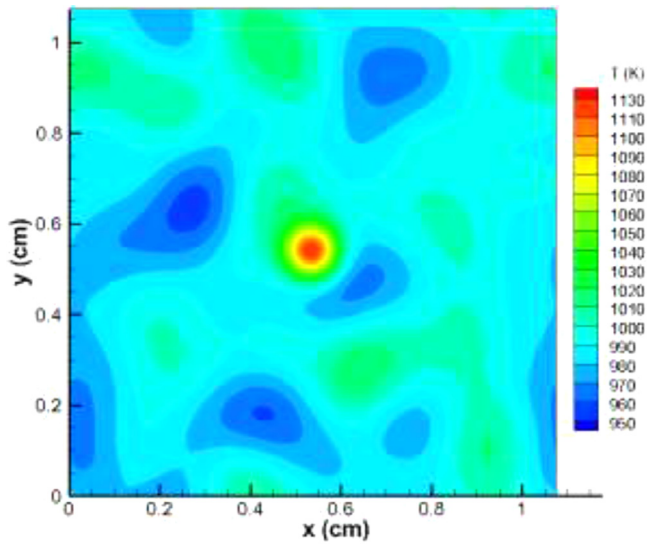

Fig. 3. Initial temperature field for case A.

to twice the amount of nitrogen present in the air, resulting in the overall molar ratio of N_2:O_2=11.28 in the reactant mixture, to ensure the pressure rise was sufficiently high to serve as an indicator of auto-ignition, but also to avoid shock wave formation [36,37], which cannot be captured by the employed computational schemes at present.

Turbulent velocity fluctuations were superimposed on a stationary mean velocity field based on an isotropic kinetic energy spectrum function [38]. A similar random temperature spectrum, uncorrelated with the turbulent kinetic energy spectrum, was superimposed on a constant mean temperature field. In addition, a thermal hot spot was superim-

Please cite this article as: P. Pal et al., Computational characterization of ignition regimes in a syngas/air mixture with temperature fluctuations, Proceedings of the Combustion Institute (2016), http://dx.doi.org/10.1016/j.proci.2016.07.059

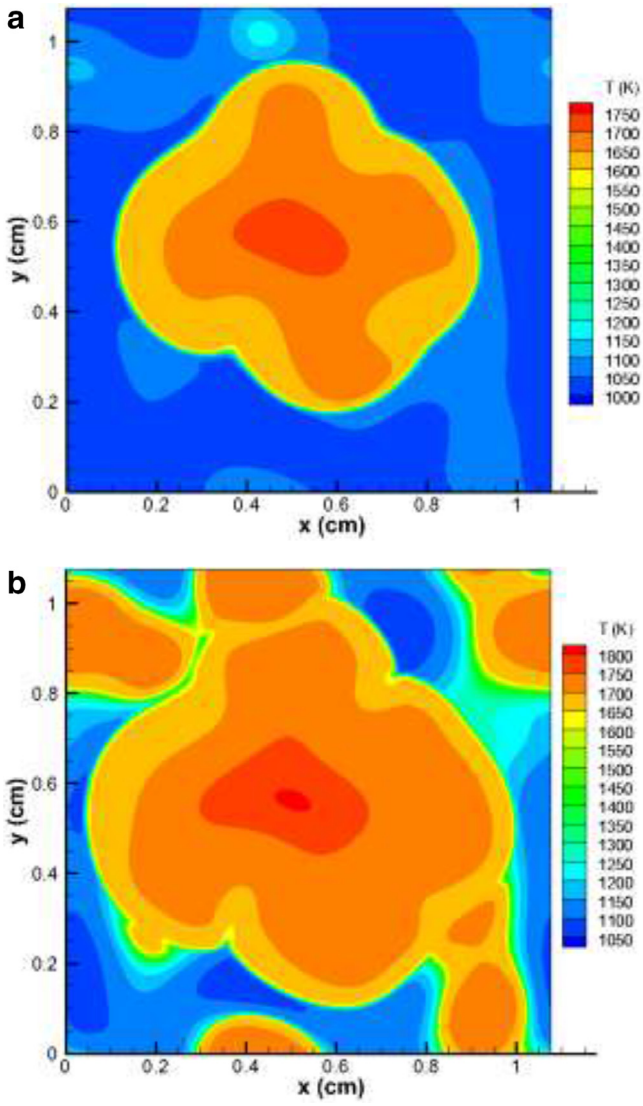

Fig. 4. Temperature fields for case A at (a) $t / \tau_{ig} = 0.41$ and (b) $t / \tau_{ig} = 0.48$.

posed on the temperature field in the form [19]:

$$T_{hs}(x, y) = \frac{A}{\pi} \exp\left[\frac{-2n^2((x - L/2)^2 + (y - L/2)^2)}{L^2}\right] - \frac{A}{2n^2} \quad (4)$$

where L is the length of each side of a 2D square box domain, $A = 450$, $n = 12$ and (x, y) represents spatial location. The peak temperature of the hot spot was approximately 100 K, which is the upper limit of the local temperature fluctuations commonly observed in ignition experiments [39].

A total of eight DNS cases A-H were considered by varying initial mean temperature (T_0), most energetic turbulent length scale (ℓ_e) and u'. For the four different T_0 values of 1100, 1020, 990 and 970 K considered, the computed $S_L$values from PREMIX [40] simulations were 67.7, 27.8, 20.5, and 16.5 cm/s, respectively. $L = 1.075$ cm and 1.5 cm for cases A–E and F–H, respectively. T' was fixed at 15 K for all cases. The turbulence time scale was defined by $\tau_t = \ell_e / u'$. The most energetic length scales of velocity and the temperature fluctuations were the same for all cases. For all simulations, the Kolmogorov length scale was resolved with at least 1 grid point [41] and the thinnest reaction fronts were resolved with at least 10 grid points.

Please cite this article as: P. Pal et al., Computational characterization of ignition regimes in a syngas/air mixture with temperature fluctuations, Proceedings of the Combustion Institute (2016), http://dx.doi.org/10.1016/j.proci.2016.07.059

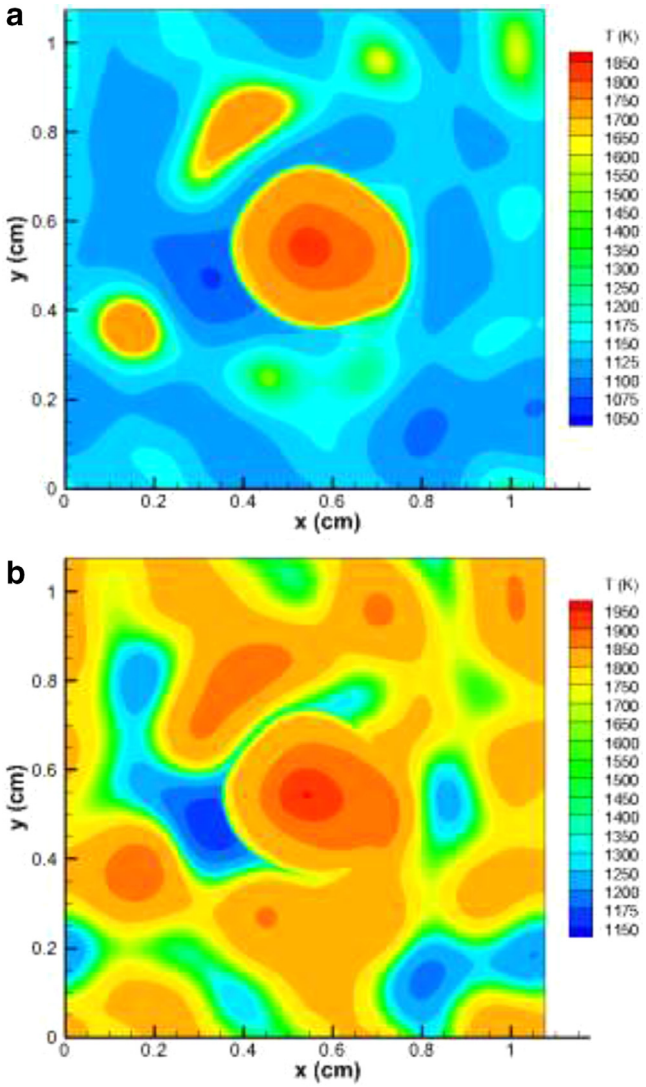

Fig. 5. Temperature fields for case B at (a) $t / \tau_{ig} = 0.63$ and (b) $t / \tau_{ig} = 0.77$.

Details of the physical parameters for the different cases and the expected ignition regimes are listed in Table 1. All the parametric cases are plotted on the regime diagram in Fig. 2. The initial temperature profile for case A is shown in Fig. 3.

4. Results and discussion

4.1. General description of auto-ignition phenomena

For the simulation cases, auto-ignition progress was investigated by monitoring the temporal evolution of the temperature fields, mean pressure and heat release rate. For all cases A–H tested, the observed ignition regimes were found to exhibit the behaviors predicted by the regime diagram as summarized in Table 1. However, for the sake of brevity, results for only the first three parametric cases A, B and C are reported here which correspond to the W, RD-S and MD-S ignition regimes, respectively. Relative to cases A and C, the initial mean temperature for case B is higher and case C has relatively higher turbulence velocity fluctuation as compared to cases A and B.

Figure 4 shows the temporal evolution of temperature field for case A. It is readily observed that a reaction front emanates from the hot spot at the center of the domain and consumes the majority

Please cite this article as: P. Pal et al., Computational characterization of ignition regimes in a syngas/air mixture with temperature fluctuations, Proceedings of the Combustion Institute (2016), http://dx.doi.org/10.1016/j.proci.2016.07.059

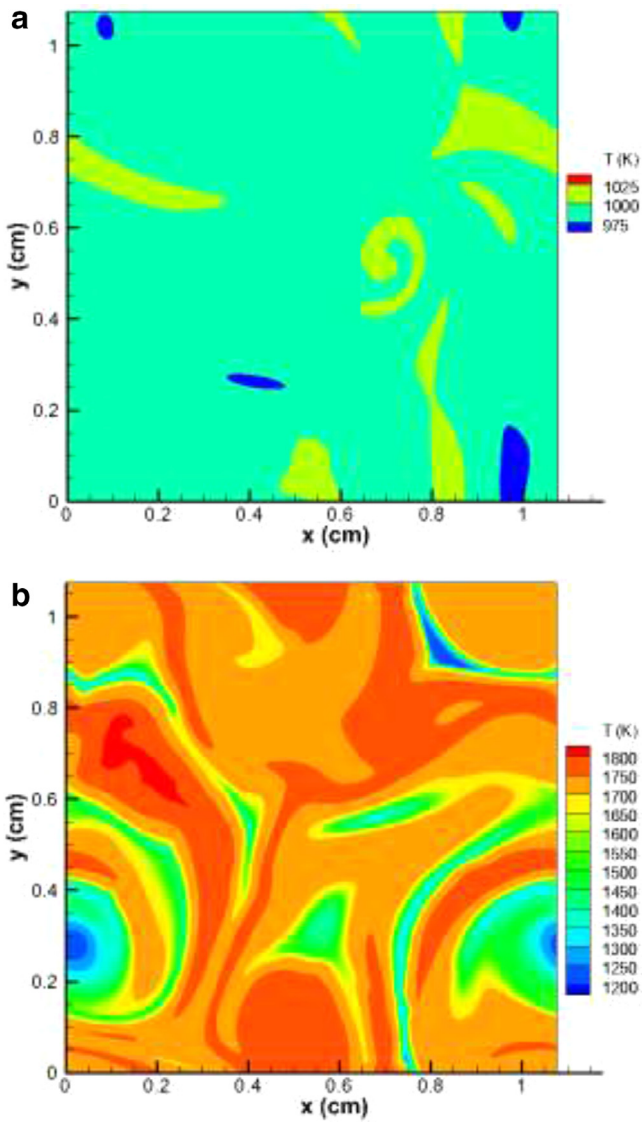

Fig. 6. Temperature fields for case C at (a) $t / \tau_{ig} = 0.33$ and (b) $t / \tau_{ig} = 0.94$.

of the reactant mixture. In contrast, for case B, although there is initially some reaction front propagation from the hot spot (Fig. 5a), the front is not able to consume much of the reactant mixture. Instead, isolated ignition fronts are formed in the end gas, consuming the rest of the mixture as shown in Fig. 5b. This is attributed to the relatively higher reactivity of the end gas which is a result of the higher initial mean temperature. Lastly, for case C, the stronger turbulence level leads to rapid scalar dissipation of the temperature fluctuations (Fig. 6a). Due to strong turbulent mixing, T' decreases from the initial value of 15 K to a minimum value of 6 K, before any ignition fronts develop. Consequently, the reactant mixture auto-ignites almost homogeneously throughout the domain as seen in Fig. 6b.

Figure 7 shows the temporal evolution of mean pressure and integrated heat release rate (HRR) for the three cases, where HRR and time are normalized by the maximum integrated HRR and τ_{ig} of the corresponding zero-dimensional (0D) cases, respectively. For comparison, the temporal evolution of 0D ignition for $T_0 = 1100$ K and 990 K are also shown. For case A, the pressure and HRR increase earlier and more slowly than the corresponding 0D case (at 990 K), resulting from the deflagrative front propagation. Based on the pressure rise curve for case A, it appears that the fractional contribution

Please cite this article as: P. Pal et al., Computational characterization of ignition regimes in a syngas/air mixture with temperature fluctuations, Proceedings of the Combustion Institute (2016), http://dx.doi.org/10.1016/j.proci.2016.07.059

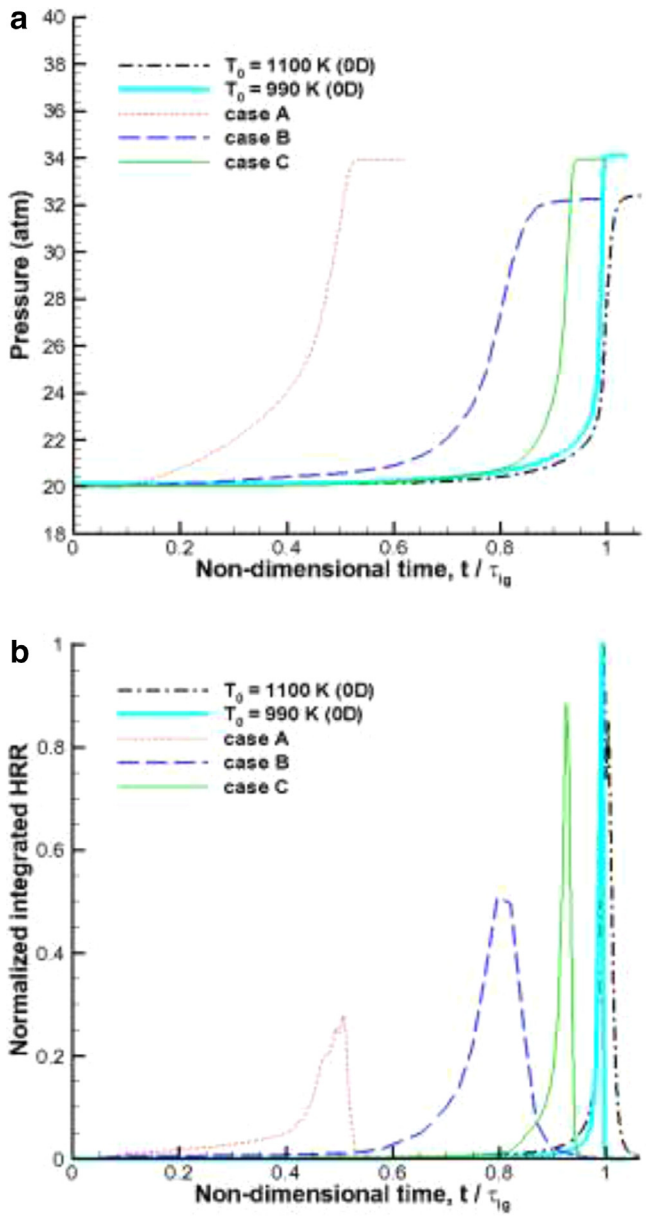

Fig. 7. Temporal evolution of (a) mean pressure and (b) heat release rate for cases A, B and C. The time is normalized by homogeneous ignition delay time at the mean initial mixture conditions for each case.

of the heat release by deflagration is about half or less, which is in agreement with the regime diagram estimate shown in Fig. 2, where case A is close to the limit between W and RD-S regimes. The maximum HRR is also much lower. In comparison, cases B and C ignite much closer to the corresponding 0D ignition delay (at 1100 K) and have much higher peak HRRs compared to case A. Moreover, the rates of pressure rise are much higher for cases B and C compared to case A.

4.2. Front speed analysis

To characterize the auto-ignition behaviors, front propagation speeds are examined for the cases. The density-weighted front propagation speed [42,43], S_d, is employed as a metric to distinguish between deflagration and spontaneous ignition fronts. The isocontour of $Y_{H_2} = 0.019$ is chosen to evaluate the mean displacement speed as this particular isocontour coincides approximately

Please cite this article as: P. Pal et al., Computational characterization of ignition regimes in a syngas/air mixture with temperature fluctuations, Proceedings of the Combustion Institute (2016), http://dx.doi.org/10.1016/j.proci.2016.07.059

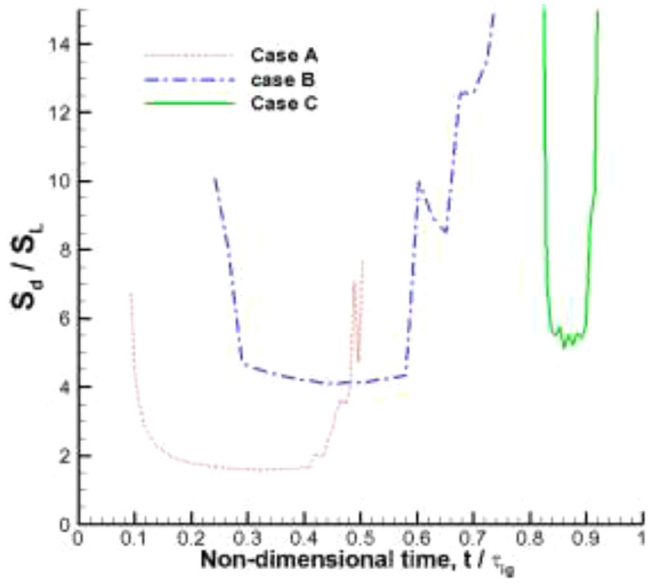

Fig. 8. Temporal evolution of mean front speed for cases A, B and C. The time is normalized by homogeneous ignition delay time at the mean initial mixture conditions for each case.

with the location of instantaneous maximum HRR, thereby capturing the propagating reaction fronts. A similar approach was used in Ref. [21], and it was found that different choices of the marker species yielded consistent results.

Figure 8 shows the temporal evolution of the mean front speed, normalized by the corresponding laminar flame speed, for cases A, B and C. The mean front speeds exhibit a characteristic U-shape [44,45], attributed to the initial thermal runaway in the nascent ignition kernel during the early phase of combustion and final stage of fuel consumption. For case A, the minimum front speed is close to S_L (within a factor of 1.5) indicating deflagrative front propagation. On the other hand, for cases B and C, the minimum front speed is much higher (by over a factor of 4) than S_L, thereby suggesting that spontaneous propagation is the dominant combustion mode. Moreover, the duration of minimum front speed is much shorter for case C, indicating that the mixture auto-ignites nearly homogeneously in this case. These results along with the qualitative description of the ignition progress in Section 4.1 suggest that the auto-ignition behaviors of cases A, B and C are in good agreement with W, RD-S and MD-S regimes, respectively, as predicted by the regime diagram.

4.3. Computational singular perturbation diagnostics

To gain further insights into the ignition characteristics, a CSP analysis [46,47,48] was employed as an automated diagnostic tool to investigate the nature of the local reaction front propagation. CSP allows projection of all relevant chemical and transport processes onto a curvilinear frame of reference spanned by the right eigenvectors of the Jacobian matrix ($d\mathbf{g}/d\mathbf{Z}$) of the chemical source term vector ($\mathbf{g}$), where $\mathbf{Z}$ is the scalar solution variable vector (N_s species and temperature). The local eigenmodes, equal to the total number of scalar variables ($N_s + 1$), are thus identified having distinct characteristic timescales. Moreover, importance indices can be identified as a non-dimensional measure of the relative contribution of an individual process to the dynamics of a target observable [49,50]. To assess the role of transport with respect to chemistry in ignition front propagation, the importance index of transport (convection and diffusion) to the slow dynamics of temperature, I^T, is analyzed in the regions ahead of the reaction fronts [50]. By definition, I^T ranges from 0 to 1; transport prevails over kinetics when this index assumes values close to unity.

Figure 9a shows the isocontours of I^T for case A at $t / \tau_{ig} = 0.41$. The corresponding temperature isocontours are shown in Fig. 4a. In addition, isocontours of HCO radical mass fraction (in black) are also superimposed to denote the active reaction zones. This approach was found to be consistent with the identification of upstream regions ahead of the reaction fronts based on the number of exhausted modes (M) [50]. It is clearly seen that I^T approaches 1 in the upstream pre-heat region of the front, indicating that the reaction zone propagates upstream by virtue of transport, i.e., as a deflagration front. This confirms that the ignition

Please cite this article as: P. Pal et al., Computational characterization of ignition regimes in a syngas/air mixture with temperature fluctuations, Proceedings of the Combustion Institute (2016), http://dx.doi.org/10.1016/j.proci.2016.07.059

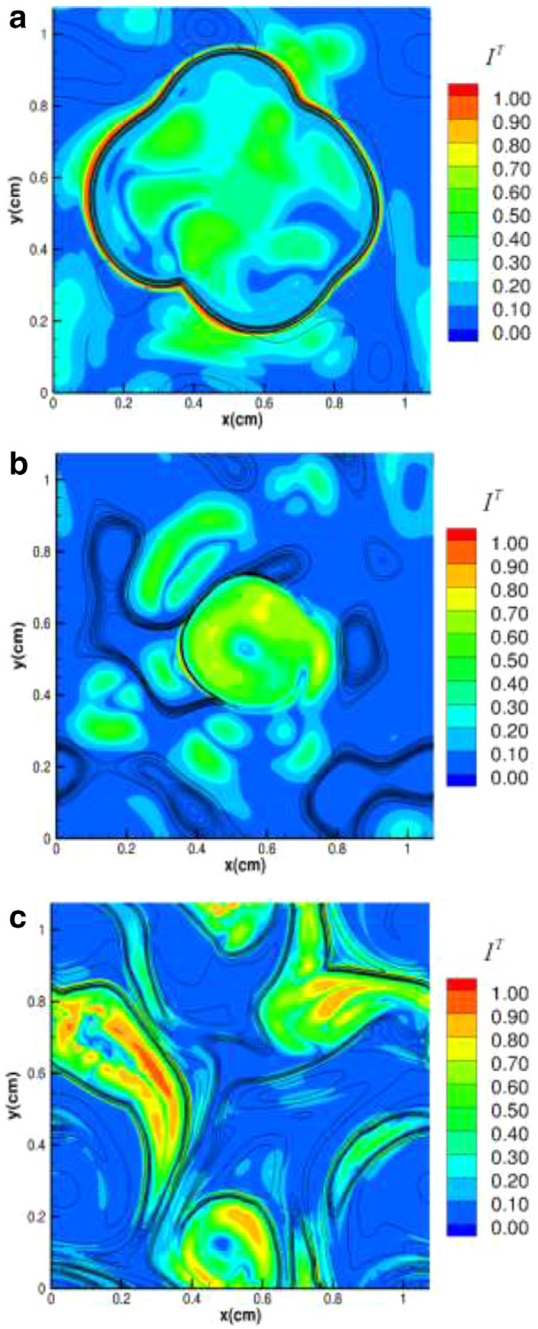

Fig. 9. I^T isocontours for (a) case A ($t / \tau_{ig} = 0.41$), (b) case B ($t / \tau_{ig} = 0.77$) and (c) case C ($t / \tau_{ig} = 0.94$). The HCO mass fraction contours are overlaid (in black).

behavior in this case is indeed in the weak (W) regime. Similarly, Fig. 9b and c shows the I^T and HCO mass fraction isocontours for cases B and C, at the same time instants for which the temperature profiles are shown in Figs. 5b and 6b, respectively. In contrast to case A, $I^T$is much lower (< 0.5) in the regions upstream of the ignition fronts. Therefore, front propagation is primarily driven by spontaneous ignition in these cases. Combining with the observations from the evolution of the respective temperature fields in Figs. 5 and 6, it can be inferred that the cases B and C fall into the

Please cite this article as: P. Pal et al., Computational characterization of ignition regimes in a syngas/air mixture with temperature fluctuations, Proceedings of the Combustion Institute (2016), http://dx.doi.org/10.1016/j.proci.2016.07.059

reaction-dominant and mixing-dominant strong ignition regimes, respectively. The results demonstrate that the ignition regime diagram is able to predict the strong and weak ignition regimes at various parametric conditions of initial turbulent velocity and temperature fluctuations with good fidelity.

5. Conclusions

In the present work, 2D DNS of auto-ignition in a uniform syngas/air mixture in the presence of turbulence and temperature fluctuations were performed, at high-pressure low-temperature conditions. Parametric cases were considered by varying the characteristic integral Damköhler and Reynolds numbers of the system, corresponding to different conditions on the ignition regime diagram of Im et al. [29]. For all cases, the observed ignition behaviors were found to agree with the predictions of the regime diagram consistently. Three representative cases A, B and C were analyzed in detail. Temporal evolution of the temperature field, mean pressure and integrated HRR showed increased propensity for reaction front propagation from a hot spot in case A; whereas for case B, isolated ignition kernels were formed; and for case C, rapid dissipation of the temperature fluctuations due to strong turbulent mixing was readily observed.

Further investigation of the ignition front characteristics was carried out using front speed and CSP importance index analyses. These additional diagnostics consistently showed that ignition in case A was driven by deflagration, whereas cases B and C were dominated by spontaneous ignition. These findings along with the above qualitative description of the ignition phenomena confirmed that the cases could be classified as weak (case A), reaction-dominant strong (case B) and mixing-dominant strong ignition (case C). These results are new and importantly demonstrate the large range of auto-ignition behaviors that can be encountered at low-temperatures and high-pressures for syngas, as well as the profound effects of turbulence and temperature fluctuations to accelerate ignition relative to 0D reference conditions. Larger advancement of overall ignition and significantly lower HRR relative to homogeneous conditions was observed in the weak ignition regime, in agreement with previous experimental observations [13]. Furthermore, the DNS results were consistent with predictions from the regime diagram based on theoretical scaling analysis. This demonstrates that the physical and chemical mechanisms controlling auto-ignition phenomena in thermally inhomogeneous turbulent reacting flows are well captured by the proposed ignition criteria by Im et al. [29].

Some of the ongoing efforts are focused on extending the applicability of the regime diagram to capture detonation by incorporating the effects of acoustics. This will have important implications in the prediction of engine super-knock phenomena. Experimental validation of the ignition regime characterization in compression ignition engines is also underway.

Acknowledgments

The authors acknowledge the financial support of U.S. DOE via NETL award number DE-FE0007465 and King Abdullah University of Science and Technology (KAUST). This research made use of the computer clusters at KAUST.

References

[1] J.E. Dec, *Proc. Combust. Inst.* 32 (2009) 2727–2742.
[2] G.A. Richards, M.M. McMillian, R.S. Gemmen, W.A. Rogers, S.R. Cully, *Prog. Energy Combust. Sci.* 27 (2) (2001) 141–169.
[3] T. Lieuwen, V. McDonell, D. Santavicca, T. SattelMayer, *Combust. Sci. Technol.* 180 (6) (2008) 1169–1192.
[4] J.A. Eng, SAE Transaction paper 2002-01-2859, 2002.
[5] V.V. Voevodsky, R.I. Soloukhin, *Proc. Combust. Inst.* 10 (1965) 279–283.
[6] J.W. Meyer, A.K. Oppenheim, *Proc. Combust. Inst.* 13 (1971) 1153–1164.
[7] E.S. Oran, T.R. Young, J.P. Boris, A. Cohen, *Combust. Flame* 48 (1982) 135–148.
[8] E.S. Oran, J.P. Borris, *Combust. Flame* 48 (1982) 149–161.
[9] R. Blumenthal, K. Fieweger, K.H. Comp, in: Proceedings of the International Symposium on Shock Waves, 20, 1995, pp. 935–940.
[10] D.J. Vermeer, A.K. Oppenheim, *Combust. Flame* 18 (1972) 327–336.
[11] K. Fieweger, R. Blumenthal, G. Adomeit, *Symp. Combust.* 25 (1994) 1579–1585.
[12] S.M. Walton, X. He, B.T. Zigler, M.S. Wooldridge, *Proc. Combust. Inst.* 31 (2007) 3147–3154.
[13] A.B. Mansfield, M.S. Wooldridge, *Combust. Flame* 161 (9) (2014) 2242–2251.
[14] E.L. Peterson, D.M. Kalitan, A.B. Barrett, et al., *Combust. Flame* 149 (2007) 244–247.
[15] C-J. Sung, C.K. Law, *Combust. Sci. Technol.* 180 (2008) 1097–1116.
[16] F.L. Dryer, M. Chaos, *Combust. Flame* 152 (2008) 293–299.
[17] M. Chaos, F.L. Dryer, *Combust. Sci. Technol.* 180 (2008) 1053–1096.
[18] D.J. Beerer, V.G. McDonell, J. Eng, *Gas Turb. Power* 130 (5) (2008) 051507.
[19] R. Sankaran, H.G. Im, E.R. Hawkes, J.H. Chen, *Proc. Combust. Inst.* 30 (2005) 875–882.
[20] Y.B. Zeldovich, *Combust. Flame* 39 (1980) 211–214.
[21] P. Pal, A.B. Mansfield, P.G. Arias, M.S. Wooldridge, H.G. Im, *Combust. Theor. Model.* 19 (5) (2015) 587–601.
[22] M. Ihme, *Combust. Flame* 159 (2012) 1592–1604.
[23] H. Wu, M. Ihme, *Combust. Flame* 161 (2014) 2317–2326.

Please cite this article as: P. Pal et al., Computational characterization of ignition regimes in a syngas/air mixture with temperature fluctuations, Proceedings of the Combustion Institute (2016), http://dx.doi.org/10.1016/j.proci.2016.07.059

[24] C.S. Yoo, T. Lu, J.H. Chen, C.K. Law, *Combust. Flame* 158 (2011) 1727–1741.
[25] C.S. Yoo, Z. Luo, T. Lu, H. Kim, J.H. Chen, *Proc. Combust. Inst.* 34 (2013) 2985–2993.
[26] H.A. El-Asrag, Y. Ju, *Combust. Flame* 161 (2014) 256–269.
[27] S.O. Kim, M.B. Luong, J.H. Chen, C.S. Yoo, *Combust. Flame* 162 (2015) 717–726.
[28] G. Bansal, A. Mascarenhas, J.H. Chen, *Combust. Flame* 162 (2015) 688–702.
[29] H.G. Im, P. Pal, M.S. Wooldridge, A.B. Mansfield, *Combust. Sci. Technol.* 187 (8) (2015) 1263–1275.
[30] K.P. Grogan, S.S. Goldsborough, M. Ihme, *Combust. Flame* 162 (2015) 3071–3080.
[31] J.H. Chen, A. Choudhary, B. de Supinski, et al., *Comput. Sci. Disc.* 2 (2009) 015001.
[32] C.A. Kennedy, M.H. Carpenter, *Appl. Numer. Math.* 14 (1994) 397–433.
[33] J. Li, Z. Zhao, A. Kazakov, M. Chaos, F.L. Dryer, J.J. Scire, *Int. J. Chem. Kinet.* 39 (2007) 109–136.
[34] R.J. Kee, F.M. Rupley, E. Meeks, J.A. Miller, *CHEMKIN-III: a fortran chemical kinetic package for the analysis of gas-phase chemical and plasma kinetics*, Sandia National Laboratories, 1996 Report No. SAND96-8216.
[35] R.J. Kee, G. Dixon-Lewis, J. Warnatz, M.E. Coltrin, J.A. Miller, *A fortran computer code package for the evaluation of gas-phase multicomponent transport properties*, Sandia National Laboratories, 1986 Report No. SAND86-8246.
[36] X.J. Gu, D.R. Emerson, D. Bradley, *Combust. Flame* 133 (2003) 63–74.
[37] J.H. Chen, S.D. Mason, J.C. Hewson, in: Proceedings of the Third Joint Sections Meeting of the U.S. Sections of the Combustion Institute, 2003.
[38] J.O. Hinze, *Turbulence*, McGraw-Hill, New York, 1975.
[39] G. Mittal, C.-J. Sung, *Combust. Flame* 145 (2006) 160–180.
[40] R.J. Kee, J.F. Grcar, M.D. Smooke, J.A. Miller, *A fortran program for modeling steady laminar one-dimensional flames*, Sandia National Laboratories, 1985 Report No. SAND85-8240.
[41] S.B. Pope, *Turbulent Flows*, Cambridge University Press, 2000.
[42] T. Echekki, J.H. Chen, *Combust. Flame* 118 (1999) 308–311.
[43] H.G. Im, J.H. Chen, *Combust. Flame* 119 (1999) 436–454.
[44] J.H. Chen, E.R. Hawkes, R. Sankaran, S.D. Mason, H.G. Im, *Combust. Flame* 145 (2006) 128–144.
[45] E.R. Hawkes, R. Sankaran, P.P. Pebay, J.H. Chen, *Combust. Flame* 145 (2006) 145–159.
[46] S.H. Lam, Corrado Casci (Ed.), Recent Advances in the Aerospace Sciences, Plenum Press, New York and London, 1985, pp. 3–20.
[47] S.H. Lam, D.A. Goussis, Twenty-Second Symposium (International) on Combustion (1988) 931–941.
[48] M. Valorani, H.N. Najm, D.A. Goussis, *Combust. Flame* 134 (2003) 35–53.
[49] M. Valorani, F. Creta, D.A. Goussis, J.C. Lee, H.N. Najm, *Combust. Flame* 146 (2006) 29–51.
[50] S. Gupta, H.G. Im, M. Valorani, *Proc. Combust. Inst.* 33 (2011) 2991–2999.

Please cite this article as: P. Pal et al., Computational characterization of ignition regimes in a syngas/air mixture with temperature fluctuations, Proceedings of the Combustion Institute (2016), http://dx.doi.org/10.1016/j.proci.2016.07.059